

Air Force Institute of Technology

AFIT Scholar

Theses and Dissertations

Student Graduate Works

12-1995

Thermo-Mechanical Fatigue Behavior of Cross-Ply Ceramic Matrix Composite under Tension-Tension Loading

Dana G. Allen

Follow this and additional works at: <https://scholar.afit.edu/etd>

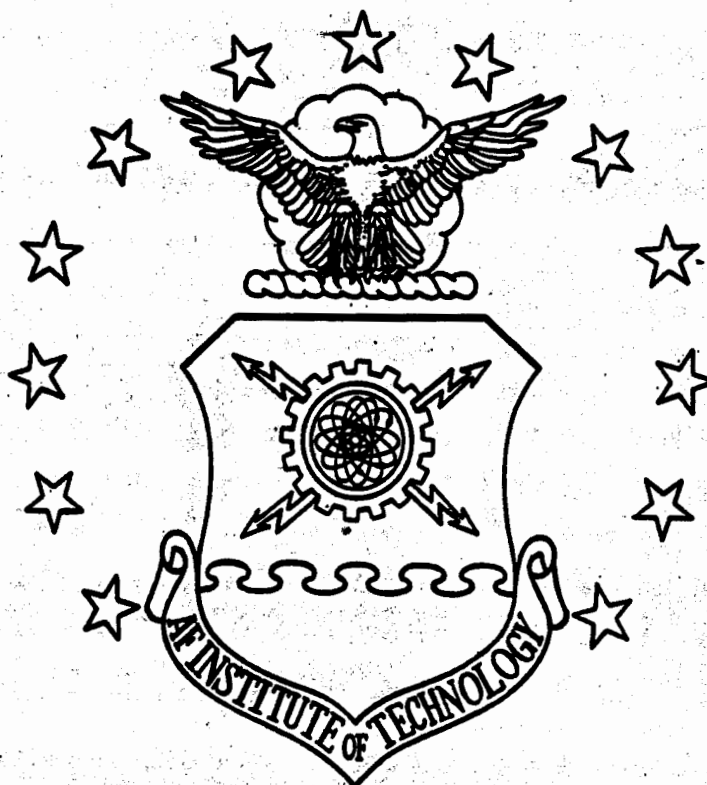


Part of the [Mechanics of Materials Commons](#), and the [Structures and Materials Commons](#)

Recommended Citation

Allen, Dana G., "Thermo-Mechanical Fatigue Behavior of Cross-Ply Ceramic Matrix Composite under Tension-Tension Loading" (1995). *Theses and Dissertations*. 6091.
<https://scholar.afit.edu/etd/6091>

This Thesis is brought to you for free and open access by the Student Graduate Works at AFIT Scholar. It has been accepted for inclusion in Theses and Dissertations by an authorized administrator of AFIT Scholar. For more information, please contact AFIT.ENWL.Repository@us.af.mil.



THERMO-MECHANICAL FATIGUE BEHAVIOR OF
CROSS-PLY CERAMIC MATRIX COMPOSITE UNDER
TENSION-TENSION LOADING

THESIS

Dana G. Allen
Captain, USAF
AFIT/GAE/ENY/95D-01

DISTRIBUTION STATEMENT A

Approved for public release
Distribution Unlimited

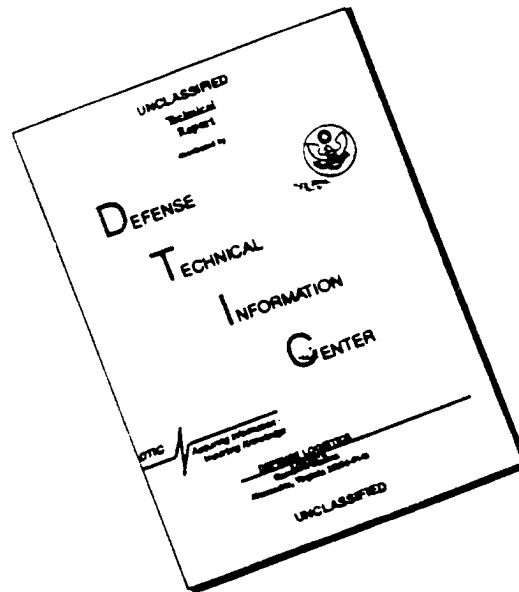
DEPARTMENT OF THE AIR FORCE
AIR UNIVERSITY
AIR FORCE INSTITUTE OF TECHNOLOGY

Wright-Patterson Air Force Base, Ohio

DTIC QUALITY INSPECTED 1

19960408 009

DISCLAIMER NOTICE



THIS DOCUMENT IS BEST QUALITY AVAILABLE. THE COPY FURNISHED TO DTIC CONTAINED A SIGNIFICANT NUMBER OF PAGES WHICH DO NOT REPRODUCE LEGIBLY.

AFIT/GAE/ENY/95D-01

THERMO-MECHANICAL FATIGUE BEHAVIOR OF
CROSS-PLY CERAMIC MATRIX COMPOSITE UNDER
TENSION-TENSION LOADING

THESIS

Dana G. Allen
Captain, USAF
AFIT/GAE/ENY/95D-01

Approved for public release, distribution unlimited

AFIT/GAE/ENY/95D-01

THERMO-MECHANICAL FATIGUE BEHAVIOR OF CROSS-PLY CERAMIC
MATRIX COMPOSITE UNDER TENSION-TENSION LOADING

THESIS

Presented to the faculty of the Graduate School of
Engineering of the Air Force Institute of Technology

Air University

In Partial Fulfillment of the
Requirements for the Degree of
Master of Science in Mechanical Engineering

Dana G. Allen

Captain, USAF

December 1995

Preface

In this study, the thermo-mechanical fatigue behavior of the cross-ply, ceramic matrix composite was investigated at elevated temperature with loading and temperature wave-forms combining the characteristics of low cycle fatigue and stress rupture. A series of tests was conducted at various stress levels, both in-phase and out-of-phase thermo-mechanical fatigue, and isothermal fatigue. In addition, the mechanisms that control the fatigue life under these different conditions were investigated.

The people I would like to thank for their inputs and support are Dr. Shankar Mall, Dr. Anthony Palazotto, and Major Dave Robertson. Thanks to Mr. Mark Derriso and Mr. Sean Coghlan who taught me to use the equipment and helped me through melt downs and other minor crises. Thank you, Mr. John Woodhouse for your help and time. I would like to thank AFOSR/NA for sponsoring this work. I would especially like to thank my wife, Lynne and my children, Katherine and Chad, for lifting my spirits at the end of each day.

Dana G. Allen

Table of Contents

Preface.....	ii
List of Tables	v
List of Figures	vi
Abstract	xi
I. INTRODUCTION	1
<i>Background</i>	1
<i>Problem statement/scope</i>	3
<i>Approach</i>	4
<i>Document Layout</i>	5
II. BACKGROUND	6
III. EXPERIMENTAL EQUIPMENT/PROCEDURE	11
<i>Equipment</i>	11
<i>Material Description</i>	13
<i>Specimen Preparation</i>	14
<i>Calibration</i>	17
<i>Test Procedure</i>	17
IV. RESULTS AND DISCUSSION	20
<i>Test Summary</i>	20
<i>Monotonic Tests</i>	21
<i>Fatigue Life</i>	27

<i>Strain Data</i>	50
<i>Modulus Degradation</i>	68
<i>Hysteresis Loops</i>	81
<i>Damage Mechanisms</i>	92
V. CONCLUSIONS	115
VI. RECOMMENDATIONS	117
BIBLIOGRAPHY	118
APPENDIX A	120
APPENDIX B	124
APPENDIX C	128
Vita.....	129

List of Tables

TABLE 1. NICALON/MAS-5 PROPERTIES	14
TABLE 2. SPECIMEN DIMENSIONS	16
TABLE 3. LOCATION OF FRACTURE	22
TABLE 4. COMPARISON OF MATERIAL PROPERTIES.....	26
TABLE 5. FATIGUE TEST SUMMARY	28

List of Figures

FIGURE 1. TEST STATION LAYOUT	12
FIGURE 2. LOW SPEED SAW	15
FIGURE 3. SPECIMEN POLISHER.....	16
FIGURE 4. SPECIMEN LAYOUT.....	18
FIGURE 5. MONOTONIC TEST: ROOM TEMPERATURE VS. 566°C.....	23
FIGURE 6. MONOTONIC TEST: PRESENT STUDY VS. STEINER'S AT 566°C.....	23
FIGURE 7. MONOTONIC TEST: 1093°C.....	24
FIGURE 8. MONOTONIC TEST: 1093°C PRESENT STUDY VS. STEINER.....	25
FIGURE 9. MONOTONIC TEST: 566°C VS. 1093°C.....	25
FIGURE 10. DAMAGE MECHANISMS AND FATIGUE LIFE DIAGRAM.....	29
FIGURE 11. IN-PHASE TMF: S-N CURVE.....	30
FIGURE 12. IN-PHASE TMF S-N CURVE: PRESENT STUDY VS. WORTHEM [17].....	31
FIGURE 13. IN-PHASE TMF S-T CURVE: PRESENT STUDY VS. WORTHEM [17]	31
FIGURE 14. OUT-OF-PHASE TMF S-N CURVE	33
FIGURE 15. OUT-OF-PHASE TMF S-N: PRESENT STUDY VS. WORTHEM [17].....	35
FIGURE 16. OUT-OF-PHASE TMF S-T: PRESENT STUDY VS. WORTHEM [17]	35
FIGURE 17. IN-PHASE VS. OUT-OF-PHASE TMF S-T.....	36
FIGURE 18. MAXIMUM FIBER STRESS VS. CYCLES.....	37
FIGURE 19. FIBER STRESS RANGE VS. CYCLES.....	38
FIGURE 20. MAXIMUM MATRIX STRESS VS. CYCLES	38

FIGURE 21. MATRIX STRESS RANGE VS. CYCLES.....	39
FIGURE 22. S-N CURVE 566°C	40
FIGURE 23. S-N CURVE 1093°C	41
FIGURE 24. S-N CURVE: 566°C VS. 1093°C.....	42
FIGURE 25. NORMALIZED S-N CURVE: 566°C VS. 1093°C	42
FIGURE 26. S-N CURVE: PRESENT STUDY VS. STEINER 566°C [15]	43
FIGURE 27. S-N CURVE: PRESENT STUDY VS. STEINER 1093°C [15]	44
FIGURE 28. S-T CURVE: PRESENT STUDY VS. STEINER 566°C [15].....	45
FIGURE 29. S-T CURVE: PRESENT STUDY VS. STEINER 1093°C [15].....	45
FIGURE 30. IN-PHASE TMF VS. 1093°C ISOTHERMAL	46
FIGURE 31. OUT-OF-PHASE TMF VS. 566°C ISOTHERMAL	47
FIGURE 32. TMF VS. ISOTHERMAL S-N CURVE	49
FIGURE 33. TMF VS. ISOTHERMAL S-T CURVE	49
FIGURE 34. IN-PHASE TMF: MAXIMUM STRAIN	51
FIGURE 35. IN-PHASE TMF: MINIMUM STRAIN	52
FIGURE 36. IN-PHASE TMF: STRAIN RANGE.....	53
FIGURE 37. IN-PHASE TMF: MAXIMUM STRAIN, NORMALIZED LIFE.....	54
FIGURE 38. OUT-OF-PHASE TMF: MAXIMUM STRAIN	55
FIGURE 39. OUT-OF-PHASE TMF: MINIMUM STRAIN	56
FIGURE 40. OUT-OF-PHASE TMF: STRAIN RANGE.....	56
FIGURE 41. OUT-OF-PHASE TMF: MAXIMUM STRAIN VS. NORMALIZED LIFE	57
FIGURE 42. MAXIMUM STRAIN: IN-PHASE TMF VS. OUT-OF-PHASE TMF.....	57

FIGURE 43. STRAIN RANGE: IN-PHASE TMF VS. OUT-OF-PHASE TMF	58
FIGURE 44. 566°C: MAXIMUM STRAIN	59
FIGURE 45. 566°C: MAXIMUM STRAIN VS. NORMALIZED LIFE	59
FIGURE 46. 566°C: MINIMUM STRAIN	60
FIGURE 47. 566°C: STRAIN RANGE.....	60
FIGURE 48. 1093°C: MAXIMUM STRAIN	61
FIGURE 49. 1093°C: MAXIMUM STRAIN VS. NORMALIZED LIFE	62
FIGURE 50. 1093°C: MINIMUM STRAIN	62
FIGURE 51. 1093°C: STRAIN RANGE.....	63
FIGURE 52. MAXIMUM STRAIN: 566°C VS. 1093°C.....	64
FIGURE 53. STRAIN RANGE: 566°C VS. 1093°C	64
FIGURE 54. MAXIMUM STRAIN: HIGH STRESS LEVELS	66
FIGURE 55. MAXIMUM STRAIN: LOW STRESS LEVELS	67
FIGURE 56. STRAIN RANGE: HIGH STRESS LEVELS	67
FIGURE 57. STRAIN RANGE: LOW STRESS LEVELS.....	68
FIGURE 58. MODULUS DEGRADATION: IN-PHASE TMF.....	70
FIGURE 59. NORMALIZED MODULUS DEGRADATION: IN-PHASE TMF.....	71
FIGURE 60. MODULUS DEGRADATION, OUT-OF-PHASE TMF	72
FIGURE 61. NORMALIZED MODULUS DEGRADATION, OUT-OF-PHASE	73
FIGURE 62. NORMALIZED MODULUS: IN-PHASE TMF VS. OUT-OF-PHASE TMF	73
FIGURE 63. MODULUS DEGRADATION: 566°C	74
FIGURE 64. NORMALIZED MODULUS DEGRADATION: 566°C.....	75

FIGURE 65. MODULUS DEGRADATION: 1093°C	76
FIGURE 66. NORMALIZED MODULUS DEGRADATION: 1093°C	77
FIGURE 67. NORMALIZED MODULUS: 566°C vs. 1093°C	78
FIGURE 68. NORMALIZED MODULUS: HIGH STRESS LEVELS	79
FIGURE 69. NORMALIZED MODULUS: LOW STRESS LEVELS	79
FIGURE 70. HYSTERESIS: 120 MPA, IN-PHASE TMF	82
FIGURE 71. HYSTERESIS: 105 MPA, IN-PHASE TMF	84
FIGURE 72. HYSTERESIS: 85 MPA, IN-PHASE TMF	84
FIGURE 73. HYSTERESIS: 110 MPA, OUT-OF-PHASE TMF	85
FIGURE 74. HYSTERESIS: 91 MPA, OUT-OF-PHASE TMF	86
FIGURE 75. HYSTERESIS: 83 MPA, OUT-OF-PHASE TMF	86
FIGURE 76. HYSTERESIS: 60 MPA, OUT-OF-PHASE TMF	87
FIGURE 77. HYSTERESIS: 160 MPA, 566°C	88
FIGURE 78. HYSTERESIS: 133 MPA, 566°C	89
FIGURE 79. HYSTERESIS: 110 MPA, 566C	90
FIGURE 80. HYSTERESIS: 100 MPA, 1093°C	91
FIGURE 81. IN-PHASE TMF, 145 MPA, FRACTURE SURFACE, 12X	94
FIGURE 82. IN-PHASE TMF: 135 MPA, FRACTURE SURFACE, 13X	95
FIGURE 83. IN-PHASE TMF: 120 MPA FRACTURE SURFACE, 12X	95
FIGURE 84. IN-PHASE TMF: 105 MPA, 13X	96
FIGURE 85. IN-PHASE TMF: 105 MPA, DAMAGE ACCUMULATION, 100X	97
FIGURE 86. IN-PHASE TMF: FRACTURE SURFACE, 100 MPA, 13X	98

FIGURE 87. IN-PHASE TMF: 100 MPa, CONCOIDAL FIBER FRACTURE, 600X	98
FIGURE 88. IN-PHASE TMF: 100 MPa, MATRIX CRACK, 100X.....	99
FIGURE 89. OUT-OF-PHASE TMF: 145 MPa, FRACTURE SURFACE, 12X.....	100
FIGURE 90. OUT-OF-PHASE TMF: 145 MPa, FIBER CONDITION, 600X	101
FIGURE 91. OUT-OF-PHASE TMF: 110 MPa, FRACTURE SURFACE, 11X	102
FIGURE 92. OUT-OF-PHASE TMF: 83 MPa, FRACTURE SURFACE, 13X.....	103
FIGURE 93. OUT-OF-PHASE TMF: 83 MPa, FIBER CONDITION, 600X	103
FIGURE 94. OUT-OF-PHASE TMF: 83 MPa, DEBOND, CRACK DEFLECTION, 100X.....	104
FIGURE 95. ISOTHERMAL FATIGUE 566°C: 160 MPa, FRACTURE SURFACE, 11X	106
FIGURE 96. ISOTHERMAL FATIGUE 566°C: 133 MPa, FIBER PULL-OUT, 550X.....	106
FIGURE 97. ISOTHERMAL FATIGUE 566°C: 133 MPa, MATRIX CRACK, 100X	107
FIGURE 98. ISOTHERMAL FATIGUE 566°C: 133 MPa, FIBER CONDITION, 1020X	107
FIGURE 99. 1093°C ISOTHERMAL FATIGUE: 115 MPa, SHORT FIBER PULL-OUT, 12X...	108
FIGURE 100. 1093°C ISOTHERMAL FATIGUE: 115 MPa, FRACTURE SURFACE, 550X.....	109
FIGURE 101. 1093°C ISOTHERMAL FATIGUE: 115 MPa, MATRIX CRACK, 10X.....	110
FIGURE 102. 1093°C ISOTHERMAL FATIGUE: 100 MPa, MATRIX, FIBER CRACK, 100X..	110
FIGURE 103. 1093°C ISOTHERMAL FATIGUE: 100 MPa, FRACTURE SURFACE, 12X.....	111
FIGURE 104. 1093°C ISOTHERMAL FATIGUE: 100 MPa, FIBER CONDITION, 550X	111

Abstract

The purpose of this study was to investigate the combined effect of cyclic temperature and loading on the fatigue life of a ceramic matrix composite with a cross ply lay-up. The material used in this study was a potassium borosilicate glass (BSG) doped (5%) magnesium aluminosilicate (MAS) cordierite matrix reinforced with Nicalon (silicon carbide, SiC) fibers in a $[0/90]_{4s}$ lay-up.

Thermo-mechanical fatigue (TMF) tests were performed with a period of 180 seconds/cycle, or 0.00556 Hz, and a triangular wave-form. The temperature was cycled between 566°C and 1093°C, and the stress levels varied between 60 MPa and 145 MPa. All tests involved tension-tension cycling with a stress ratio of 0.1. These two temperatures and the stress ratio were chosen to correspond with previous studies on this material.

Six tests were performed under in-phase TMF conditions, and five tests were performed out-of-phase TMF condition. Four fatigue tests were performed isothermally at 566°C, and three more at 1093°C. Monotonic tests were also performed at room temperature, 566°C and 1093°C.

Load and strain data were measured during all tests. This data was then used to get histories for maximum strain, minimum strain and strain range, modulus degradation, stress-strain hysteresis loops, and fatigue life curves. Post-mortem fractographic analysis, with optical and scanning electric microscopes, was also performed on the specimen. Damage and fracture mechanisms were thus determined.

These results indicate a much higher damage for thermo-mechanical fatigue than for high temperature isothermal mechanical fatigue, with the out-of-phase TMF being much higher than the in-phase TMF. By comparing with previous data, it is shown that frequency has no effect, thus the damage is a time dependent phenomenon involving environmentally assisted crack growth and fiber-matrix debonding. The fatigue life for the in-phase TMF condition was found to be equivalent to the isothermal fatigue tests for low stress values. At higher stress values it fell between the isothermal fatigue at 566°C and 1093°C, and was within half the life of the 1093°C condition. The fatigue life for the out-of-phase TMF condition was consistently lower than the other fatigue conditions.

THERMO-MECHANICAL FATIGUE BEHAVIOR OF CROSS-PLY
CERAMIC MATRIX COMPOSITE UNDER TENSION-TENSION
LOADING

I. Introduction

Background

The use of composites has been around for centuries, but it is only recently that advanced composites have surfaced. Advanced composites are the latest breed of materials consisting of high strength and a large modulus of elasticity fibers impregnated within a matrix material. These fiber reinforced composites have been produced for only the last three decades. These composites are being pushed by the growing need for high technology, and especially for higher performance in aircraft. Loads that are experienced in aerospace applications are unsteady, causing a great deal of fatigue over the life of the structure. Composites promise to offer excellent strength and fatigue life with reduced weight, a desirable feature for aerospace applications. High performance requires more powerful and more efficient turbine engines. The limiting factor in turbine engine technology is the turbine inlet temperature. Higher temperature means higher performance, but a very few materials can withstand the high temperature and stresses applied in such a cyclical manner.

Monolithic ceramics have good high temperature properties, but are very brittle in nature. By adding reinforcing fibers, it is hoped to combine high toughness associated with fiber reinforcement with the high temperature resistance and strength of monolithic ceramics. Ceramics, however, do have their drawbacks. Typically ceramics are very susceptible to preexisting flaws, which then cause stress concentrations, and thus very low fatigue lives. They also do not exhibit plastic flow like most metals, they have a very brittle behavior. Adding fiber reinforcement increases the ceramic's toughness, and lessens its susceptibility to preexisting flaws, hence greatly increases the fatigue life.

Ceramic matrix composites (CMCs) have a great potential in high temperature regimes. The Nicalon fiber, invented by Yajima in 1980 [5] is one of the most promising step in this direction. There have been several studies of this material with different ceramic matrices, such as silicon carbide (SiC) [11], lithium aluminosilicate (LAS) [12], and calcium aluminosilicate (CAS) [1,6,8,17,18]. They are all glass-ceramic matrices. These glass-ceramics exhibit the same trends in fatigue life and stress rupture. They all experience oxygen embrittlement of the fiber/matrix interface. The use of the magnesium aluminosilicate (MAS) matrix has only recently been looked at as matrix material in ceramic matrix composites. Larsen studied the effects of doping the MAS matrix with borosilicate glass (BSG) to improve the high temperature properties of the fiber/matrix interface by decreasing the oxidation of the interface [7], thus it is hoped that MAS would provide a better ceramic matrix composite system.

There have been a few studies [3,15] of this material to investigate the properties at constant elevated temperature, i.e. under isothermal conditions. Both Steiner and Grant

looked at Nicalon/MAS-5 at elevated temperatures[3,15]. Real life applications, such as turbine blades in a turbofan engine, dictate the need to determine the behavior of this material in an environment involving both cycling loads and cycling temperature which is commonly known as thermo-mechanical fatigue (TMF). Since thermo-mechanical fatigue involves many factors, it is much more difficult to build an analytical model to accurately predict the behavior of such a composite in a varying load and temperature environment, thus it is necessary to perform thermo-mechanical fatigue testing. There has been a limited number of studies involving thermo-mechanical fatigue of ceramic matrix composites. One such study was done by Worthem [17]. He compared the fatigue lives of Nicalon/CAS with Nicalon/MAS-5, and found that the doped MAS matrix is better than the CAS in TMF conditions. He also compared the fatigue lives of unidirectional Nicalon/MAS-5 with cross-ply Nicalon/MAS-5. The cross-ply laminate had the same fatigue life at half the maximum stress indicating that fiber failure was the controlling factor in fatigue life. Thus, there is a limited amount of information available about the thermo-mechanical fatigue behavior of ceramic matrix composites. This study will further investigate the behavior of this material. This study will also provide a follow-on investigation of two previous studies involving isothermal fatigue of this material [3,15].

Problem statement/scope

The objective of this study is to investigate the effects of cycling temperature along with the cycling of load on a silicon carbide/magnesium aluminosilicate ceramic matrix composite. This will not only characterize the behavior of this material, it will

also provide trends to extrapolate new data, or possibly use the simpler testing methods for new data, since TMF testing is much more complex to set up than simple isothermal fatigue testing. It may also help to build the foundation from which an analytical model can be built, saving countless hours of costly laboratory work to test specimen.

Approach

To achieve the objective, a test program was designed which included both in-phase and out-of-phase thermo-mechanical fatigue testing, and isothermal tests at the maximum and minimum temperatures of the TMF, and at the same frequency of the TMF tests. The thermo-mechanical fatigue tests involve cycling both temperature and load. In reality, these cycles will have various phase differences, and will not be together at the same frequency. The two simple cases would be if the load and temperature were at the same frequency and either in-phase, where the load and temperature peak together, and out-of-phase TMF, where the load peaks while the temperature is at a minimum value, and the temperature peaks while the load is at a minimum value. The isothermal tests will be similar to the previous study [3,15], but at a frequency that is equal to the frequency of thermo-mechanical fatigue.

All thermo-mechanical fatigue tests involved a triangular waveform, at a period of 180 seconds. All tests had a stress ratio of 0.1. The maximum temperature was 1093°C and the minimum was 566°C. These were chosen to compare with Steiner [15] and Grant's [3] studies who conducted isothermal fatigue tests at these two temperatures. These tests were performed on an MTS servohydraulic test machine under load control

mode. Several tests were conducted at different maximum stress levels in order to effectively determine the fatigue characteristics, and to develop the fatigue life diagrams, i.e., S-N curves. Monotonic tests were also performed to obtain baseline data for the tested composite and to compare material properties with previous studies. This provided information such as modulus, yield stress, failure stress, and strain at failure for the different temperatures. Next, in-phase TMF testing was performed at different stress levels. Out-of-phase TMF testing was then performed at stress levels chosen to give similar fatigue life values as the in-phase TMF tests. Finally, isothermal fatigue tests were run at both 566°C and 1093°C, at the same frequency as of the thermo-mechanical test to provide a comparison with them, and to also continue previous isothermal studies [3,15] at the same temperatures but different frequencies.

Document Layout

The remainder of this document is set in the following manner. Chapter 2 has background information, Chapter 3 discusses the test machine, specimen preparation, and the procedures used to run tests. Chapter 4 is broken up into seven sections, the first being acquisition and reduction of test data, with a summary of the test results. The second section deals with the monotonic tests. The third is the discussion of the fatigue life curves, the fourth about strain data. Section five looks at the modulus degradation, and section six provides the strain hysteresis loops. Section seven discusses the failure damage mechanisms. Chapter five summarizes the conclusion of this study and Chapter six provides recommendations for further research.

II. Background

Silicon carbide (SiC)/magnesium aluminosilicate (MAS) is one of many new advanced ceramic matrix composites manufactured for high temperature environments. It falls into the category of glass-ceramic composites. These composites offer high strength and durability at high temperatures. They promise to raise the operating temperature of turbine engines while lowering the weight. They could also operate without the cooling devices which metals require, thus reducing complexity and cost.

Several studies have been undertaken to determine the properties of the glass-ceramic composites with the silicon carbide fiber, Nicalon. Nicalon is very promising and has been studied with several different matrices, most of which are glass-ceramics, similar to MAS. These studies have predominantly involved only monotonic loading, or high cycle fatigue. When they have been studied under thermal conditions, they have been under isothermal conditions.

Static tests were performed first to characterize the properties of the material. Daniel, Anastassopoulos and Lee [2] looked at Nicalon/CAS under room temperature longitudinal loading and found that the initial failure was transverse matrix cracks, occurring at stress levels above 100 MPa. The cracks increased in density as the stress level increased. Mall and Kim [8] investigated the failure mechanisms in Nicalon/CAS of three different lay-ups. These tests were at room temperature. They found that

matrix cracking occurred below the proportional limit, and at random. The matrix cracks did not propagate through the laminate, but would end at each ply.

A similar study was performed by Karandikar and Chou [6]. Upon loading, the 90 degree plies of a Nicalon/CAS experienced microcracking. The microcracking occurred until a saturation point was reached. The saturation point corresponded with the proportional limit of the laminate. The cracking led to a significant degradation in elastic modulus. Thus, these studies characterized the room temperature static performance of similar ceramic matrix composites.

The eventual application of a material in aerospace application leads to the need for fatigue testing. Prewo [12] studied Nicalon/LAS and found that both the flexural and tensile fatigue lives were dependent on the stress level. For maximum fatigue stresses below the proportional limit no damage accumulation was found, but for stresses above the proportional limit, there was a gradual decrease in specimen stiffness, indicating damage accumulation.

Since ceramic matrix composites will be subjected to high temperature environments, such as turbine engines, testing at those operating temperatures is required. Steiner [15] performed isothermal fatigue testing of Nicalon/MAS-5 at both 566°C and 1093°C. He ran tests at 1 Hz and 10 Hz and a variety of stress levels. He found that the fatigue life and the damage mechanisms were not dependent on the frequency of cycles. The fatigue life was dependent on the stress level and the temperature. At high stress levels, the fatigue life was reduced, likewise for elevated temperature. The damage mechanisms were consistent with the fatigue life findings.

Grant [3] also performed isothermal study of Nicalon/MAS-5. His study involved fatigue testing with various hold times at maximum stress. He found that exposure time was the predominant factor in fatigue life, but both stress and environment played a part at high temperatures. These studies showed that the limiting factor in the fatigue life of the ceramic composite system is severe reduction of mechanical properties at high temperatures due to oxidation of the fiber matrix interface.

SiC/MAS has a problem common to many ceramic matrix composites, at high temperature the fiber matrix interface oxidizes rapidly, thus altering the bond between the fiber and matrix. It strengthens the bond, but making it more brittle. With prolonged exposure to high temperature, the bond becomes strong enough to restrain the fibers. Any matrix cracking that occurs will simply propagate across the matrix and through the fibers. The composite needs a weaker interfacial bond so the fibers can strain at a different rate than the matrix.

Any type of cyclic loading, thermal or mechanical, can cause plastic deformation in a composite, which can initiate cracking. Even at maximum stress levels below that of the elastic limit a material may fail due to stress concentration from preexisting flaws. These flaws can be voids and inclusions, but in the case of composites, the fiber matrix interface can act as a flaw, from which cracks can initiate. This is even more prevalent in ceramic matrix composites, which are very susceptible to flaws due to their brittle nature.

There have been some attempts to improve the high temperature characteristics of ceramic matrix composites. Ishikawa studied the high temperature properties of a Nicalon/SiC (Nicaloceram) composite. He modified the Nicalon fiber into HI-Nicalon,

and got good tensile strength up to 1500°C. Toreki, et. al. [16]. found that by improving the process in which the fibers are made, there can be an increase in the thermo-mechanical stability of a Nicalon/ceramic composite.

Larsen [7] doped Nicalon/MAS with different levels of BSG to modify the interface. His investigation was under stress rupture loading at both 566°C and 1093°C. He found that BSG added boron to the interface, making it thinner and less susceptible to oxidation. High quantities of BSG (7.5%) decreased the refractoriness, and is unacceptable. He concluded that 5% doping was optimal for maintaining material properties throughout the temperature range as well as reducing the interface oxidation.

Very few real world applications involve constant temperature or load. Both temperature and stress cycles would be present in many applications. Temperature cycling does damage in many ways, first, the simple difference in the coefficient of thermal expansion (CTE) between the fiber and the matrix causes both shear stresses and hoop stress, which then cycle with the cycling temperature. Also the mere exposure to the extreme temperatures of this test cause a breakdown of the fiber matrix interface, which can initiate cracking.

Butkus and Holmes [1] investigated thermo-mechanical fatigue of unidirectional Nicalon/CAS II and found that the primary damage mechanism for low stress, long exposure time specimens, was matrix creep, with the thermo-mechanical tests having much higher creep and matrix damage accumulation than the isothermal tests.

Worthern [17] performed Thermo-mechanical fatigue testing on Nicalon fibers with three different matrix materials, CAS, MAS-5, and SiC. The MAS-5 was both

unidirectional and cross-ply. In comparing the results to those of a previous study, he found that thickness had little effect on fatigue life in 3 to 6 mm range. He also showed that the MAS-5 matrix performed considerably better than CAS, due to the improved interface and a better match of CTE. The unidirectional MAS-5 had the same fatigue life at twice the stress level as the cross-ply, showing failure was dependent only upon the failure of the fibers. This was observed for both in-phase and out-of-phase TMF testing.

Wortherm also tested the TMF properties of Nicalon/CAS and found the life was significantly shorter under TMF than isothermal conditions. The effect of phase angle was also significant, but this significance may vary with material properties [18].

The significance of residual stresses was emphasized by Powell, Smith and Yeomans [11]. They predicted the residual shear stresses at room temperature were enough to debond the fibers from the matrix in Nicalon/CAS. There were also significant compressive hoop stresses on the fibers, and consequently, tension on the matrix.

III. Experimental Equipment/Procedure

This chapter deals with the experimental details. The test equipment is described, as well as its calibration. A description of the material studied and its preparation into a test specimen is included. Finally, the procedure for running the tests is outlined. All the tests were performed in the Department of Aeronautics and Astronautics Structures Laboratory of the Air Force Institute of Technology.

Equipment

The test station consisted of testing equipment, a control system, heating and cooling equipment, and a data acquisition system. The testing equipment was composed of a hydraulic actuator, hydraulic grips, and an extensometer. The hydraulic actuator was a 22.24 kN model 204.13 servoram actuator, manufactured by MTS. The grips were an MTS model 685.03 20.685 MPa Hydraulic grip supply. The extensometer was an MTS 632.65B-03, with a gage length of 2.54 cm. The control system was an MTS model 458.20 Microconsole. The load cards used were the ± 11.12 kN and the ± 4.448 kN. Both air and water provided cooling for the test station. Air cooling was provided by a laboratory supplied pneumatic system, and water cooling was available from a closed system refrigerated recirculator, model HX-75, manufactured by Neslab. Due to the extremely high temperatures involved, extra cooling shields had to be installed on the grips to protect the sensitive equipment. Heat was provided by a total of eight 1000 watt Sylvania quartz bulbs, in two locally manufactured housings, four bulbs in each. The

lamps were provided with feedback by four ANSI code K chromel-alumel thermocouples, firmly attached to the specimen. The thermocouples and the load feedback were attached to microconsole which also took strain data via a ceramic rod extensometer. The raw data was then acquired by a Zenith 486DX33 using MATE program via a 12 bit A/D board. See Figure 1 for the test station layout.

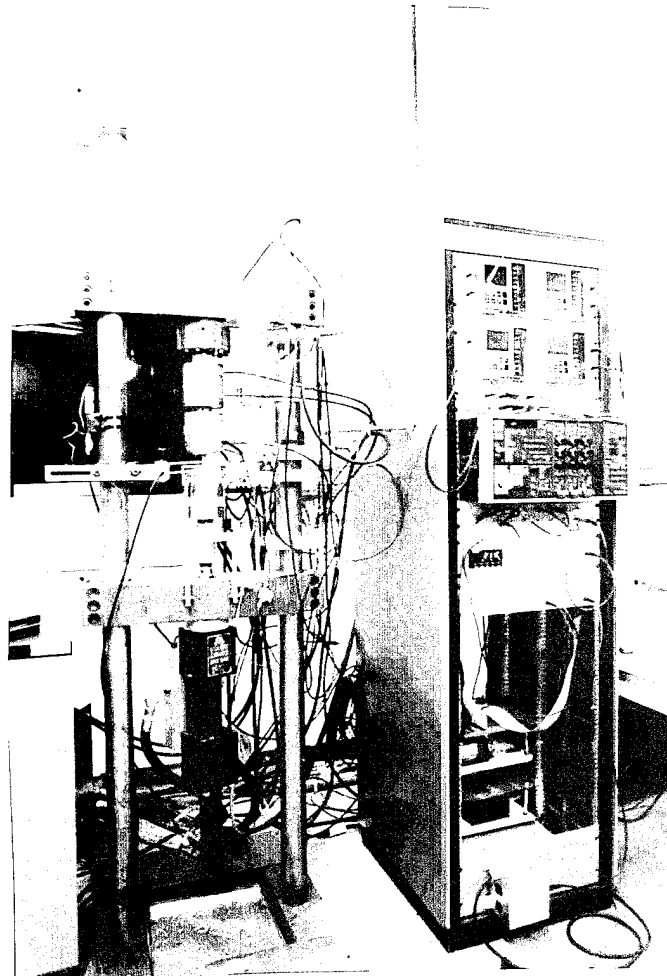


Figure 1. Test Station Layout

Material Description

Nicalon/MAS-5 incorporates a silicon carbide (SiC) fiber manufactured by Nippon under trade name of Nicalon, in a magnesium aluminosilicate matrix that has been doped with 5% borosilicate. The borosilicate adds boron to the fiber matrix interface, which then becomes more stable than the commonly used carbon interface in the present ceramic matrix composites, such as SiC/LAS and SiC/CAS. Nicalon is not a pure silicon carbide fiber, its chemical composition is $\text{SiC} - \text{C} - \text{SiO}_2$. The matrix is $2\text{MgO} - 2\text{Al}_2\text{O}_3 - 5\text{SiO}_2$, based on cordierite. A typical graphite/epoxy or boron/epoxy composite has a large difference between the fiber modulus and the matrix modulus, a ratio of around 10 to 1, but with this type of ceramic/ceramic composite, the ratio is less than 2 to 1. Obviously, the fibers are not added to increase stiffness, but they are there to increase toughness, of which monolithic ceramics are decidedly lacking. This toughness comes from the fact that matrix cracks will stop at the fiber matrix interface, and crack bridging and crack tip deflection will occur. Both of these are energy absorbing phenomena, which greatly increase the toughness. However, these important fiber/matrix interfaces oxidize rapidly with exposure to high temperatures. This oxidation causes the interface strength to increase, which does not allow the fibers to slide or give, and reduces the amount of fiber debonds. This leads to undesirable properties that are essentially in monolithic ceramic material, where cracks are uninhibited, and can quickly traverse the composite. See Table 1 for the material properties.

Table 1. Nicalon/MAS-5 Properties

	Nicalon*	MAS-5**	Lamina***	Laminate***
Composition (wt %)	59 Si, 31 C, 10 O	Mg Al S O		
Young's Modulus (GPa)	200	138	162	159.6
CTE per °C	4.0×10^{-6}	2.4×10^{-6}	3.17×10^{-6}	3.08×10^{-6}
Poisson ratio	0.25	0.25	0.25	0.25
Ultimate Strength	2.8 - 3.0 GPa	250 MPa		
Ultimate Strain	1%-1.4%	0.8 %		
Volume Fraction	0.39	0.61		

* [5]

** [4]

***calculated, see Appendix A

Specimen Preparation

Specimens were cut from two plates, both serial number 9324305L, using a 10.16 cm diamond wafering blade, shown in Figure 2. Since the blade diameter was shorter than the specimen length, two cuts had to be made to complete the cutting of specimen. The two cuts had a very slight mismatch, which resulted in a small notch, as well as a slightly non-uniform width. If the notch was left untreated, it could cause a stress concentration and initiate unwanted cracking. The first polishing step was a medium grind with 68 micron diamond wheel to level both sides of the specimen and ensure the notch no longer remained and the specimen had a uniform width. This created some differences among the specimen in the final width. The specimen dimensions are shown in Table 2. Next, using the polisher shown in Figure 3, a series of finer grades

of diamond powder in a suspension fluid were used on a texmet pad to successively polish one edge of the specimen, starting with 45 micron, and ending up with 1 micron. This provided a smooth, clear edge which could later be examined under a microscope for micromechanical damage. Aluminum tabs, 2.54 cm in length, were then fixed to both ends of the specimen using a one to one mixture of an epon resin and curing agent. This was then cured for one hour at 160 degrees. These tabs give a higher coefficient of friction, as well as allow for a higher grip pressure in the testing machine without damaging the ceramic.

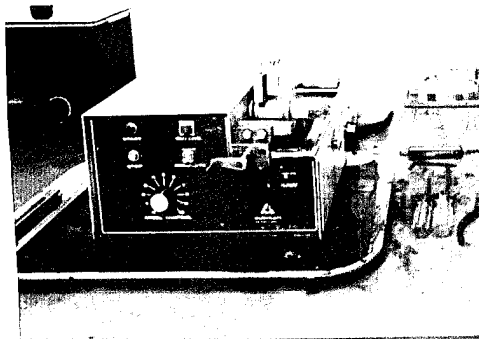


Figure 2. Low Speed Saw

Table 2. Specimen Dimensions

SPECIMEN	THICKNESS (mm)	WIDTH (mm)	CROSS-SECTIONAL AREA (mm ²)
1	3.2258	4.7498	15.3219
2	3.2385	4.5212	14.6419
3	3.2512	4.5720	14.8645
4	3.2385	4.5720	14.8064
5	3.1750	4.6736	14.8387
6	3.2385	3.3528	10.8580
7	3.2512	3.1750	10.3226
8	3.2385	6.8834	22.2919
9	3.2512	4.0640	13.2129
10	3.2258	4.9784	16.0593
11	3.2385	3.7084	12.0097
12	3.2258	5.7150	18.4354
13	3.2512	4.8895	15.8967
14	3.2512	4.9022	15.9380
15	3.2258	4.6690	15.0613
16	3.2512	3.8862	12.6348
17	3.2512	5.3594	17.4245
18	3.2512	4.5720	14.8645
19	3.2258	4.3688	14.0929
20	3.2385	3.8608	12.5032
21	3.2385	4.3688	14.1484

Note: All specimens were 152 mm long

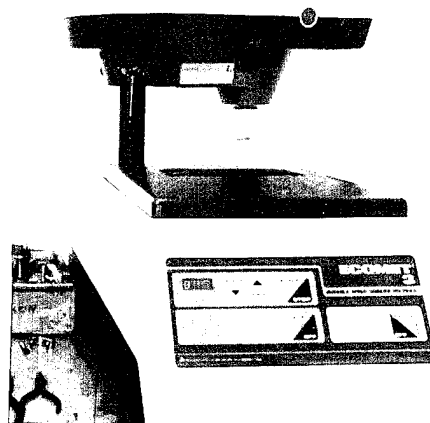


Figure 3. Specimen Polisher

Calibration

Grips were aligned using a calibrated specimen with four strain gages to ensure that no bending stress would be put on the specimen. The extensometer was calibrated using the calibration software in MATE and a vertical micrometer manufactured by MTS.

Test Procedure

The machine was warmed up for a period of five minutes prior to each test. The warm up involved cycling the grip at 1 Hz with a total stroke of 5 cm under displacement control. The specimen was placed into the grips, such that the grips covered the tabs, and checked to ensure it was perfectly vertical. If the specimen was not vertical, it would undergo bending stresses which would not be detected during the test and thus render the data useless, so this was a small but important step in the setup. The grips were adjusted for the length of the specimen and then the machine was switched to load control, then the lower grip was closed. The grip pressure was 1112 N for the initial tests, but midway through, the lower set of grips had to be changed due to a water leak, and the grip pressure had to be adjusted to 2224 N to compensate for the new grips. This higher pressure did not damage the specimen, nor did it alter the data in any way. The 1112 N was the minimum practical pressure and previous tests with this material have been successfully run with grip pressures of 4448 N.

With the specimen properly aligned in the grips, and the load was set to zero. The four thermal couples were then tied to the specimen using 36 gage alumel wire, two in the front and two in the back. They were placed where they would be centered between the

pair of lights for which they would be providing feedback, as shown in Figure 4. Once they were secure in their proper positions and flat against the specimen, a high temperature alumina oxide (903 Green) adhesive was applied to ensure they would not slip and to cover any exposed thermocouple wire.

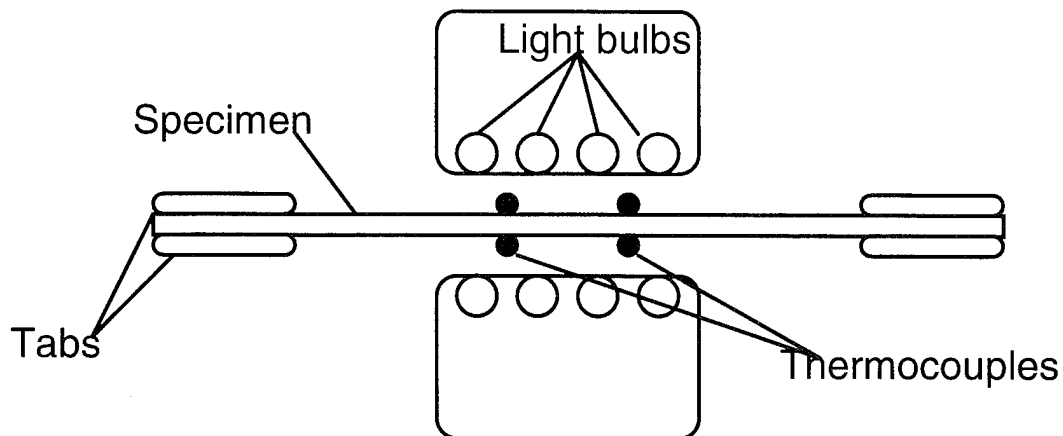


Figure 4. Specimen Layout

The ceramic rods of the extensometer were then placed on the unpolished edge of the specimen using moderate pressure, since too much could induce small bending stress and too little could cause the extensometer to slip. The rods were at either end of the 2.54 cm gage section in the center of the specimen, and carefully zeroed out. The two lamps, holding four bulbs each, were then placed into position, one in front and one in back, approximately 1 cm from the specimen and centered vertically.

The alumina adhesive was then cured for a period of two hours at 250°C, with the circulating air and water cooling systems on. This also provided an opportunity to ensure all eight bulbs were fully functional, and the thermocouples were properly controlling them.

MATE, a program written by Hartmann of the University of Dayton Research Institute, was run on a Zenith 486DX33. This program provides control to the lamps and the hydraulics to accurately create the correct loading and temperature profile. The inputs to the program were input interactively into the appropriate program. The program first brought the specimen to temperature, and then it was allowed to soak the heat for a period of ten minutes to stabilize the lamps and ensure uniform heating through the thickness of the specimen. This was performed on three specimens, first at room temperature, then at a temperature of 566°C and finally at 1093°C. The program recorded the stress and strain, and steadily increased the load until failure.

The remainder of the tests were performed under low cycle fatigue, with a specified maximum stress, load ratio of 0.1, and cycled between 566°C and 1093°C, or in the case of the isothermal tests, at a constant temperature of either 566°C or 1093°C. The period of all the fatigue was 180 seconds, chosen due to the limitations in the speed at which the specimen should be heated and cooled evenly at the high temperatures. All of these test were run until specimen failure or a number of cycles more than 2000 were reached. The program recorded number of cycles, zone temperature, stress and strain data.

IV. Results and Discussion

Test Summary

The purpose of this study was to investigate the thermo-mechanical fatigue behavior and damage mechanisms of Nicalon/MAS-5 cross ply ceramic matrix composite. The material was subjected to TMF cycles from 566°C to 1093°C at various maximum stress levels under tension-tension condition with a load ratio of 0.1 and a period of 180 seconds. Isothermal fatigue tests were also performed at 566°C, as well as at 1093°C at various maximum stress levels under tension-tension condition with a load ratio of 0.1 and a period of 180 seconds.

Stress and strain data obtained during the test were used to determine modulus degradation, strain histories, and hysteresis loops. Post-mortem fractography using optical and scanning electron microscopes was used to determine the damage mechanisms.

The data was taken based on a 2.54 cm gage length in the center of the specimen. Within the gage length, uniform thermal conditions were applied. This gage length was far enough from the grips to not be effected by the pressure of the grips, and ensure a uniform stress level. The quartz lamps were centered to ensure uniform heating of the gage length.

All isothermal fatigue tests at 566°C failed within the gage length, as well as most of the in-phase TMF tests, however, the isothermal fatigue tests at 1093°C and the out-of-phase TMF tests rarely failed within the gage length, and instead failed just outside of it.

This phenomenon was also recorded by Worthem, who ran similar TMF tests. Worthem used dogbone specimens, and found that "Consistently, the specimens experience final failure in the lower transition between the straight-sided gage sections and the gripped ends rather than in the straight sided gage section" [63-3: 18]. Table 3 lists each test and shows where fracture occurred on the specimen.

The rest of this chapter is divided into six sections dealing with the fatigue behavior and damage mechanisms of the tested material. The first section deals with the results of the monotonic tests, the second section deals with the fatigue life curves in terms of both cycles and time. The modulus degradation during fatigue is discussed in the third section. Strain data is discussed in the fourth section, and the strain hysteresis in the fifth. Finally, damage mechanisms are discussed in the sixth section.

Monotonic Tests

Figure 5 shows the stress strain response of the monotonic tensile tests at room temperature and at 566°C. The same elastic modulus, 120 GPa, was observed at room temperature and 566°C. Both also had the same proportional limit, as seen by the knee at 80 MPa. This is the point at which the matrix in the 90 degree plies fail, known as first ply failure. After first ply failure, the material exhibits a linear response up to failure, at 290 MPa for the 566°C, as opposed to 380 MPa at room temperature. The ultimate strain at 566°C is 0.8 percent, but extends to just over 1 percent at room temperature. This corresponds well with Steiner's data [15], as shown in Figure 6. Steiner reports an initial modulus of 117.99 GPa, 0.8 percent strain at failure, and ultimate strength of 270 MPa.

Table 3. Location of Fracture

Test type	Temperature	Maximum Stress	Fracture from Center	Within gage length
Isothermal				
	27°C			
		Monotonic	33.02 mm	no
	566°C			
		290 MPa	1.27 mm	yes
		160 MPa	7.62 mm	yes
		133 MPa	2.54 mm	yes
		110 MPa	unbroken	N/A
	1093°C			
		208 MPa	8.89 mm	yes
		125 MPa	12.32 mm	yes
		115 MPa	30.48 mm	no
		100 MPa	26.67 mm	no
TMF				
	In-Phase			
		145 MPa	15.24 mm	no
		135 MPa	30.48 mm	no
		120 MPa	3.81 mm	yes
		105 MPa	12.32 mm	yes
		100 MPa	25.4 mm	no
		85 MPa	2.54 mm	yes
	Out-of-Phase			
		145 MPa	7.62 mm	yes
		110 MPa	3.81 mm	yes
		91 MPa	22.86 mm	no
		83 MPa	33.02 mm	no
		60 MPa	Unbroken	N/A

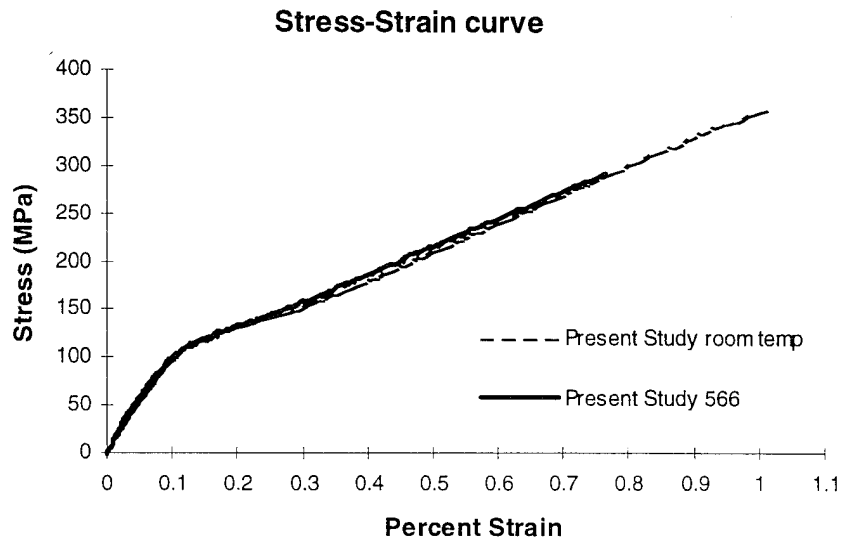


Figure 5. Monotonic Test: Room Temperature vs. 566°C

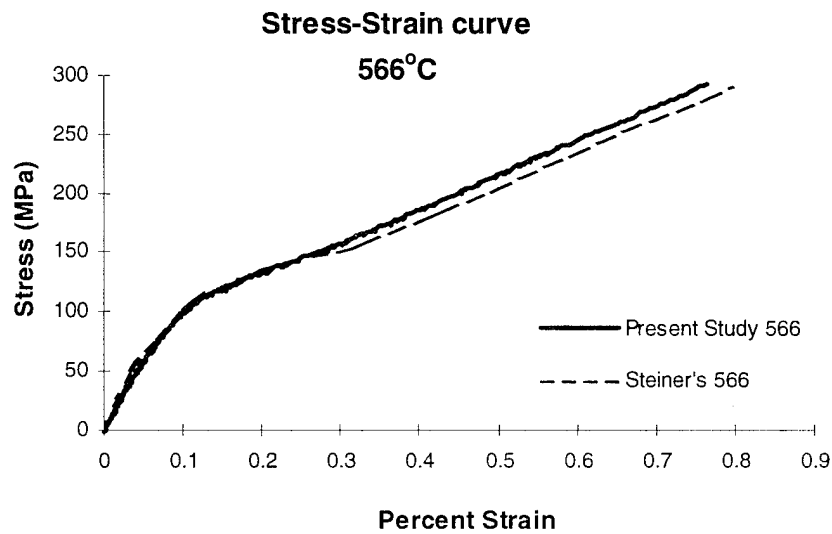


Figure 6. Monotonic Test: Present Study vs. Steiner's at 566°C

Figure 7 shows the stress strain response of the monotonic tensile test at 1093°C. The elastic modulus was observed to be 90 GPa at 1093°C. The proportional limit was

60 MPa, as seen by the knee in the figure. This is the point at which the matrix in the 90 degree plies fail, known as first ply failure. After first ply failure, the material exhibits a linear response up to failure, at 200 MPa for the 1093°C case. The ultimate strain at 1093°C is 0.8 percent. This corresponds well with Steiner's data [15], as shown in Figure 8. Steiner reports an initial modulus of 96.19 GPa, 0.82 percent strain at failure, and ultimate strength of 209.6 MPa.

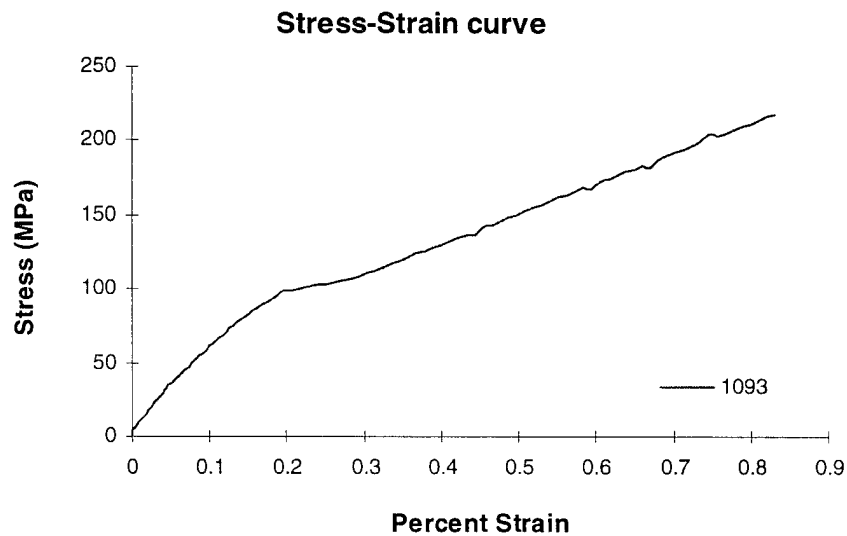


Figure 7. Monotonic Test: 1093°C

Figure 9 shows the stress strain response of the monotonic tensile test at 566°C compared with 1093°C. These curves are of similar shape. At 1093°C, the initial modulus was much lower, and the knee occurred earlier than at 566°C. Ultimate strength occurred at a much lower stress at the higher temperature. Strain at failure was slightly lower at 566°C.

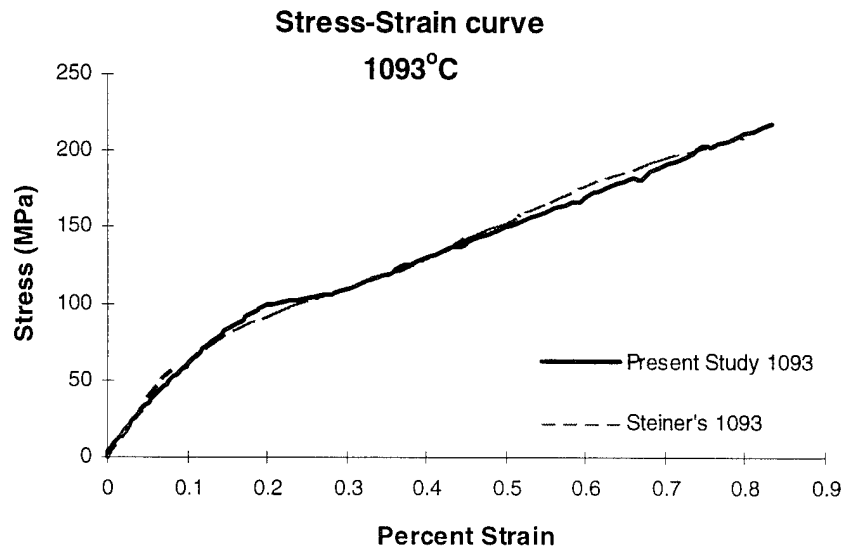


Figure 8. Monotonic Test: 1093°C Present Study vs. Steiner

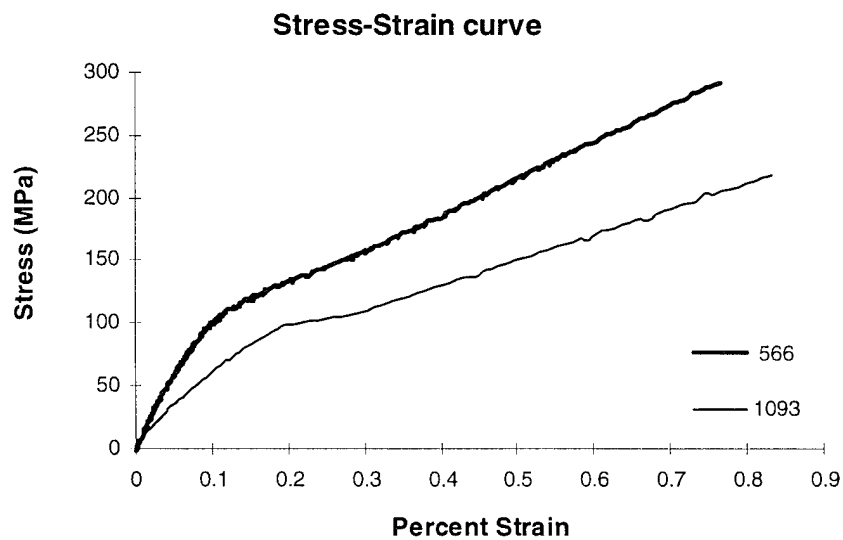


Figure 9. Monotonic Test: 566°C vs. 1093°C

Table 4 shows a comparison of material properties at 566°C and 1093°C, the maximum and minimum test temperatures, as well as at room temperature. There is also a comparison with the properties found by Steiner [15], who used the same material, but a different batch.

Table 4. Comparison of Material Properties

MATERIAL PROPERTY	TEMPERATURE	PRESENT STUDY	STEINER [15]
ULTIMATE STRENGTH	ROOM TEMP	380 MPa	
	566°C	290 MPa	292.41 MPa
	1093°C	200 MPa	209.26 MPa
STRAIN AT FAILURE	ROOM TEMP	1.05 %	
	566°C	0.8 %	0.80 %
	1093°C	0.82%	0.82 %
INITIAL MODULUS	ROOM TEMP	120 GPa	
	566°C	120 GPa	117.99 GPa
	1093°C	90 GPa	96.19 GPa
PROPORTIONAL LIMIT	ROOM TEMP	80 MPa	
	566°C	80 MPa	50 MPa
	1093°C	60 MPa	34 MPa

Fatigue Life

Fatigue Test Summary

The fatigue life curves were developed from the total number of cycles to failure of each specimen and the maximum stress applied during those tests. The in-phase TMF tests were run at a maximum stress of 145 MPa, 135 MPa, 120 MPa, 105 MPa, 100 MPa, and 85 MPa. The out-of-phase TMF tests were run at 145 MPa, 110 MPa, 91 MPa, 83 MPa, and 60 MPa. The test conducted at 60 MPa was terminated prior to failure because it was felt that cycle run-out (i.e., more than 2000 cycles) had occurred. The 566°C isothermal fatigue tests were run at 290 MPa, 160 MPa, 133 MPa and 110 MPa. The test conducted at 110 MPa was terminated prior to failure because it was believed that cycle run-out (i.e., more than 2000 cycles) had occurred. The 1093°C isothermal fatigue tests were run at 210 MPa, 135 MPa, 115 MPa and 100 MPa. All the fatigue data are summarized in Table 5.

The fatigue life curves all had the same shape, a steeply sloped early portion, and a shallow sloped latter portion. Figure 10 shows a typical fatigue life diagram. It shows the typical relationship between stress and fatigue life. The upper band is a high stress region where the failure results from fiber breakage, known as fiber controlled failure. The middle, steeply sloped region is characterized by a combination of failure controlled by the matrix as well as fiber failure, fiber debonding and fiber sliding. The next, shallow sloped region, is characterized by matrix controlled failure. The lower region is below a stress level where matrix damage does not occur and the material has an infinite fatigue

Table 5. Fatigue Test Summary

Test Condition	Maximum Stress (MPa)	Cycles to Failure	Time to Failure (sec)
Isothermal 566°C	290	1/2	90
	160	12	2160
	133	25	4500
	110*	>4000	>720000
Isothermal 1093°C	208	1/2	90
	125	10	1800
	115	102	18360
	100	304	54720
In-Phase TMF	145	1.5	270
	135	2.5	450
	120	398	71640
	105	16	2880
	100	360	64800
	85	590	106200
Out-of-Phase TMF	145	1.5	270
	110	5	900
	91	20	3600
	83	59	10620
	60*	>2465	>443700

* did not fail

life. This is known as the fatigue limit. There are methods of determining what type of damage is occurring, which include the strain, and rate of change in strain per cycle, the secant modulus, the stress-strain hysteresis during fatigue, and by post-mortem microscopy. Each of these will be investigated in subsequent sections of this chapter, as well as a discussion of how they can be used to characterize the damage and failure mechanisms.

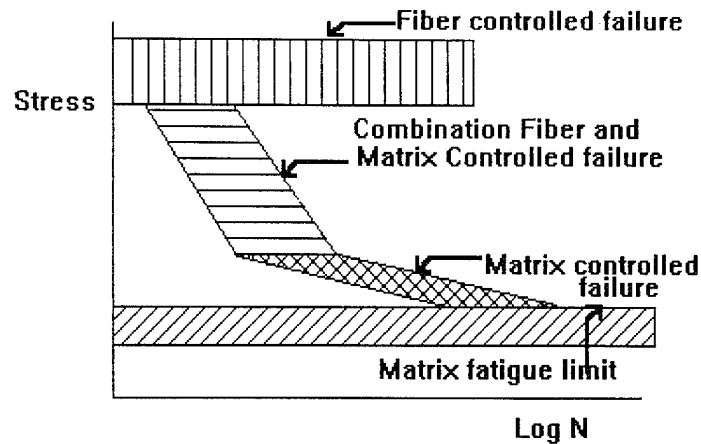


Figure 10. Damage Mechanisms and Fatigue Life Diagram

In-Phase TMF

Figure 11 shows the maximum stress to number of cycles to failure (S-N) relationship of the in-phase TMF condition. The data shows a bit of scatter, this is very common in composites, especially in brittle ceramics. The data shows that the fatigue life is inversely proportional to maximum stress. The curve is relatively flat over the entire life and the slope becomes almost horizontal after 10 cycles. The first portion of the curve, prior to 10 cycles, is the region where fiber controlled failure is predominant. Reducing the stress from 145 MPa to 125 MPa will reduce the number of fibers that fail in each cycle, thus it would take slightly longer to fail all of the fibers at 125 MPa than it would at 145 MPa. The second portion (i.e., beyond 10 cycles) is more of a matrix controlled failure. In this region, the fibers do not fail until the fibers become so degraded that they begin to fail or the matrix cracks finally propagate through them.

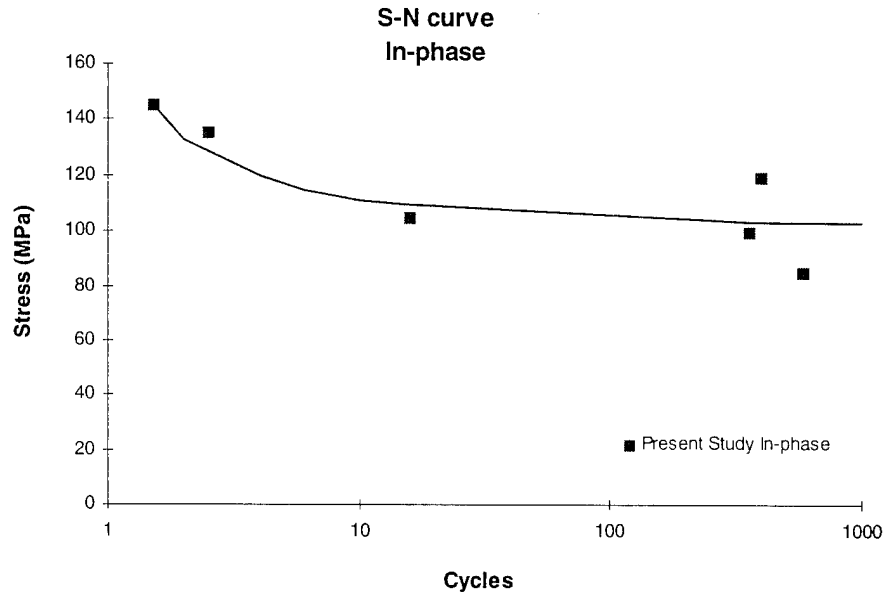


Figure 11. In-Phase TMF: S-N Curve

Present Study vs. Worthem

Worthem studied the thermo-mechanical fatigue behavior of Nicalon/MAS-5 [17]. His conditions were similar, except the cycle period was 300 seconds, and the maximum and minimum temperatures were 1100°C and 600°C, respectively. As expected, the present in-phase data matched well with Worthem's data as shown in Figure 12.

In order to determine the time dependency of the material, the S-N data was converted to maximum cyclic stress vs. time of failure (S-T). This is done by multiplying the number of seconds per cycle by the number of cycles until failure. The S-T curves from the present study and Worthem's study [17], Figure 13, match with each other. This indicates that the fatigue of the tested CMC is a time-dependent phenomenon under

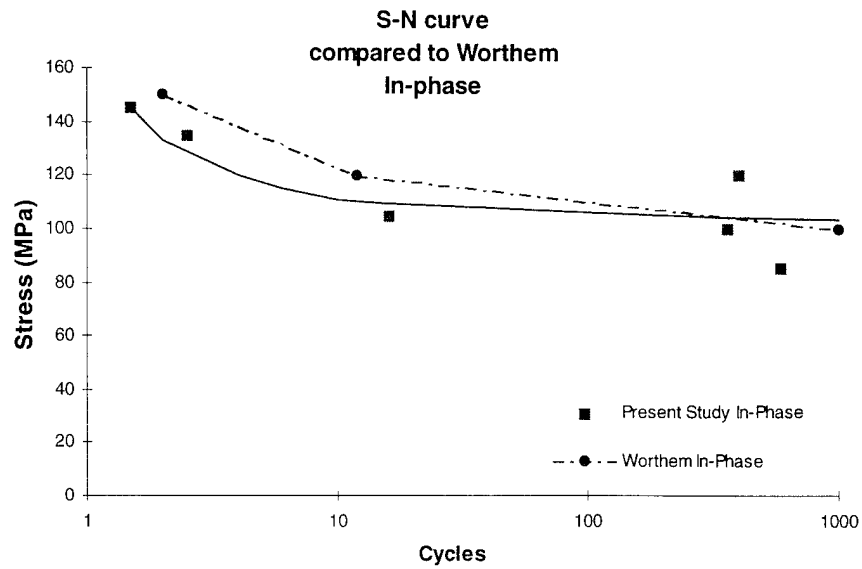


Figure 12. In-Phase TMF S-N Curve: Present Study vs. Worthem [17]

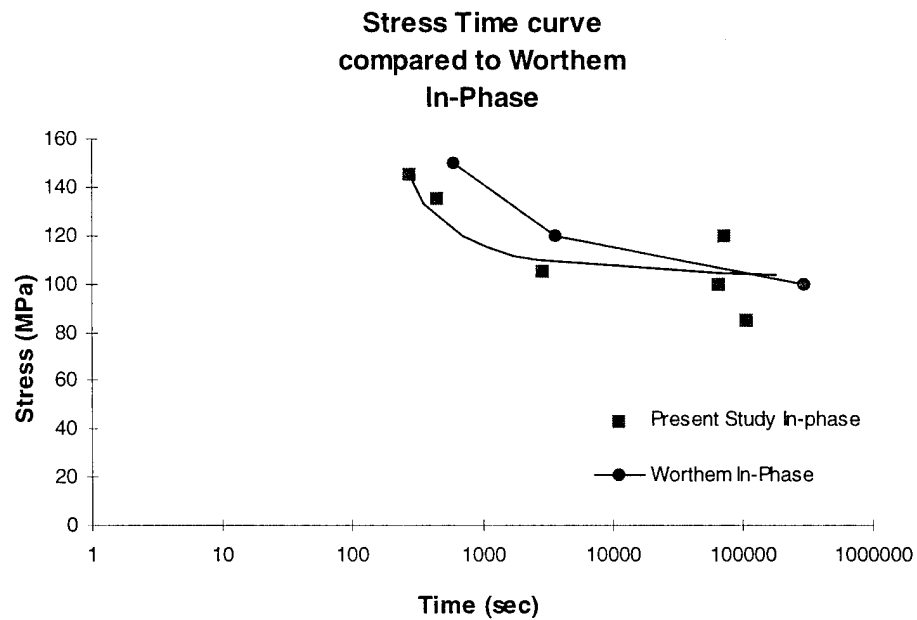


Figure 13. In-Phase TMF S-T Curve: Present Study vs. Worthem [17]

in-phase TMF loading. Worthem's tests were conducted at a lower frequency, 300 second cycles while this study used an 180 second cycle.

Out-of-Phase TMF

Figure 14 shows the S-N relation for the out-of-phase TMF condition. The fatigue life is inversely proportional to the maximum stress level. The curve has two distinct regions. The first is portion with the low number of cycles, high maximum stress level. This portion has a high negative slope, where a large reduction in maximum stress will result in a small increase in the fatigue life. This depicts the stress levels that result in fiber controlled failure. The second region has a small negative slope, and represents more of a matrix controlled failure. This portion of the curve is very flat, where a small reduction in maximum stress will result in a large increase in fatigue life, until the proportional limit is reached, below which the fatigue life is infinite.

Fatigue life of the out-of-phase TMF condition was considerably shorter than those of the in-phase TMF condition as well as of both isothermal fatigue conditions which will be shown later. There are two points to note regarding this phenomenon. First, the life is shortened simply due to the exposure to the temperature, which alters the fiber matrix interface, reducing the composite's toughness and shortening its fatigue life. If this were the only phenomenon occurring, it would be expected that the in-phase and out-of-phase TMF tests would have similar lives. Also the thermo-mechanical tests would have shorter lives than the isothermal tests at 566°C and longer than the isothermal tests at 1093°C. Therefore something else must be happening. This is related to the

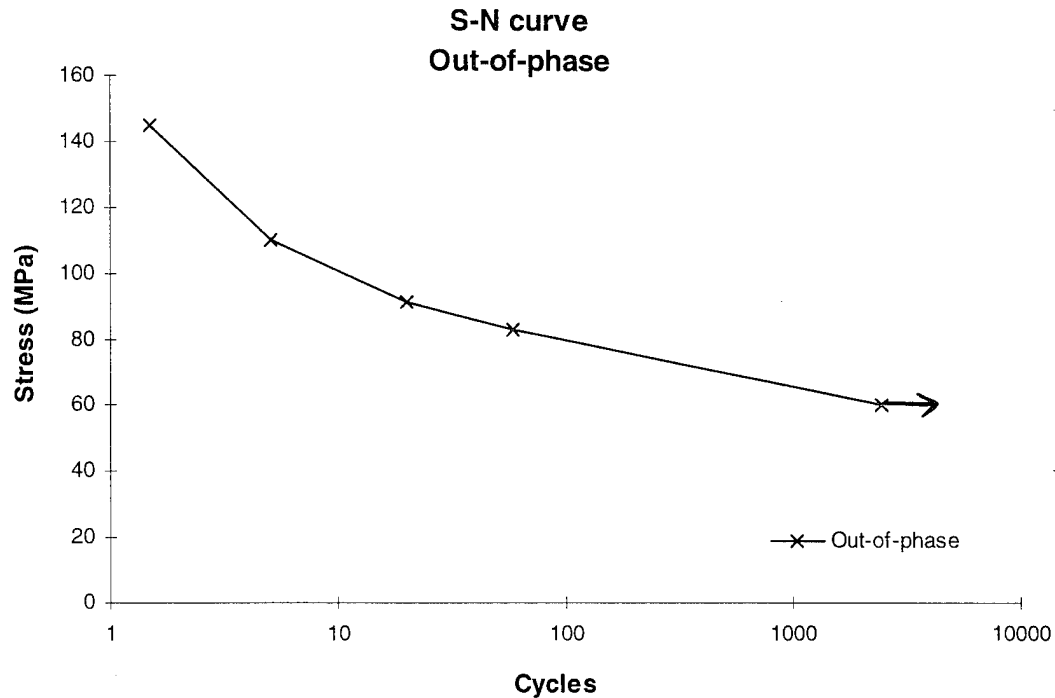


Figure 14. Out-of-Phase TMF S-N Curve

processing of the composite. When the Nicalon fibers are embedded in the MAS matrix, it is done at approximately 1400°C. At this temperature, the fibers and the matrix are stress free, and there are no internal stresses. As the composite cools during processing, the difference in the coefficient of thermal expansion (CTE) causes the fibers to shrink longitudinally more than the matrix, but due to the bonding between the matrix and fibers, they are restrained to deform by the same amount. This causes internal stresses, also called residual stresses, and these are present in almost all composites. These residual stresses are in the form of hoop and axial stresses. It is logical that when the composite is then reheated, the internal stresses relax until the temperature reaches 1400°C at which the composite is stress free. Therefore the internal stresses are much

less at 1093°C than they are at 566°C. With in-phase TMF testing, the maximum stress occurs at the maximum temperature, which, as was just explained is the point of lowest residual stress. In out-of-phase TMF tests, the maximum stress is applied at the lowest temperature, and therefore at the point of highest residual stress. These are additive, and thus the out-of-phase TMF tests incur the maximum net stress. The stresses in the fibers for out-of-phase TMF are considerably higher than the applied stress. Appendix B includes these residual stress calculations. The maximum total stress in the out-of-phase TMF is the same as the maximum total stress for the isothermal fatigue at 566°C, and in fact, the isothermal at 566°C has a higher average stress during each cycle. This higher average stress is not as damaging as the extreme temperatures the out-of-phase TMF encounters, and thus the out-of-phase TMF condition is the most damaging to the composite.

Present Study vs. Worthem

Figure 15 shows the out-of-phase TMF cycles to failure compared with Worthem's corresponding data [17]. Worthem ran similar tests, except the temperature peaks were 600°C and 1100°C, and the period was 300 seconds. As with the in-phase TMF data, the out-of-phase TMF data of the present study compares well with Worthem's data. Both S-N curves have similar shapes.

When compared on the basis of time to failure, Figure 16 shows both sets of data are almost identical, indicating that exposure time is the predominant factor in deciding the fatigue life, not the cycles.

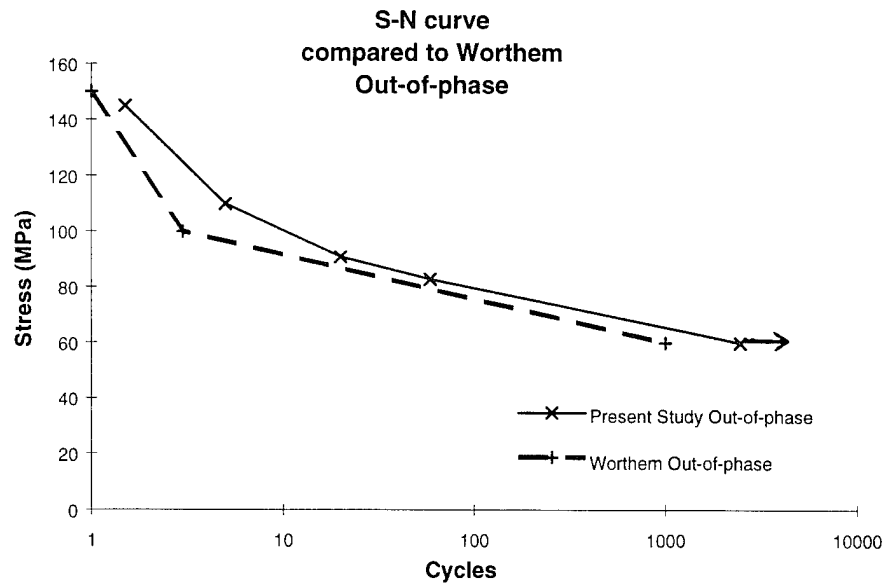


Figure 15. Out-of-Phase TMF S-N: Present Study vs. Worthem [17]

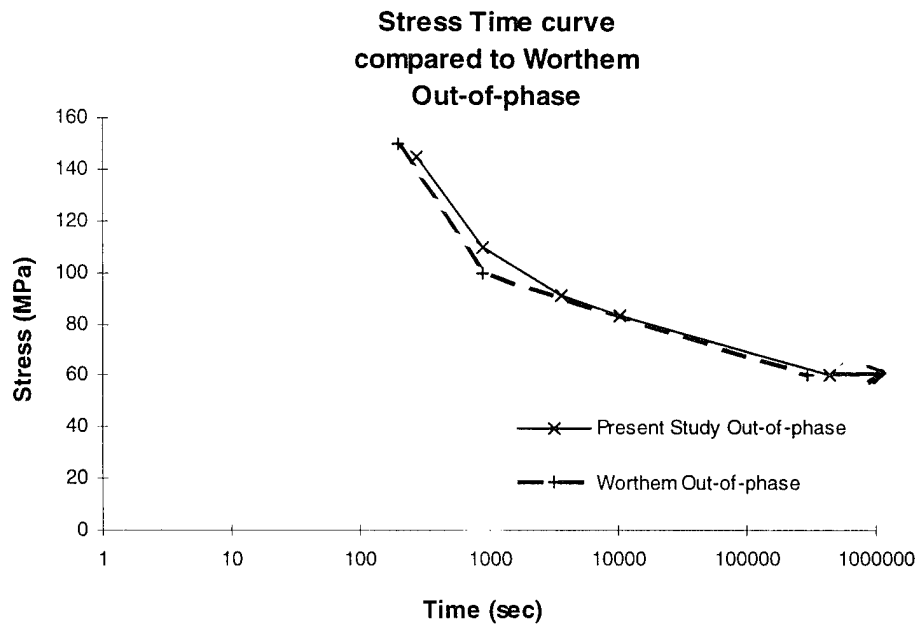


Figure 16. Out-of-Phase TMF S-T: Present Study vs. Worthem [17]

In-Phase TMF vs. Out-of-Phase TMF

The in-phase and out-of-phase TMF S-T relations are very different. Figure 17 shows these two curves together. Both curves begin almost identically, indicating a region of fiber controlled failure. The in-phase TMF starts with a shallower slope, showing a faster transition toward a matrix controlled failure. The out-of-phase TMF does not transit to matrix controlled failure until much after the in-phase TMF does. This supports the previous discussion on the residual stresses causing the fiber stress to increase in out-of-phase TMF, and likewise, decrease with in-phase TMF.

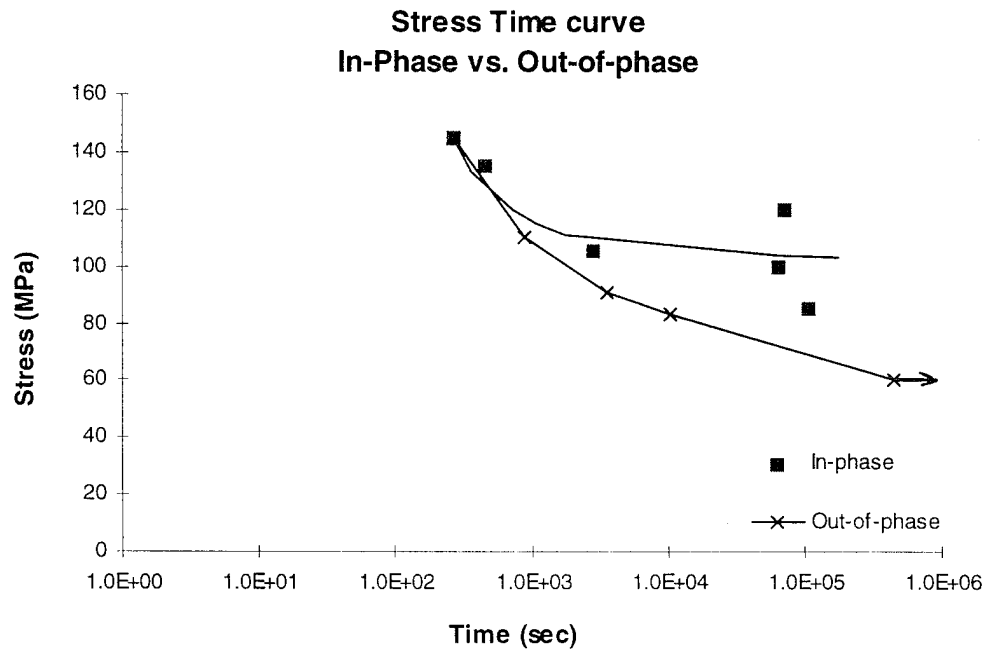


Figure 17. In-Phase vs. Out-of-Phase TMF S-T

In order to determine if the fiber stresses are the controlling factor during TMF fatigue, the maximum fiber stresses were calculated and then plotted against fatigue cycle, as shown in Figure 18. The fiber stress range during the cycle was also plotted against fatigue cycle, as shown in Figure 19.

The same calculations were done for the matrix stress. The plot of maximum matrix stress vs. fatigue life is Figure 20. Figure 21 shows the plot of matrix stress range vs. fatigue cycle for both in-phase and out-of-phase TMF.

Figure 18 to Figure 21 show that neither the fiber stress (maximum or range) nor the matrix stress (maximum or range) agree with each other for the both TMF conditions (i.e., in-phase vs. out-of-phase). Therefore both fiber and matrix stresses influences the fatigue lives of in-phase and out-of-phase TMF conditions, and hence their S-N or S-T relationships are different as shown in Figure 17.

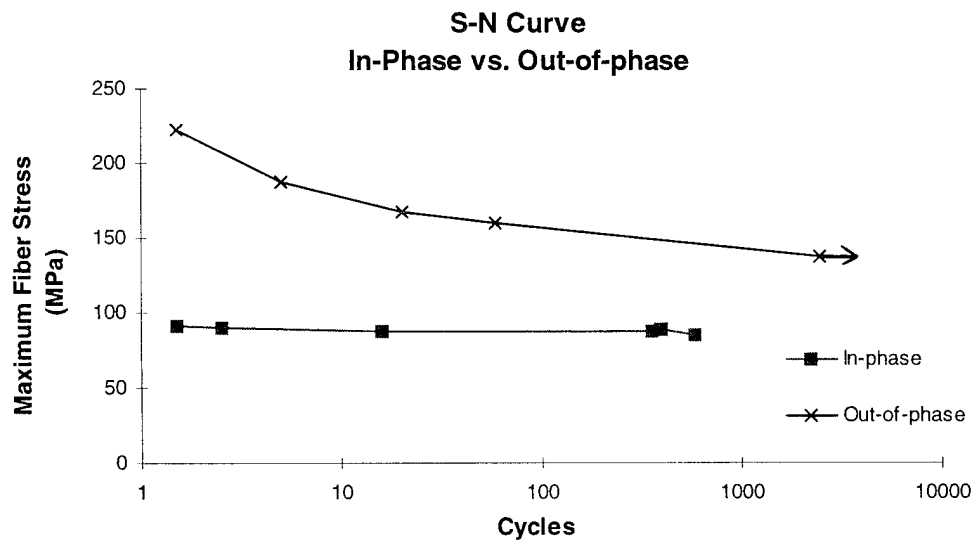


Figure 18. Maximum Fiber Stress vs. Cycles

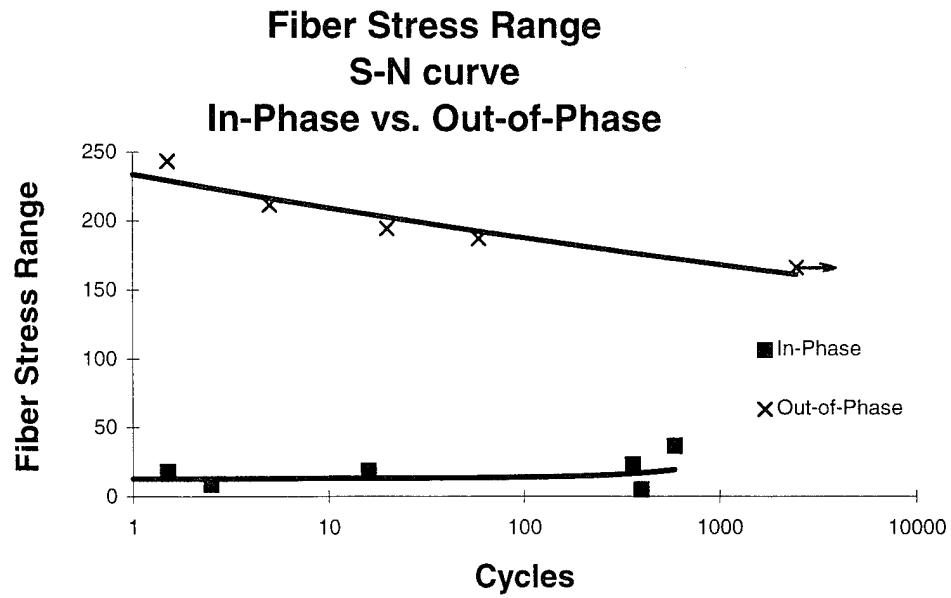


Figure 19. Fiber Stress Range vs. Cycles

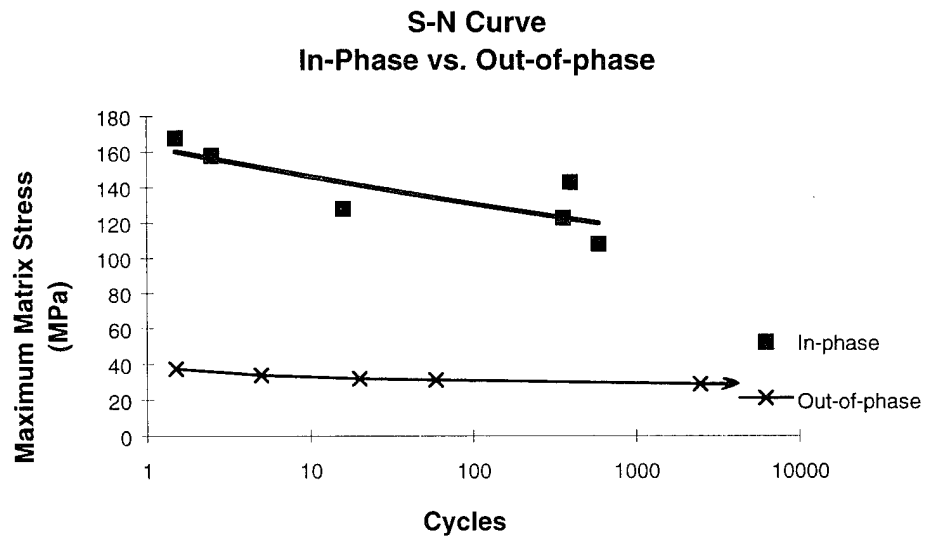


Figure 20. Maximum Matrix Stress vs. Cycles

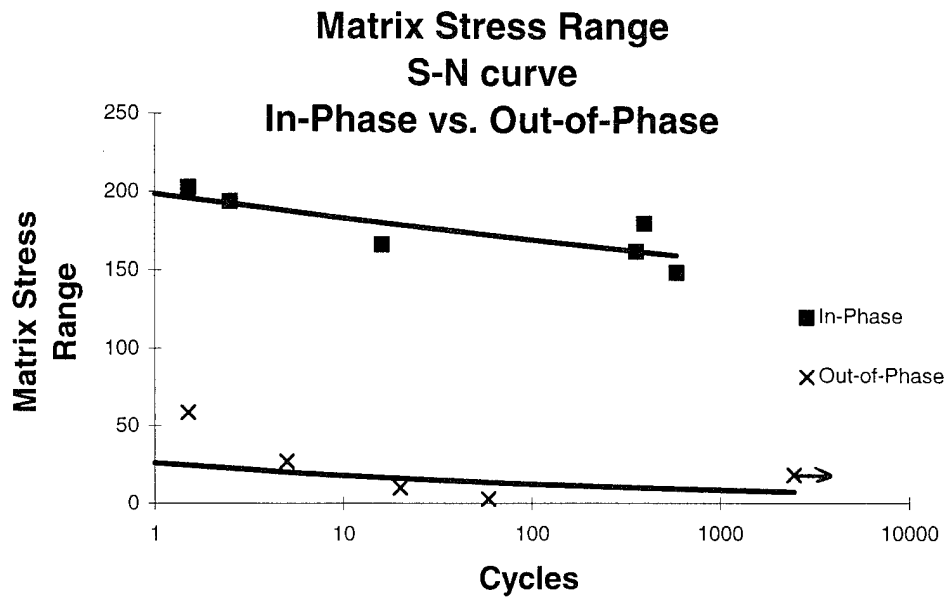


Figure 21. Matrix Stress Range vs. Cycles

Isothermal Fatigue

Present isothermal fatigue specimens were tested with the same frequency as the thermo-mechanical fatigue test. In previous studies, the same composite system have been investigated at higher frequencies of 1 Hz and 10 Hz [3,15]. They, thus, provided a comparison with both Steiner's [15] and Grant's [3] work, as well as a baseline data for comparison to the thermo-mechanical fatigue. The isothermal fatigue specimens were tested under the TMF low cycle fatigue program in MATE, with the maximum and minimum temperatures set to the same temperature, either 566°C or 1093°C. This served to validate the TMF low cycle fatigue data, by showing it matched with Grant's, who ran the high cycle fatigue program in MATE.

566°C Isothermal

Figure 22 shows the fatigue life of the material under isothermal condition at a temperature of 566°C. It can be seen that the fatigue strength decreases with cycles. The fatigue life is inversely proportional to the maximum cyclic stress applied to the specimen. At a maximum stress of 110 MPa or below, the material has reached the fatigue limit and the specimen can withstand an infinite number of cycles.

1093°C Isothermal

Figure 23 shows the S-N relationship under isothermal fatigue condition at 1093°C. The trend at 1093°C, seen in this figure, is similar to that of the data at 566°C. The fatigue life is inversely proportional to the maximum stress level. The transition from fiber controlled failure to matrix controlled failure seems to occur at approximately 12 cycles and 120 MPa.

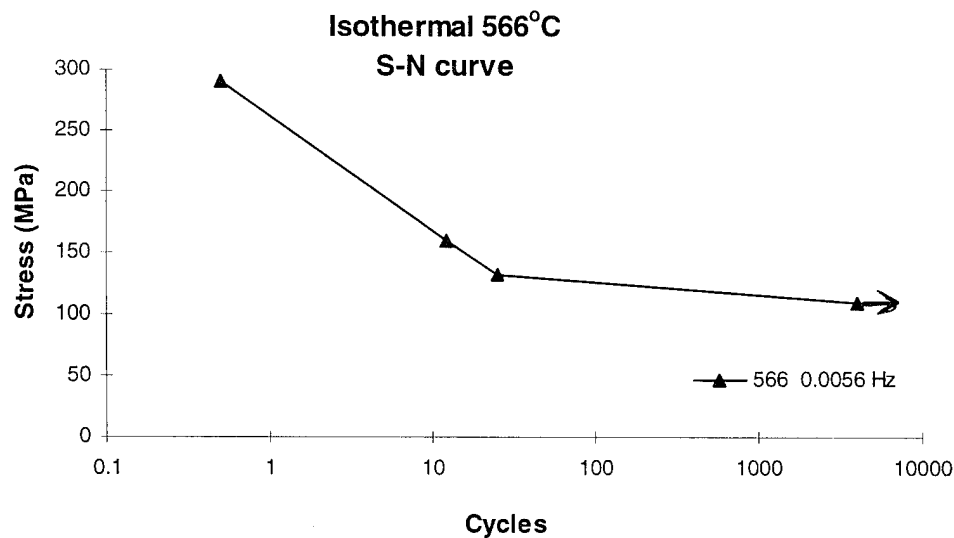


Figure 22. S-N Curve 566°C

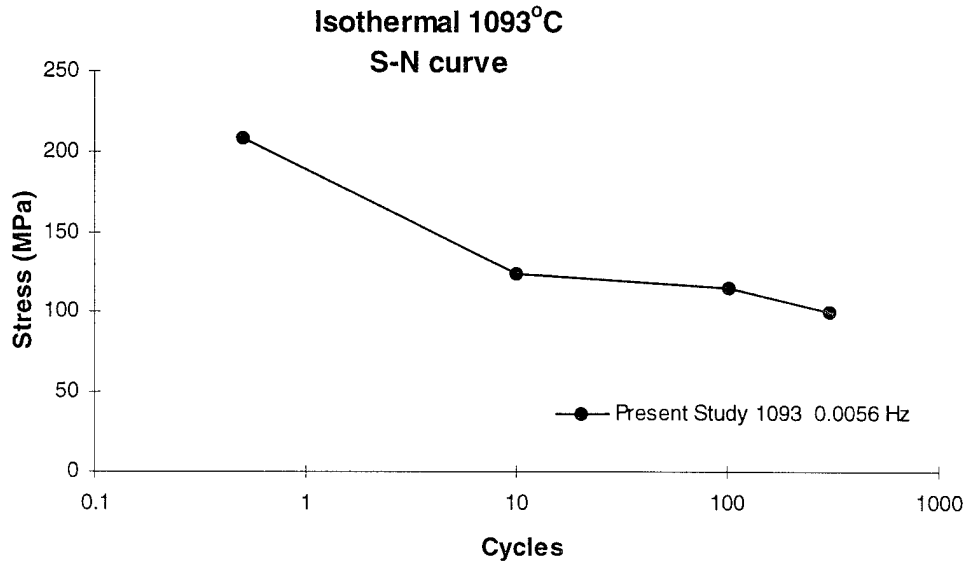


Figure 23. S-N Curve 1093°C

566°C vs. 1093°C

Figure 24 shows a comparison between the isothermal fatigue tests at 566°C and 1093°C. The fatigue strength and fatigue life are reduced with increased temperature. The increased temperature reduces the stress required to fail the fibers, as reflected in the monotonic stress-strain relations. Both curves changeover to the flatter portion at approximately the same stress level. The 1093°C data changes to matrix controlled failure in a fewer number of cycles than the 566°C data.

Figure 25 shows the normalized fatigue life curves for the isothermal fatigue at 566°C and 1093°C. The fatigue strength was normalized with respect to the ultimate stress obtained during the monotonic tensile tests at their respective temperatures. This figure shows that the material performs better at the higher temperature relative to

monotonic ultimate tensile strength. This is due to the reduction in residual stresses at the higher temperature.

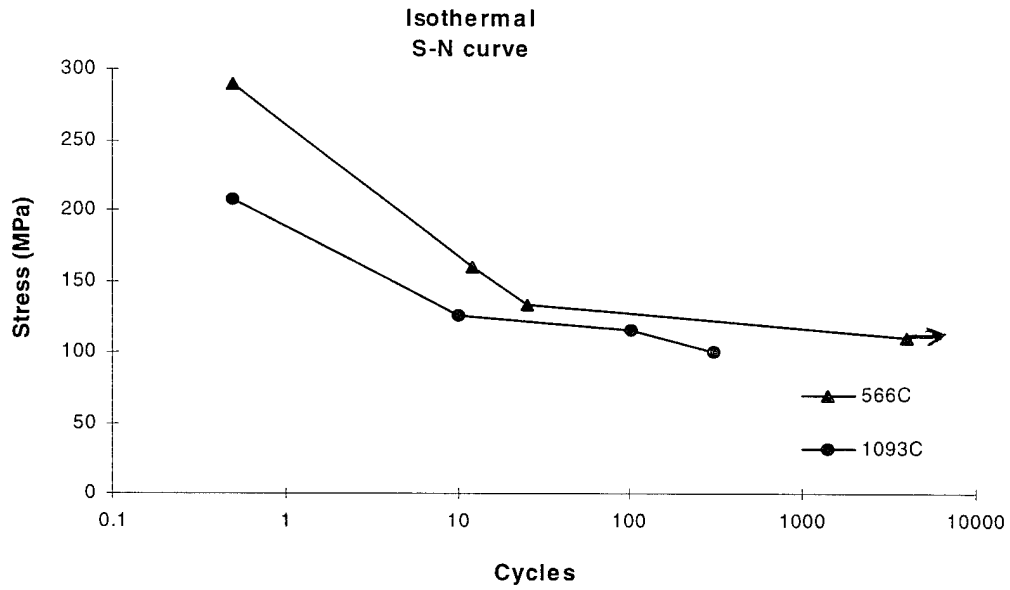


Figure 24. S-N Curve: 566°C vs. 1093°C

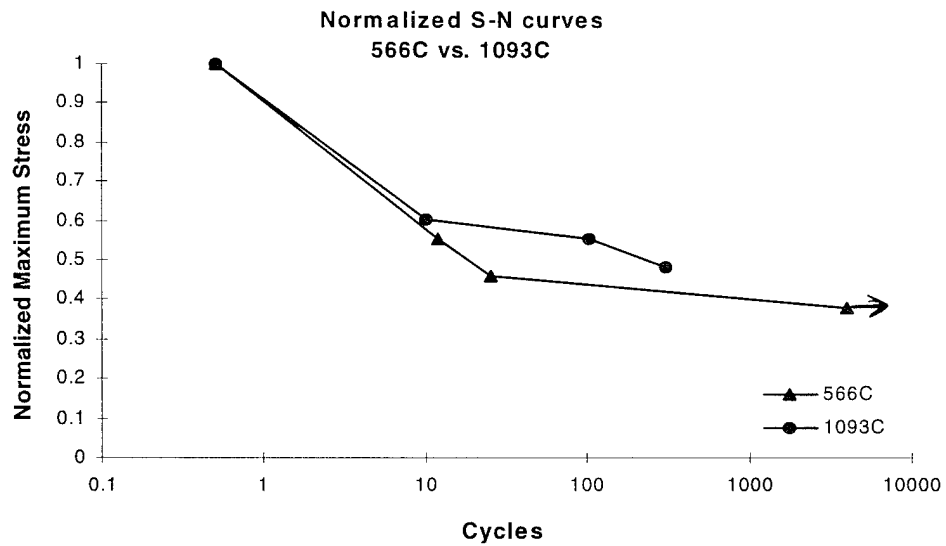


Figure 25. Normalized S-N Curve: 566°C vs. 1093°C

Present Study vs. Steiner [15]

Figure 26 and Figure 27 show the isothermal fatigue S-N data at 566°C and 1093°C of the present study, respectively, compared to Steiner's [15] data at the same temperature. The low frequency fatigue caused failure in noticeably fewer cycles than the high frequency fatigue. This shows that the material has a greater cyclic fatigue life expectancy at higher frequencies. These curves have the same shape, indicating the transition in the different damage mechanisms is a function of stress, not cycles.

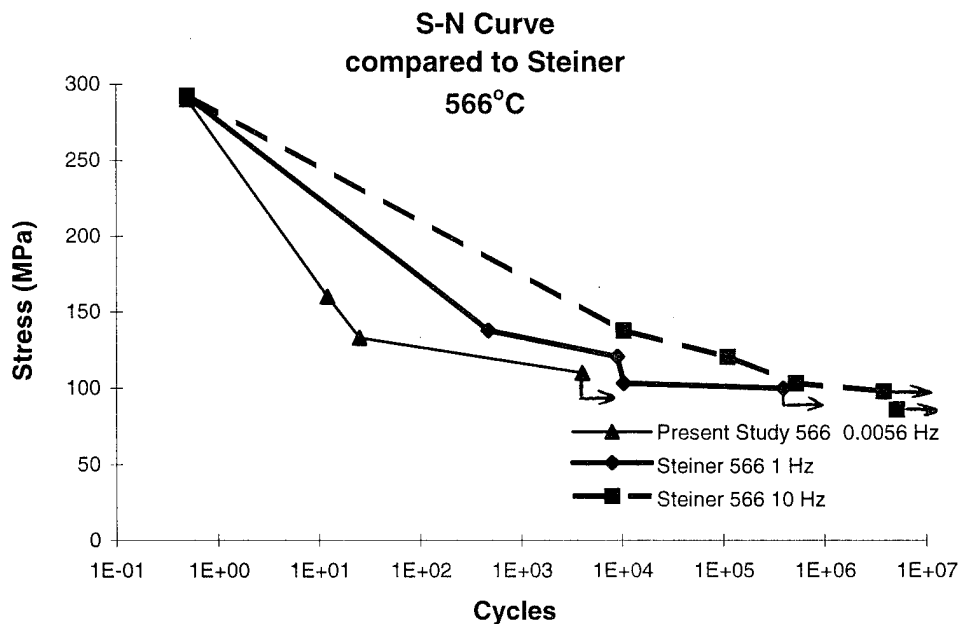


Figure 26. S-N Curve: Present Study vs. Steiner 566°C [15]

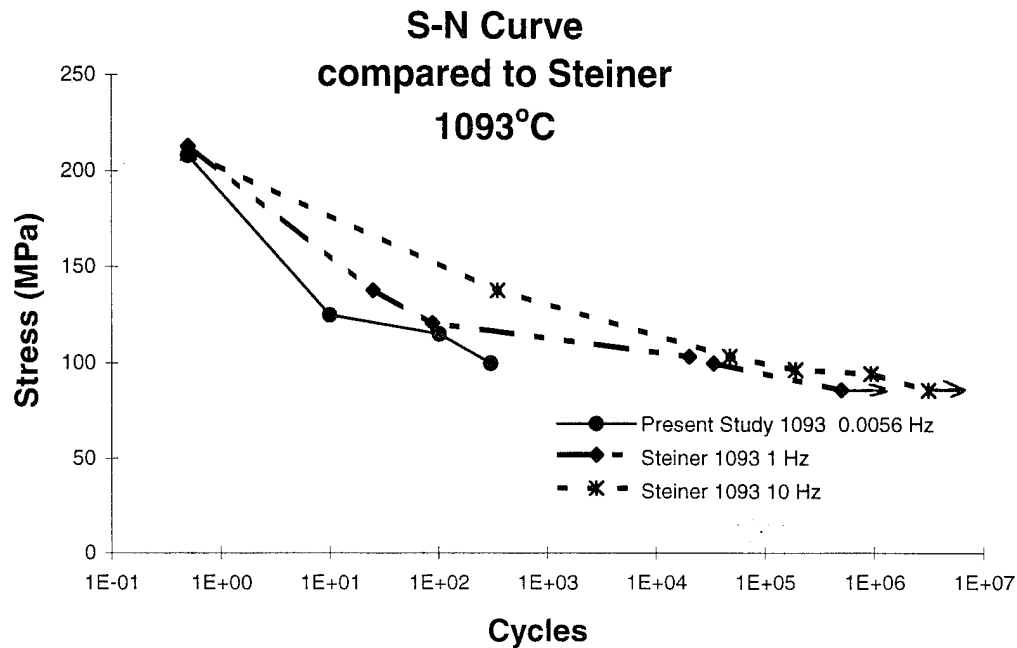


Figure 27. S-N Curve: Present Study vs. Steiner 1093°C [15]

Figure 28 and Figure 29 show the maximum cyclic stress plotted against the time to failure for 566°C and 1093°C, respectively. These figures show the results of the present study compared to Steiner's results [15]. They show that when looking on the basis of time, the results are nearly identical for both temperatures. The only difference comes in the early region of the curve, where fiber failure is dominant. This difference comes from the different frequencies at which the experiments were run. Failure at one half of one cycle occurred in ninety seconds for the present study, whereas the same failure would occur in one half of one second, or one twentieth of one second in Steiner's study. These results reaffirm Steiner's conclusion that the fatigue life is based on the

time to which the specimen is exposed to the high temperature environment, not the number of cycles it experienced.

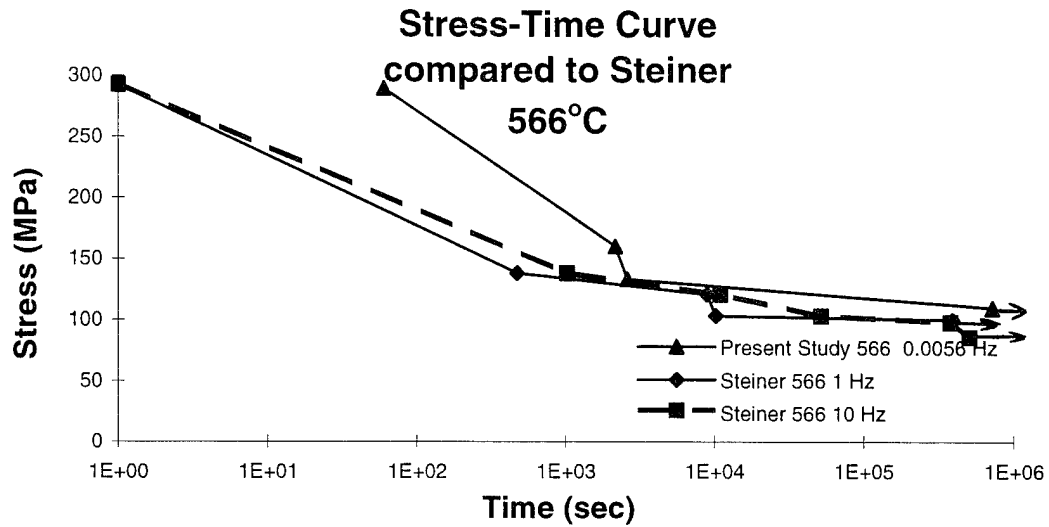


Figure 28. S-T Curve: Present Study vs. Steiner 566°C [15]

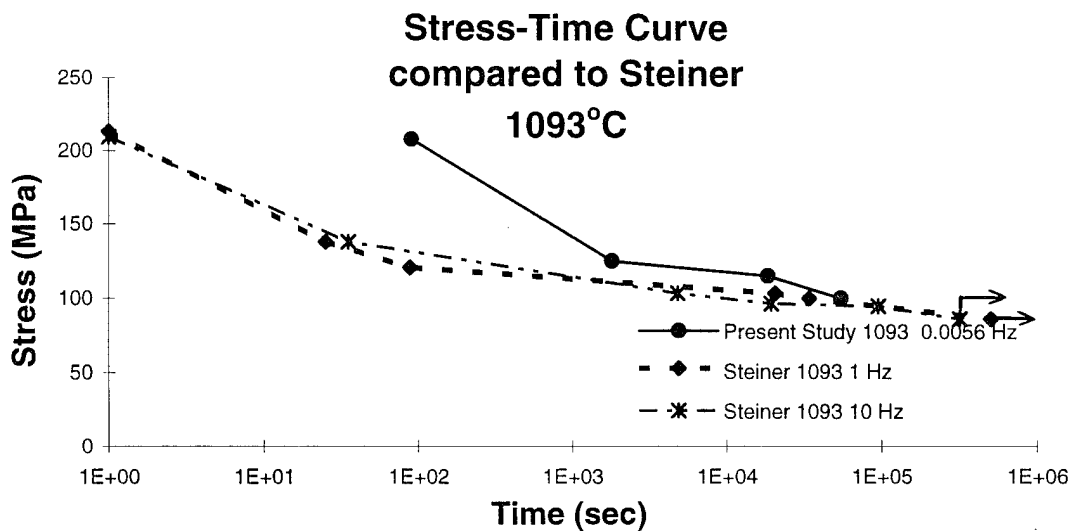


Figure 29. S-T Curve: Present Study vs. Steiner 1093°C [15]

TMF vs. Isothermal Fatigue

The comparison between TMF fatigue life data and existing isothermal fatigue data is important. It is thought that a comparison could be made between in-phase TMF and isothermal fatigue at 1093°C, since they both experience peak stresses at the same temperature. The same is true for a comparison between the out-of-phase TMF and the isothermal fatigue at 566°C. An overall comparison needs to be made as well. The results of these comparisons can be used to distinguish the effects of time, temperature and fatigue loading condition.

Figure 30 shows the S-N curve for the in-phase TMF tests compared with the isothermal fatigue test run at 1093°C. At stress levels above 120 MPa, both conditions generate fatigue lives within 10 cycles of each other. The TMF was more damaging at these stress levels. At low stress levels, below 120 MPa, the fatigue lives are equivalent.

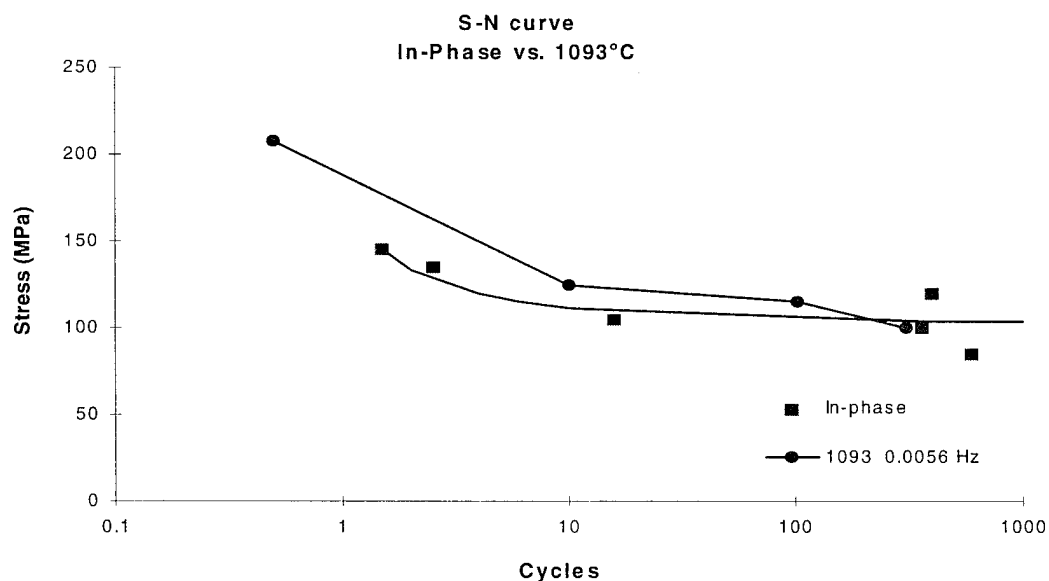


Figure 30. In-Phase TMF vs. 1093°C Isothermal

A comparison between the fatigue lives of the out-of-phase TMF with the isothermal fatigue at 566°C is shown in Figure 31. The transition from a combination of fiber and matrix failure to matrix controlled failure occurs at a lower stress for the out-of-phase TMF than it does for the isothermal fatigue. This shows there is an effect of both stress level and loading conditions on the failure mechanisms. At all stress levels the fatigue life of the isothermal fatigue is consistently longer than the fatigue life of the out-of-phase TMF.

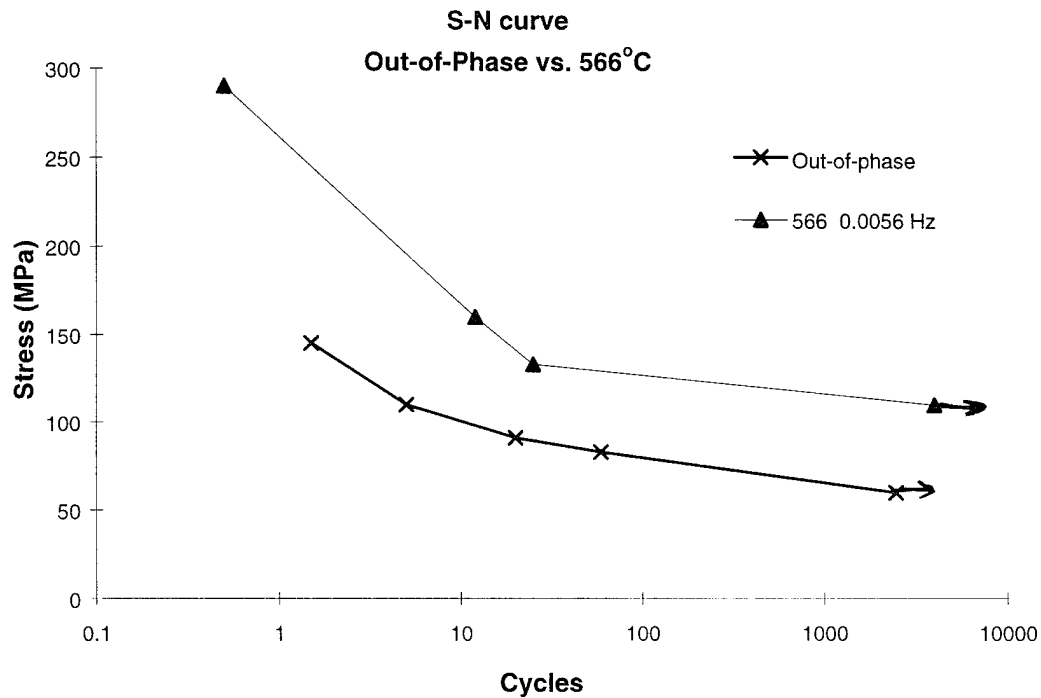


Figure 31. Out-of-Phase TMF vs. 566°C Isothermal

Figure 32 shows the S-N curves for all cases from this study, as well as Steiner's isothermal fatigue data [15]. This shows the material has the greatest cyclic fatigue life expectancy at 10 Hertz and 566°C. The material has the lowest life expectancy, in terms of cycles, in the out-of-phase TMF condition.

When compared on the basis of time, all of the S-N curves fall within a reasonable scatter of each other, with the exception of the out-of-phase TMF condition. At stress levels below 150 MPa all of the curves except for the out-of-phase TMF seemed to be converging. This indicates that time is the dominant factor in fatigue life, regardless of the temperature, frequency or loading condition except for out-of-phase TMF. The in-phase TMF falls between the isothermal fatigue at 566°C and the isothermal fatigue at 1093°C, although it is much closer to the curve at 1093°C. This was expected, since the peak residual stresses are the same for both the in-phase TMF and the 1093°C, but the in-phase TMF spends less time in the elevated temperature environment.

Summary

In summary, fatigue life is primarily dependent on fatigue time. This holds for in-phase and out-of-phase TMF as well as isothermal fatigue at both 566°C and 1093°C. The environment has a large impact on the fatigue life. The curves indicate two different failure mechanisms at work, with the transition from one to the other being a function of stress level and environment. Higher temperatures reduce the fatigue life, and out-of-phase TMF is more damaging than in-phase TMF. In-phase TMF is more damaging than isothermal fatigue at high stress levels, but both are essentially the same at lower stress

levels. Out-of-phase TMF is the most damaging condition, consistently exhibiting one-twentieth the cyclic fatigue life of isothermal fatigue at 1093°C.

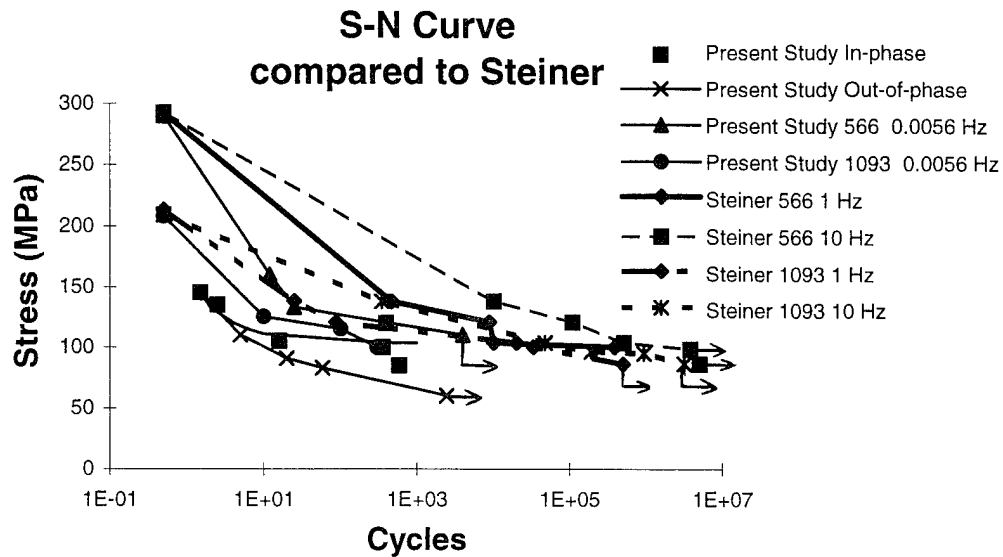


Figure 32. TMF vs. Isothermal S-N Curve

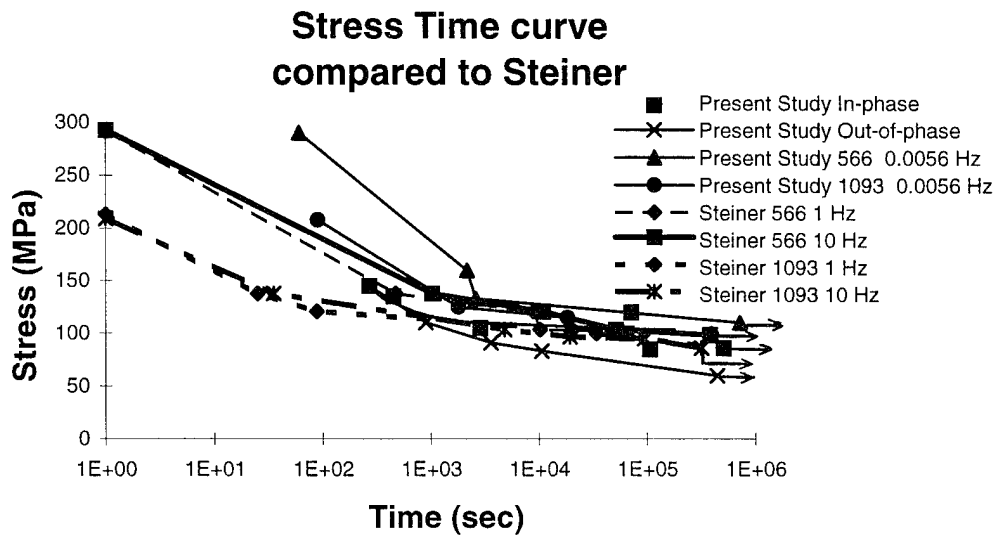


Figure 33. TMF vs. Isothermal S-T Curve

Strain Data

Much can be learned from the variations of the strain levels seen by the specimen during cycling. This strain data indicates the damage accumulation occurring within the specimen during cycling. Strains were measured directly from displacement of the extensometer, and converted to engineering strain by normalizing it by the gage length of 2.54 centimeters. This was automatically performed by MATE. The total strain was then converted to mechanical strain by subtracting the thermal strain. The thermal strain was calculated by multiplying the change in temperature by the laminate's coefficient of thermal expansion that was found by taking the average of the experimentally measured coefficients of thermal expansion, which was $2.9 \times 10^{-6}/^{\circ}\text{C}$. This matched well with the theoretical value of the laminate coefficient of thermal expansion (CTE), $3.08 \times 10^{-6}/^{\circ}\text{C}$. This was computed from the reported values of coefficients of thermal expansion of both the fibers and the matrix, and using a rule of mixtures, calculating the lamina coefficient of thermal expansion, and finally generating the laminate's CTE. The CTE calculations are included in Appendix B.

In-Phase TMF

Figure 34 shows the maximum strain during cycling for the four in-phase TMF specimens. There is creep occurring at the higher stress levels. This is characterized by an increase in strain without an increase in strain range, and without a decrease in modulus. Strain ratcheting is also evident in this figure. The ratcheting is strain due to damage accumulation in the matrix material. This ratcheting occurs in the midrange

stress levels. At low stress levels, there is no increase in strain, showing lack of damage and creep.

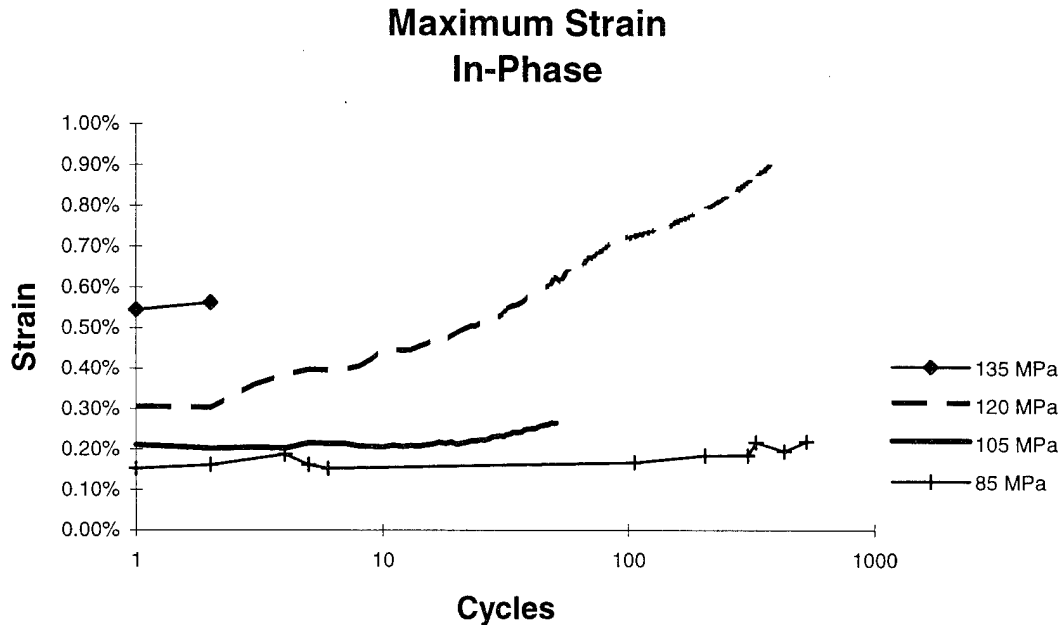


Figure 34. In-Phase TMF: Maximum Strain

Figure 35 shows minimum strain follows the same trend as the maximum strain. This is also illustrated by the constant difference between maximum and minimum strain, known as strain range, shown in Figure 36. Higher stress levels produce a larger strain, as well as a higher rate of change in strain. Both the maximum and minimum strains are directly proportional to maximum stress. A change in strain without a change in strain range is an indicator of creep.

A different view of how the strain changes over the life of each specimen can be taken by normalizing the number of cycles by the cycles to failure for each specimen.

When the cycles are normalized, the ratcheting effect is more visible as shown in Figure 37. At high stress levels, the strain increased rapidly over the first 20% of the life, and continued to slowly increase over the remainder of the life. The specimen is straining due to a combination of creep and fiber failure. At low stress levels, the strain increased rapidly over the first 1% the life, then leveled off. This shows most of the damage occurs in the first few cycles in these specimens.

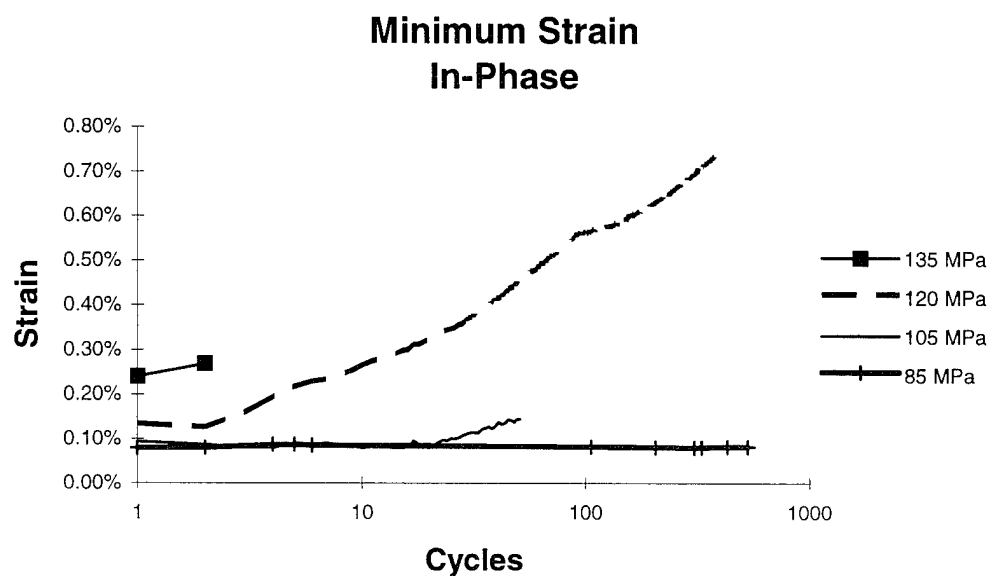


Figure 35. In-Phase TMF: Minimum Strain

Out-of-Phase TMF

The out-of-phase TMF tests experienced the negative ratcheting in the earlier part of cycling, where the maximum total strain (sum of mechanical and thermal strains) decreases with each cycle. This is not shown graphically, but important enough to bring

up. This strain ratcheting occurred rapidly over the first few cycles, then began to level off. This agreed with Worthem's statement "out-of-phase tests show a negative ratcheting that stabilizes within about 100 cycles" [63-3: 18]. Worthem ran a similar series of TMF tests.

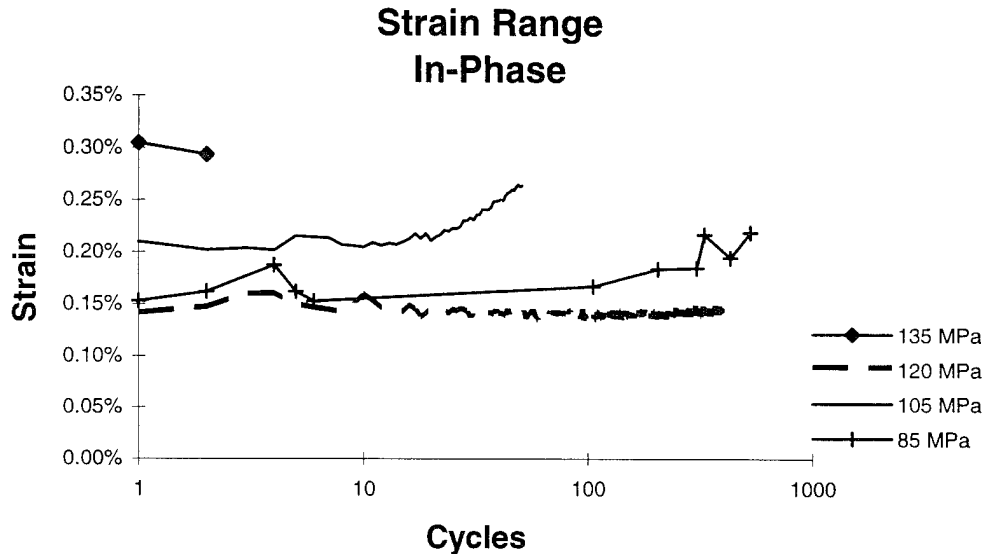


Figure 36. In-Phase TMF: Strain Range

An investigation into this phenomenon showed that the coefficient of thermal expansion (CTE) decreases with damage accumulation to the specimen. When this slight decrease in CTE was used to subtract the thermal strains from the total strain to get mechanical stress, the mechanical strains were constant or increased slightly. Figure 38 shows the maximum mechanical strain for all out-of-phase TMF tests. It was also found that, due to the out-of-phase TMF condition, the strain range was barely at the resolution of the data acquisition system. During out-of-phase TMF cycling, the maximum load

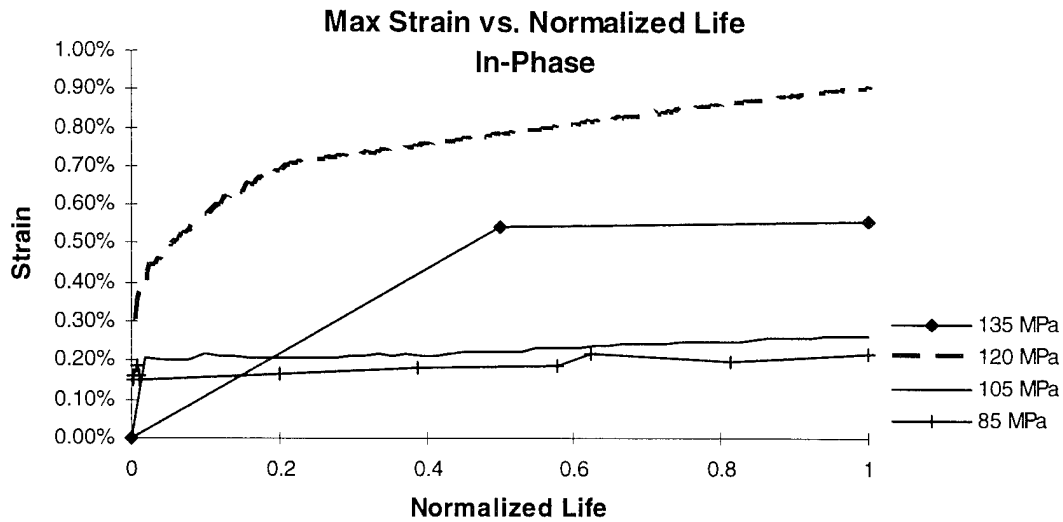


Figure 37. In-Phase TMF: Maximum Strain, Normalized Life

occurs at the minimum temperature. This minimum temperature is the point of highest residual stresses. Among other things, these residual stresses cause the fibers to go into compression longitudinally. The mechanically applied stress must overcome this compression. The behavior is similar to cold working of metals, where the material is deformed, creating residual compression within the material. This creates a low maximum strain and the opposite effect creates a high minimum strain, shown in Figure 39. This combination makes the strain range a small quantity, as seen in Figure 40.

The magnitude of the strain range of the out-of-phase TMF tests varied from 0.05% to 0.14%. Strain range is directly proportional to the maximum stress levels, shown in Figure 40. Strain range remains constant at lower stress levels, and increases slightly at higher stress levels. This show very little creep occurred in the out-of-phase TMF condition.

Figure 41 shows the maximum mechanical strain of the out-of-phase TMF condition with normalized fatigue lives. When normalized, the maximum strain is almost constant throughout the life. There is a small amount of ratcheting occurring in the early portion of the life, indicating early damage, but none little more after the first few cycles.

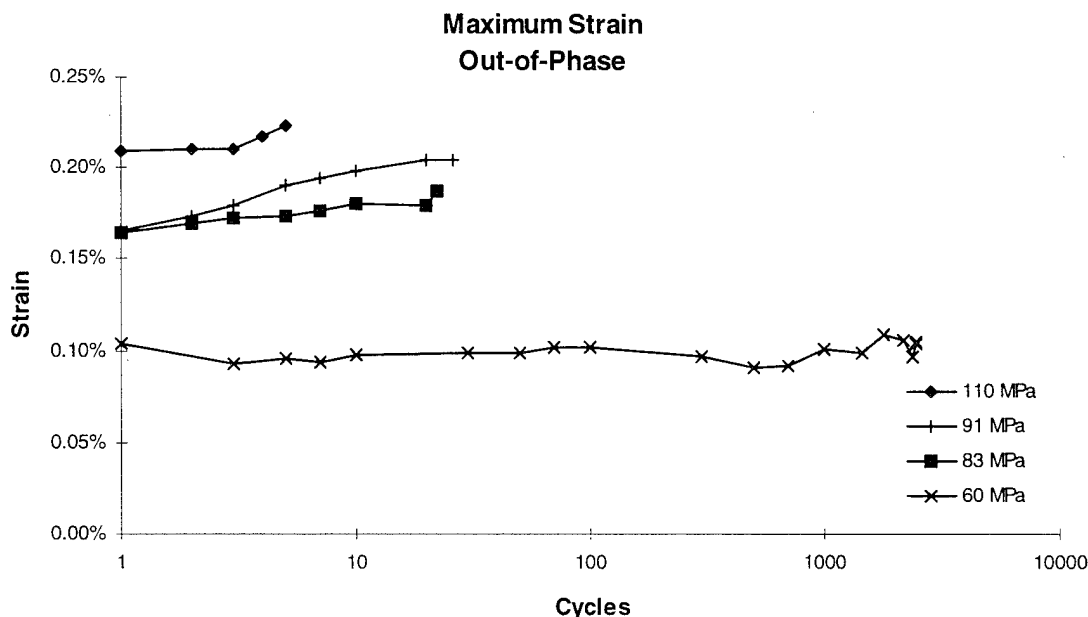


Figure 38. Out-of-Phase TMF: Maximum Strain

In-Phase TMF vs. Out-of-Phase TMF

Figure 42 and Figure 43 show the maximum strain and the strain range for both the in-phase and the out-of-phase TMF condition, respectively. There is little difference in the maximum strain between in-phase and out-of-phase TMF, for any given stress level. The strain range for the in-phase TMF is higher than the out-of-phase TMF strain range. This shows that damage depends on the TMF conditions.

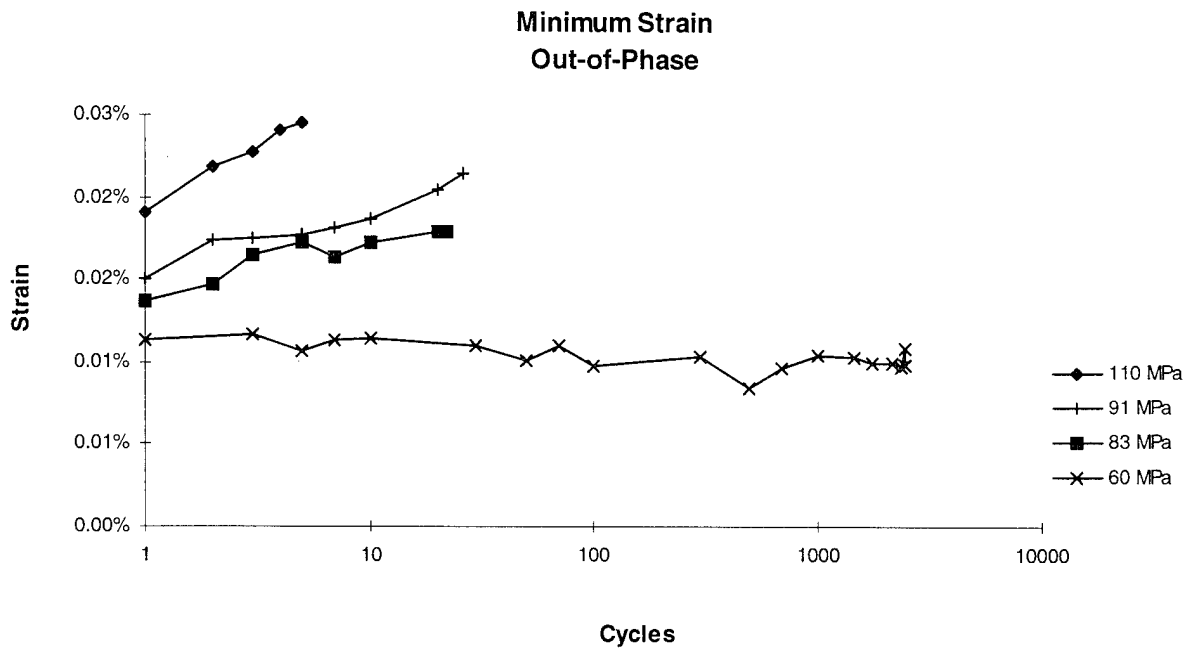


Figure 39. Out-of-Phase TMF: Minimum Strain

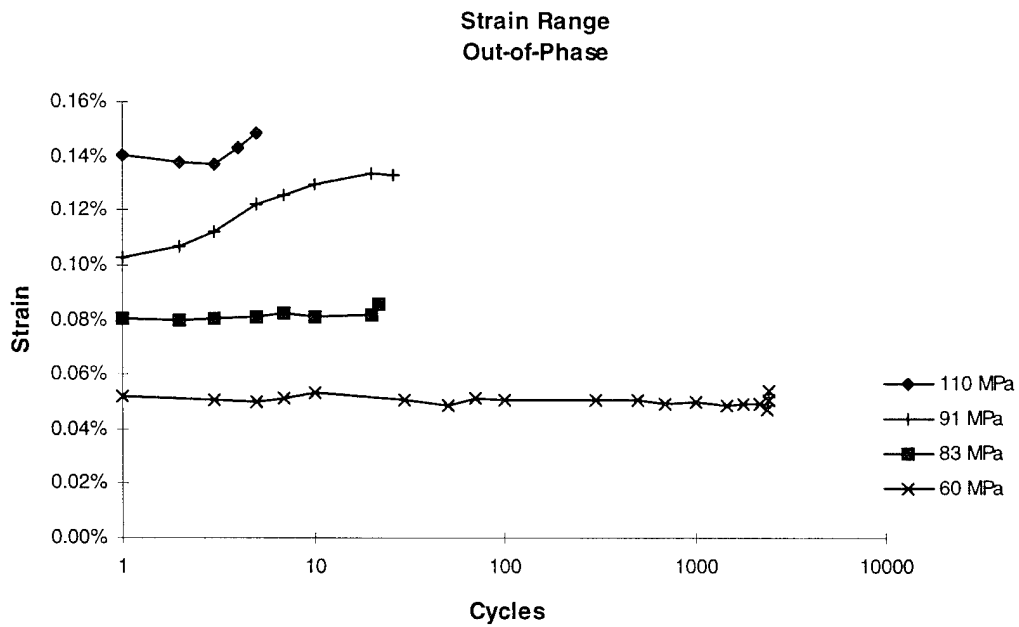


Figure 40. Out-of-Phase TMF: Strain Range

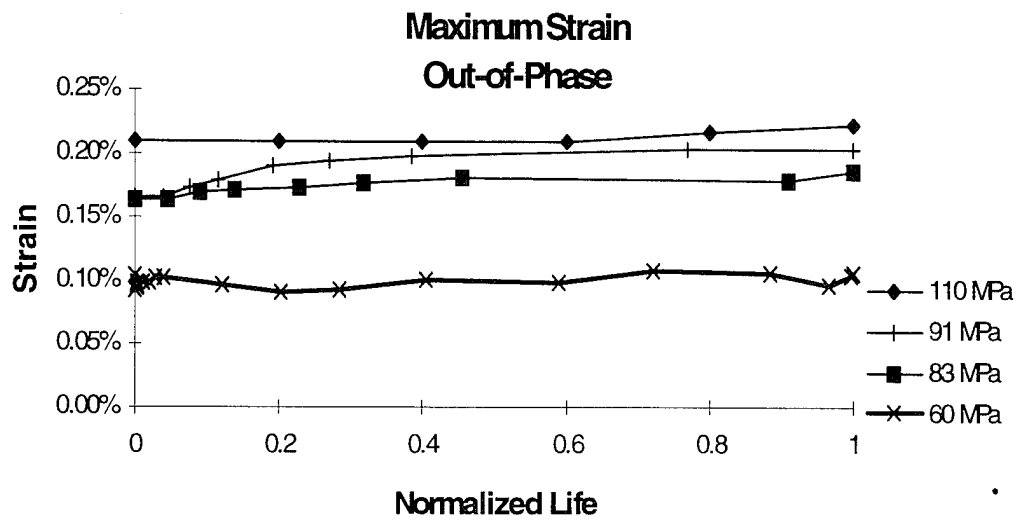


Figure 41. Out-of-Phase TME: Maximum Strain vs. Normalized Life

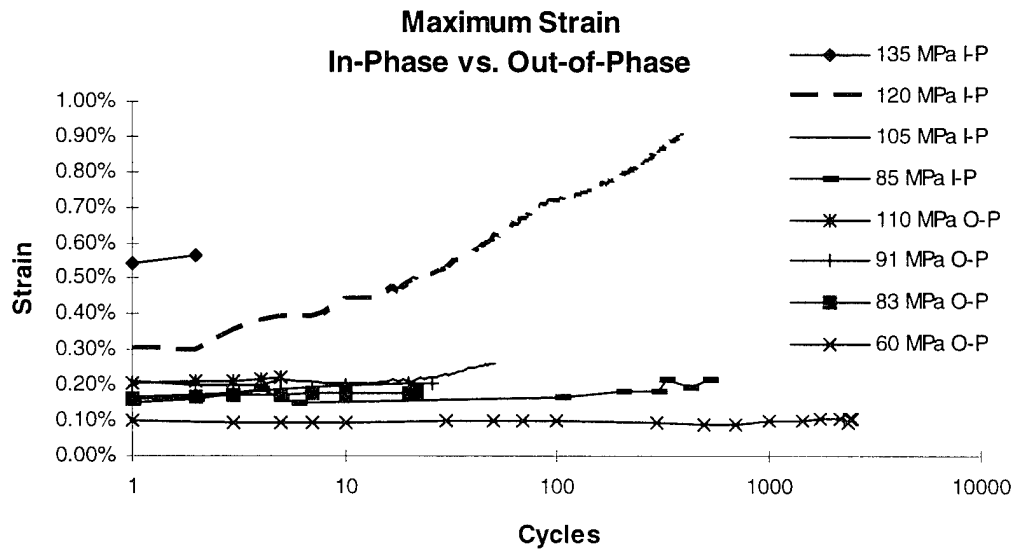


Figure 42. Maximum Strain: In-Phase TME vs. Out-of-Phase TME

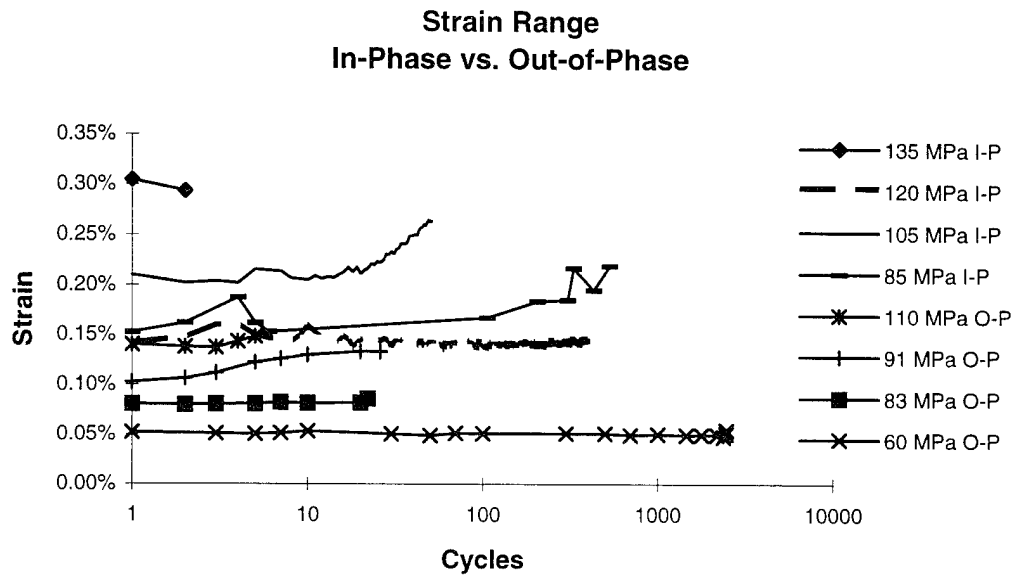


Figure 43. Strain Range: In-Phase TMF vs. Out-of-Phase TMF

566°C Isothermal

The maximum strains for the isothermal fatigue tests at 566°C are shown in Figure 44. The maximum strain is directly proportional to the maximum stress. The rate of change in these strain is very small. This small increase in strain is due to a combination of strain ratcheting and creep. The effect is more clearly seen when the strains are plotted against normalized life in Figure 45. The creep is much less than the in-phase TMF. Figure 46 shows the minimum strain follows the same trend as the maximum strain. This is also seen by the constant strain range shown in Figure 47.

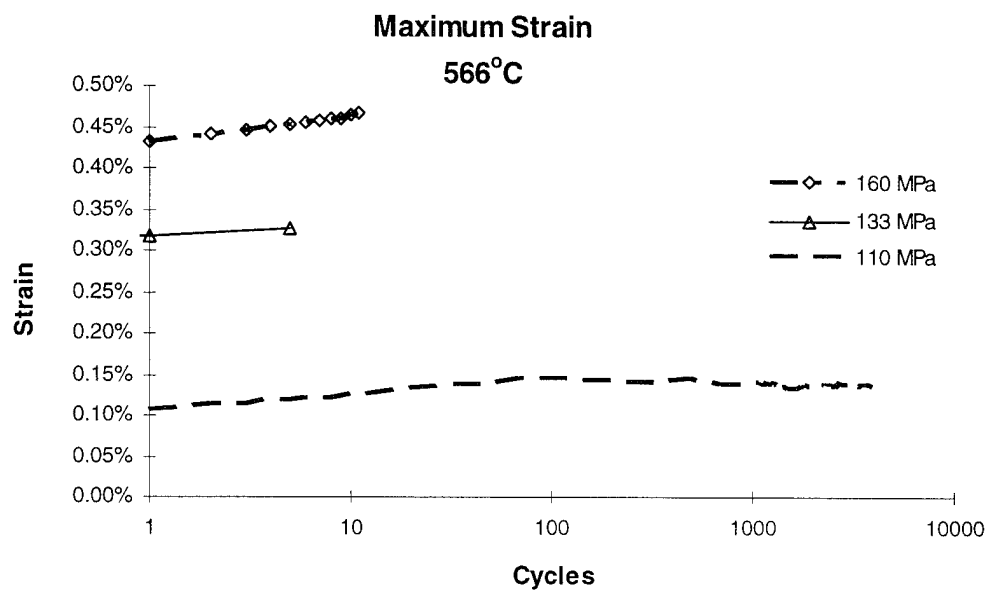


Figure 44. 566°C: Maximum Strain

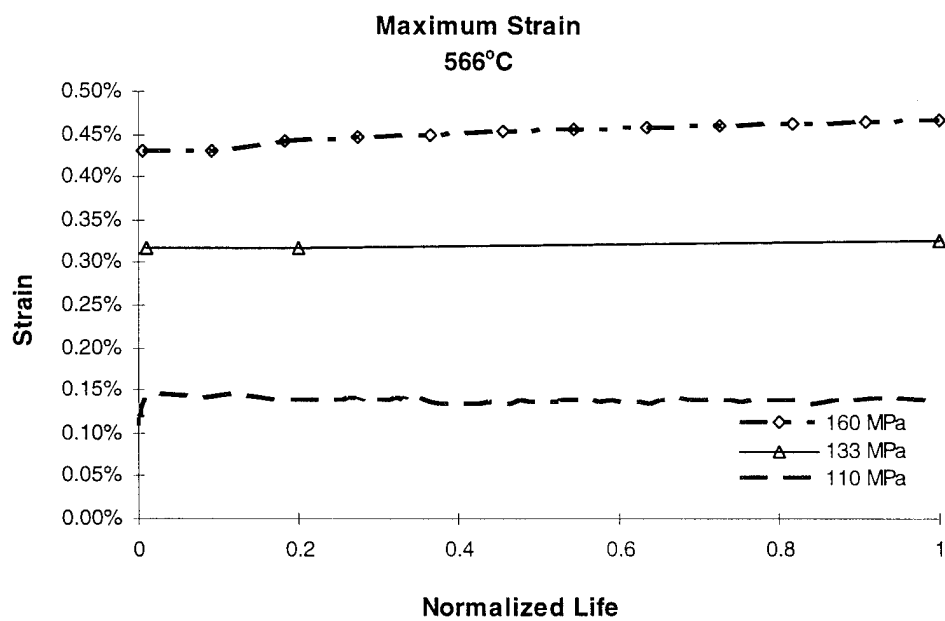


Figure 45. 566°C: Maximum Strain vs. Normalized Life

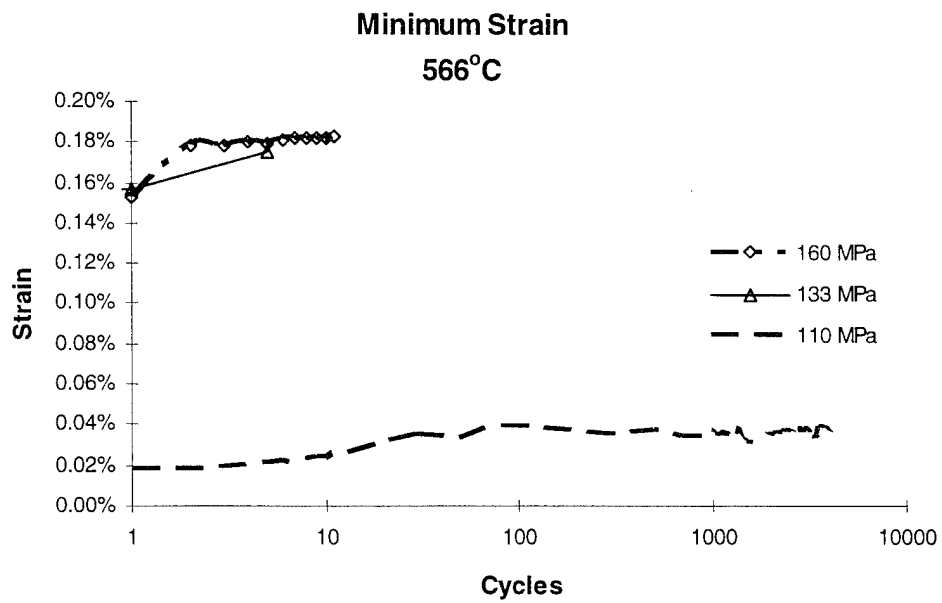


Figure 46. 566°C: Minimum Strain

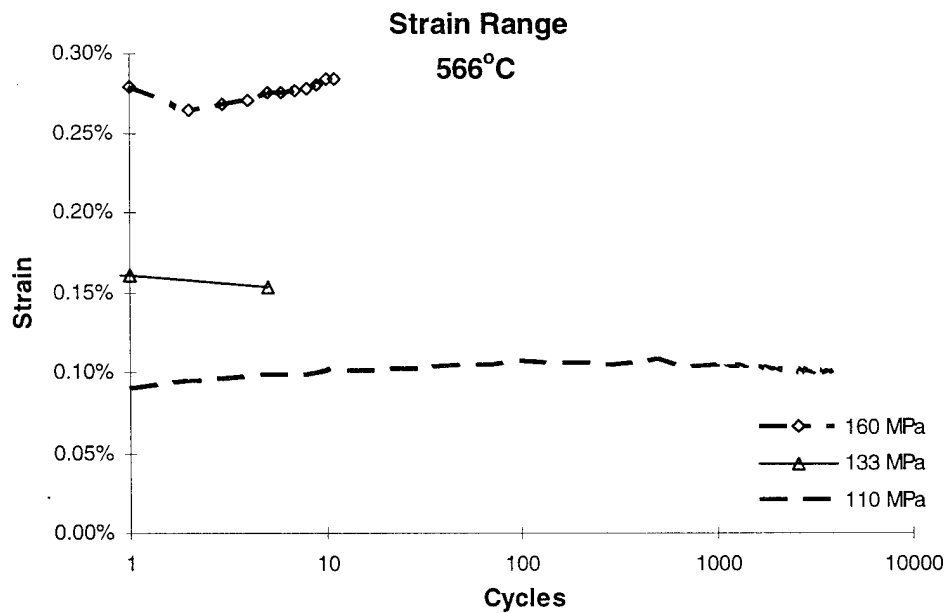


Figure 47. 566°C: Strain Range

1093°C Isothermal

The maximum strains for the isothermal fatigue tests at 1093°C are shown in Figure 48. The rate of change in strain is large at higher stress. The combination of ratcheting and creep is seen more clearly when the strains are plotted against normalized life in Figure 49. Figure 50 shows the minimum strain follows the same trend as the maximum strain. This is also seen by the constant strain range shown in Figure 51.

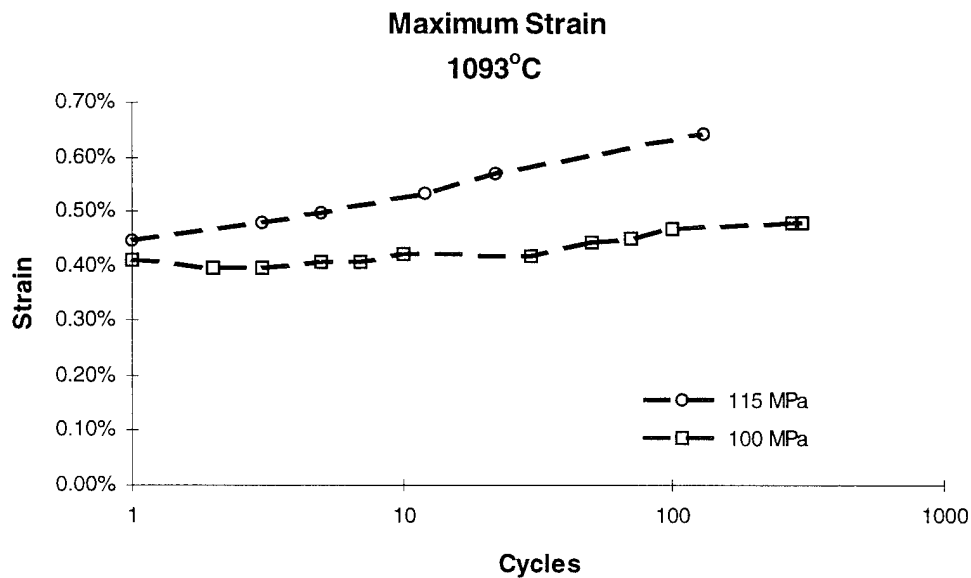


Figure 48. 1093°C: Maximum Strain

566°C vs. 1093°C

Figure 52 and Figure 53 show a comparison of maximum strain and strain range between the 566°C and the 1093°C conditions of isothermal fatigue. There are clearly

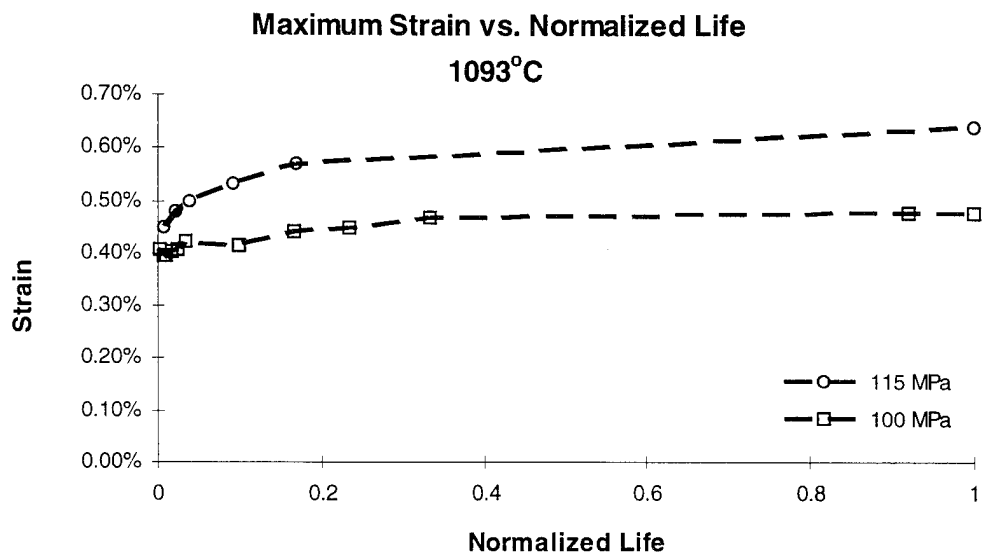


Figure 49. 1093°C: Maximum Strain vs. Normalized Life

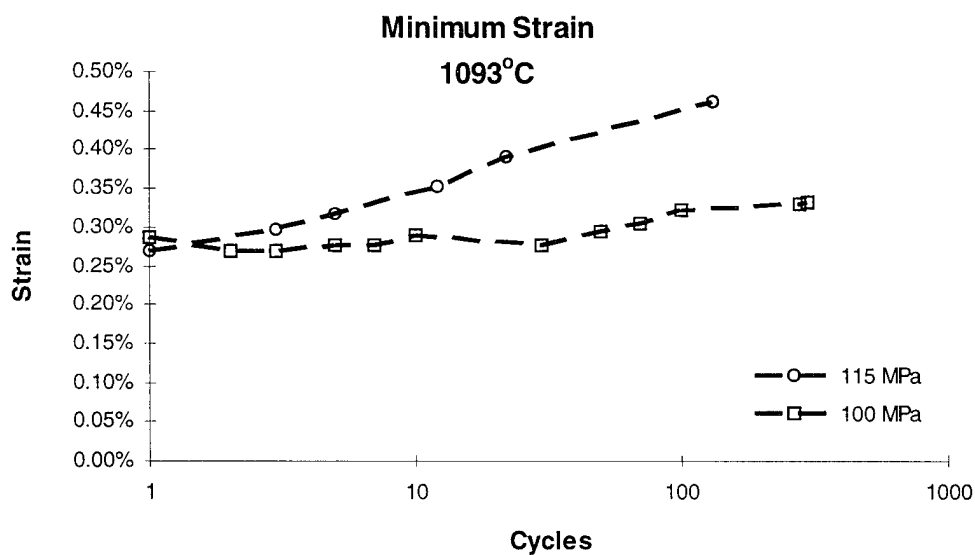


Figure 50. 1093°C: Minimum Strain

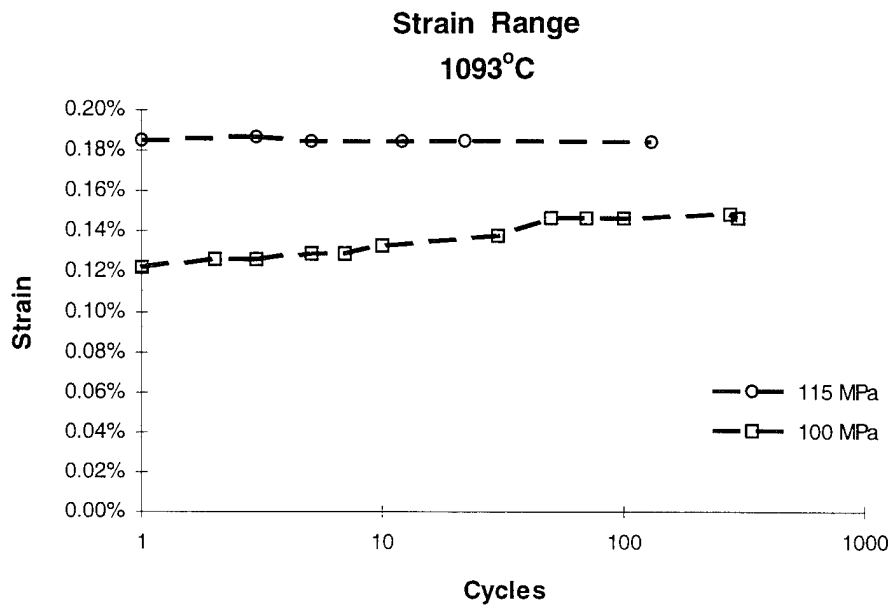


Figure 51. 1093°C: Strain Range

some differences in these cases. The 1093°C condition has a much higher strain as well as strain range. The strain range remains constant at 566°C and 1093°C. The rate at which the strain is changing per cycle is much higher at higher temperatures as well. This shows the temperature effects, which are also reflected in the monotonic tensile tests, as well as in the modulus degradation, as discussed later. The lower residual stresses at 1093°C allow the fibers to slide more readily at this temperature, allowing for higher strain. Oxidation is occurring much more rapidly at higher temperatures, degrading the fibers and embrittling the fiber/matrix interface. This will be supported when the failure mechanisms are investigated.

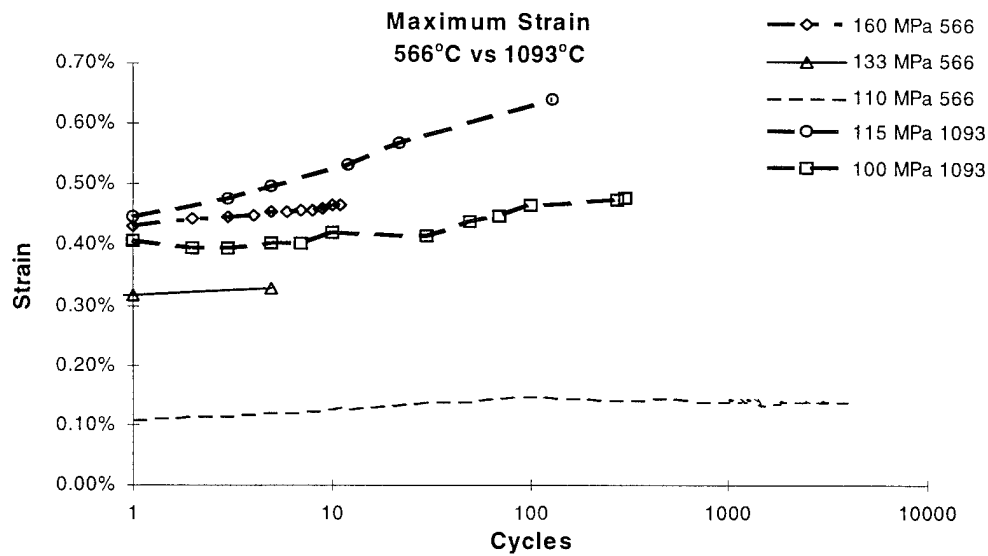


Figure 52. Maximum Strain: 566°C vs. 1093°C

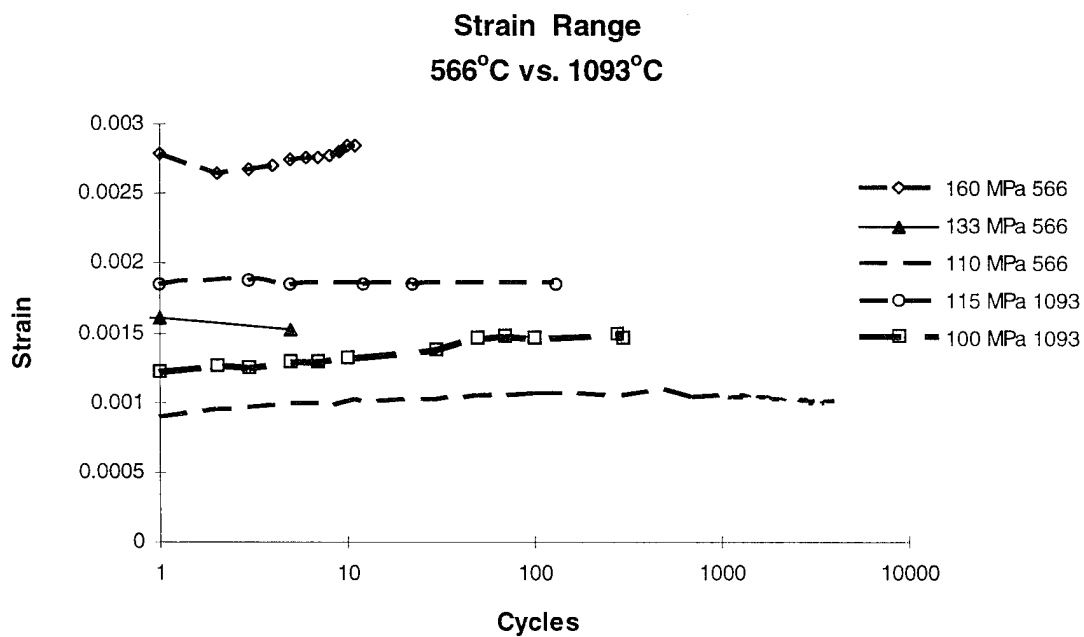


Figure 53. Strain Range: 566°C vs. 1093°C

TMF vs. Isothermal Fatigue

A comparison was made for the maximum strain and the strain range between thermo-mechanical fatigue and isothermal fatigue. For clarity, the curves were broken up in to high stress levels (110 MPa - 160 MPa) and low stress levels (60 MPa - 110 MPa). Figure 54 and Figure 55 show the maximum strain at high and low stress levels, respectively. The specimens run under isothermal fatigue conditions at 1093°C strained the most and had the highest rate of change in strain per cycle. The isothermal fatigue conditions at 566°C showed the least amount of strain and no change in strain over the life of the specimens. Both TMF tests were between the two isothermal conditions, with out-of-phase TMF straining slightly less for any given stress level than the in-phase TMF. The in-phase TMF specimens had the increase in strain over their life, especially at high stress levels. The out-of-phase TMF had a very small change in strain at high stress levels, but none at low stress levels.

Figure 56 and Figure 57 show the strain range at high and low stress levels respectively. At all stress levels, the out-of-phase TMF and the isothermal fatigue at 566°C have low strain ranges compared to in-phase TMF and 1093°C. This is due to the fact that maximum stress occurs at 566°C for both out-of-phase TMF and 566°C isothermal, and maximum stress occurs at 1093°C for in-phase TMF and 1093°C isothermal. The in-phase TMF was slightly less than the isothermal fatigue at 1093°C at high stress levels, but they were the same at lower stress levels. The out-of-phase TMF and 566°C showed the same amount of strain range at high stress levels, but the out-of-phase TMF was slightly higher than the 566°C at low stress levels. The strain range

remained constant at 566°C and 1093°C, and the TMF strain ranges rose slightly, showing more damage occurred in the TMF condition. This illustrates the effect that fatigue condition had on the damage.

Summary

In summary, the strain data shows the material undergoes a combination of strain ratcheting and creep during fatigue cycling. Isothermal fatigue at 1093°C produced the largest change in strain, followed by the in-phase TMF. Both the out-of-phase TMF and the isothermal fatigue at 566°C had very small rates of change in strain, especially at lower stress levels. The 1093°C had the highest strain, and the 566°C had the lowest.

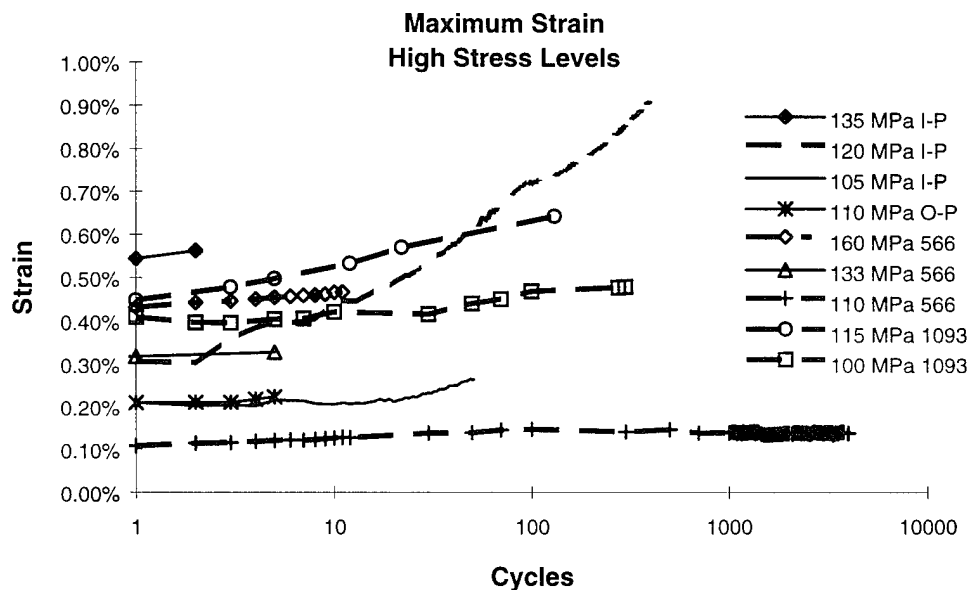


Figure 54. Maximum Strain: High Stress Levels

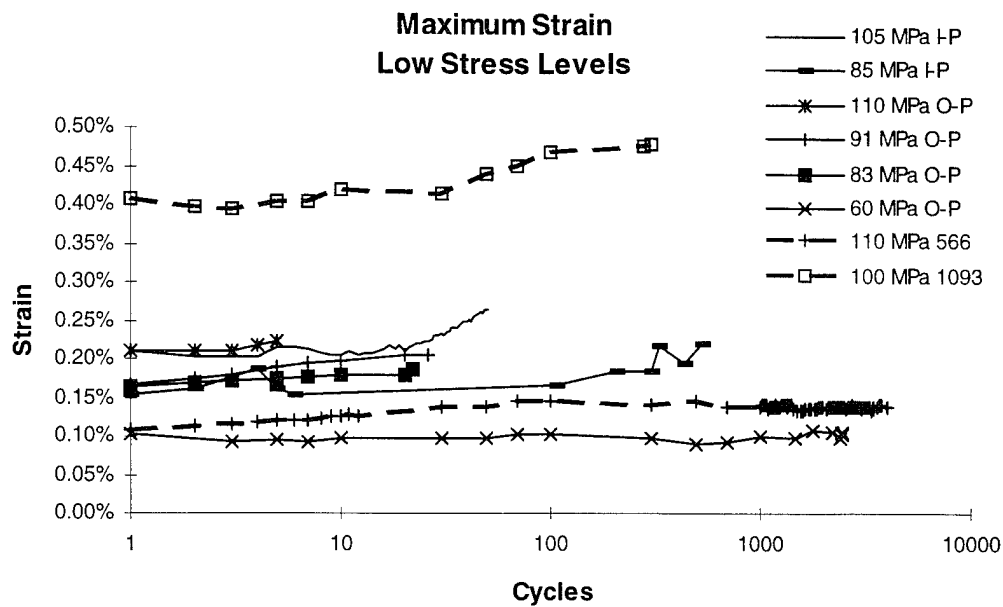


Figure 55. Maximum Strain: Low Stress Levels

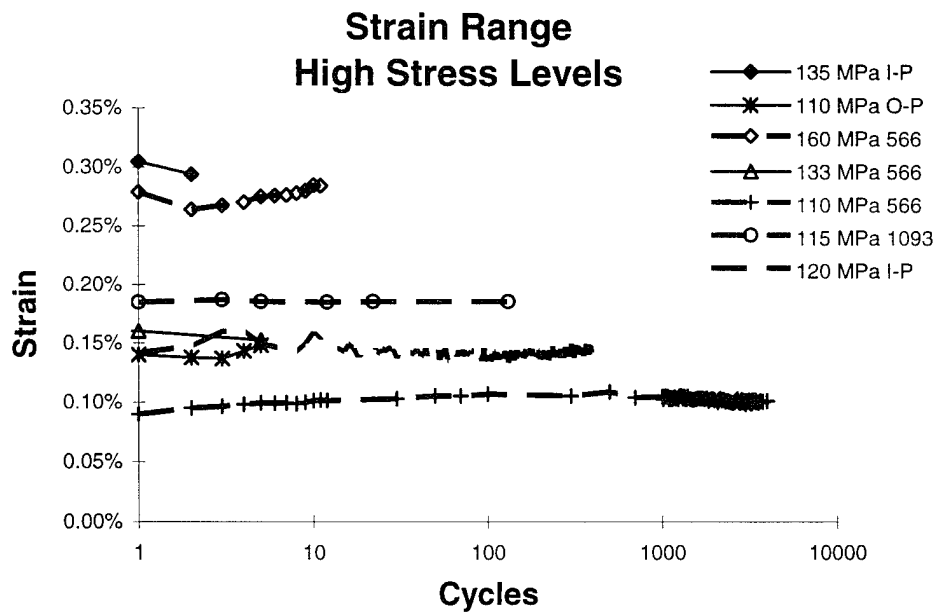


Figure 56. Strain Range: High Stress Levels

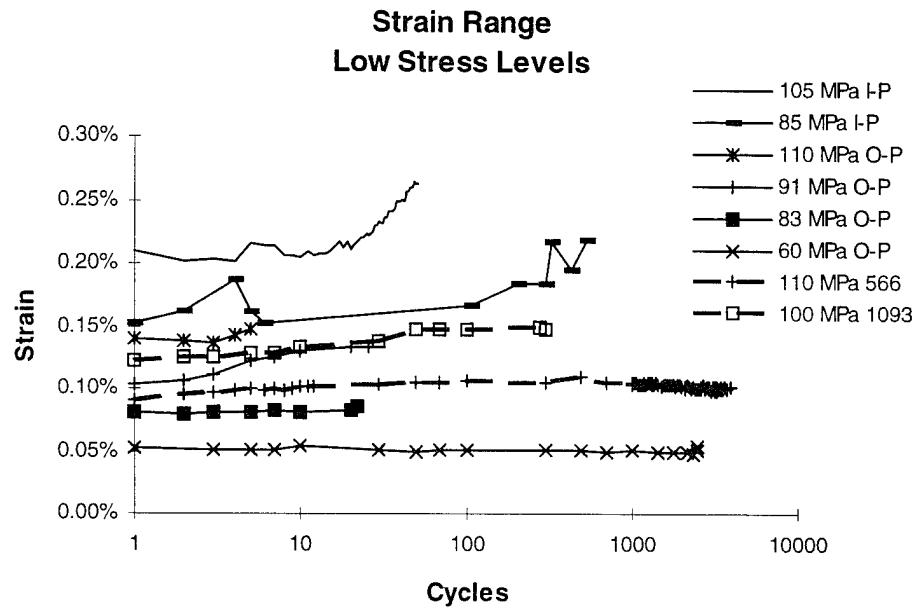


Figure 57. Strain Range: Low Stress Levels

The TMF tests had strain levels between the two isothermal tests. The creep experienced by the specimens was mostly a function of temperature at the time maximum stress was applied. The mechanisms occurring are a function of time, stress level, residual stresses and fatigue environment.

Modulus Degradation

The investigation of the modulus of elasticity over the life of the specimen gives an indication of the damage. This modulus was the secant modulus which was calculated by taking the difference between maximum stress and minimum stress and dividing by the difference in maximum mechanical strain and minimum mechanical strain. Dividing the secant modulus by the initial modulus normalizes the modulus

degradation. The initial modulus was taken from an average of first cycle moduli of all the tests in that group. There is a different initial modulus for both sets of isothermal tests, 566°C and 1093°C, and for both sets of TMF tests, in-phase and out-of-phase. For the isothermal tests at 566°C, the initial modulus was 120 MPa. For the isothermal tests at 1093°C, the initial modulus was 90 MPa. In-phase TMF testing had an initial modulus of 112 MPa, and out-of-phase TMF testing had an initial modulus of 112 MPa as well. In general, the modulus degraded rapidly initially and then leveled out. The total amount of modulus degradation was directly proportional to the maximum stress level.

In-phase TMF

Figure 58 shows the secant modulus plotted over the life of specimens under in-phase TMF conditions. During in-phase TMF cycling, the secant modulus of elasticity degraded rapidly over the first few cycles, then leveled off, with the modulus remaining fairly constant for the remainder of the life. This is the same effect as discussed in the previous section dealing with strain, where it was shown that strain range was constant after the first cycle. The damage occurs early, then not much new damage is occurring, until the 0° fibers fail, which causes the specimen to fail. This damage is in the form of cracks in the matrix of the 90° plies and debonding of the fiber/matrix interface. After the first few cycles, the crack density is saturated and the modulus can degrade no more. Localized fiber breakage at high stress levels accounts for some of the modulus degradation as well. A higher stress level produces a greater reduction in modulus.

Another way to look at this damage degradation is by normalizing the secant modulus (E_i) by the initial modulus (E_0), and normalizing the fatigue life (N_i) by the number of cycles to failure (N_f). Figure 59 shows this normalized modulus as a function of fatigue life for the in-phase TMF condition. The test at 135 MPa degraded rapidly to 55.4% of the initial modulus, in the first 50% of its life. The modulus at 120 MPa degraded 60% in less than 1% of its life then slowly climbed back up to about 66%. The same phenomenon occurred at 105 MPa, which degraded to 68% in the first 3% of its life and then crept up to 70%, and again at 85 MPa, which went down to 78% in the first 2% of its life, but eventually came back up to 84%. The rise in modulus could be attributed to an increase in shear stress between the fiber and matrix as the interface oxidizes.

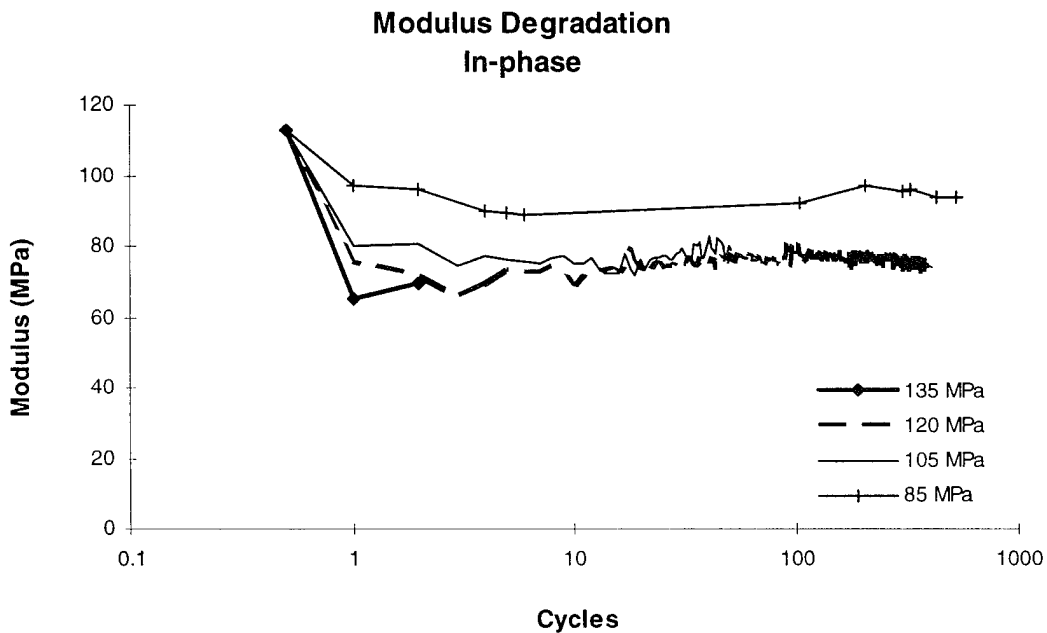


Figure 58. Modulus Degradation: In-Phase TMF

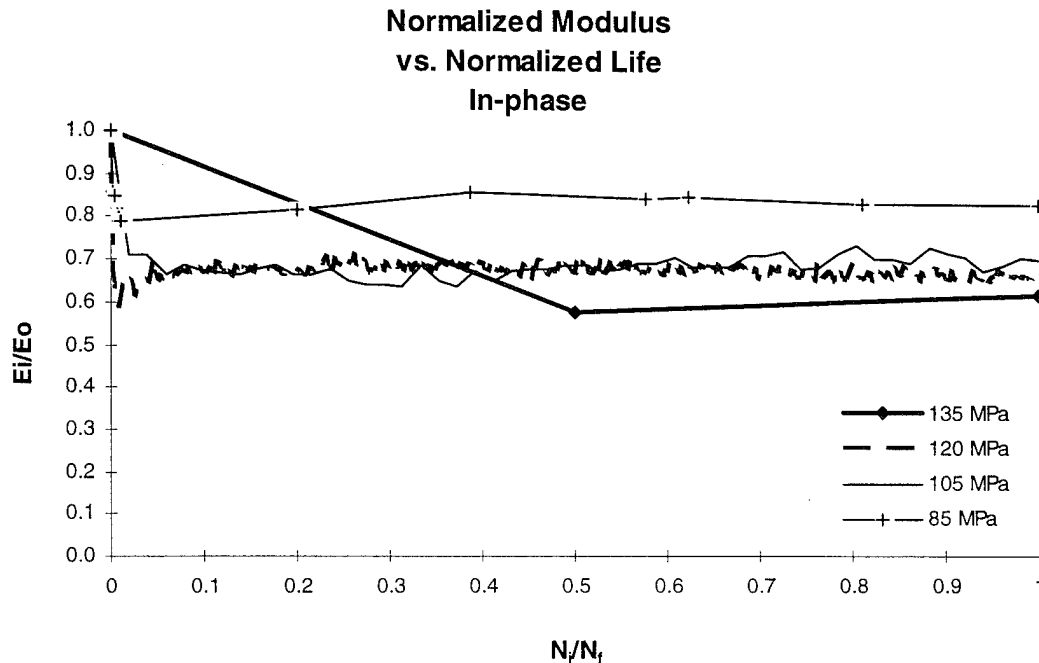


Figure 59. Normalized Modulus Degradation: In-Phase TMF

Out-of-Phase TMF

Figure 65 shows the modulus degradation of the out-of-phase TMF tests. This data shows that the modulus decreased over the life of the specimen. This is due to the damage accumulation in the specimen. It can be seen in this figure that the modulus degraded rapidly in the early cycles, then leveled off to a constant. This indicates that most of the damage to the specimen occurred early. The specimen tested at a maximum stress level of 60 MPa did not have any modulus degradation at all. This agrees with the strain range which does not change over the life of the specimen. Very little damage is occurring within the specimen. These similar results are expected, since the modulus degradation is calculated using the strain range.

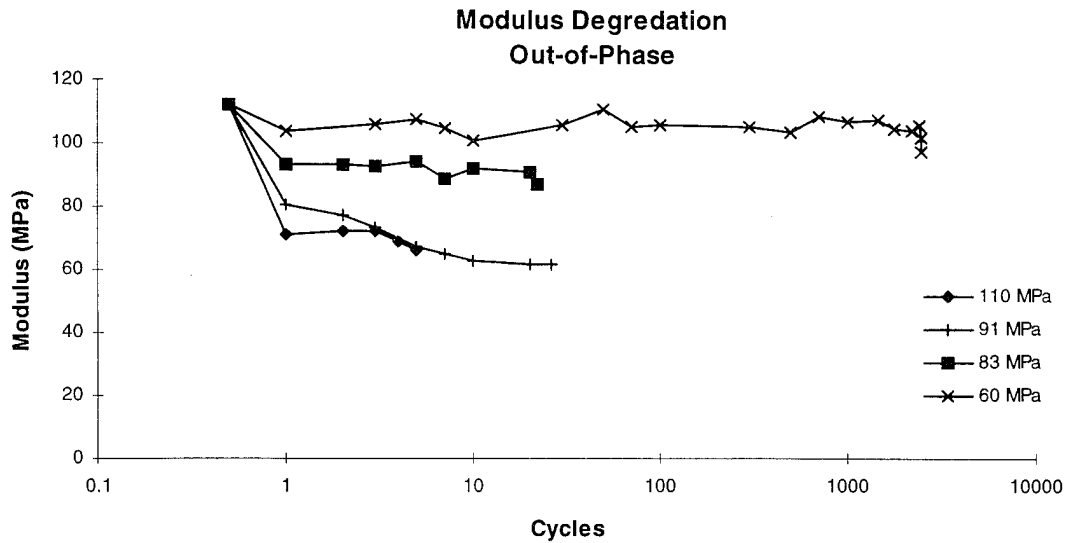


Figure 60. Modulus Degradation, Out-of-Phase TMF

A clearer picture of the amount of degradation that is occurring is shown by normalizing the modulus and fatigue life. Figure 61 shows the normalized modulus degradation data for the out-of-phase TMF condition. At 110 MPa, the modulus decreased by almost 60% of the initial modulus in the first 20% of its life. At 91 MPa, the specimen took 40% of its life to decrease the modulus by 58%. The modulus of the specimen tested at 83 MPa decreased very slightly to about 87.5% in only 5% of its life. The modulus of the specimen tested at 60 MPa remained very close to 100%. The modulus does not exhibit the slight recovery as seen in the in-phase TMF data.

In-Phase TMF vs. Out-of-Phase TMF

Figure 62 shows a comparison between the normalized modulus for both the in-phase and the out-of-phase TMF conditions. There is about the same amount of

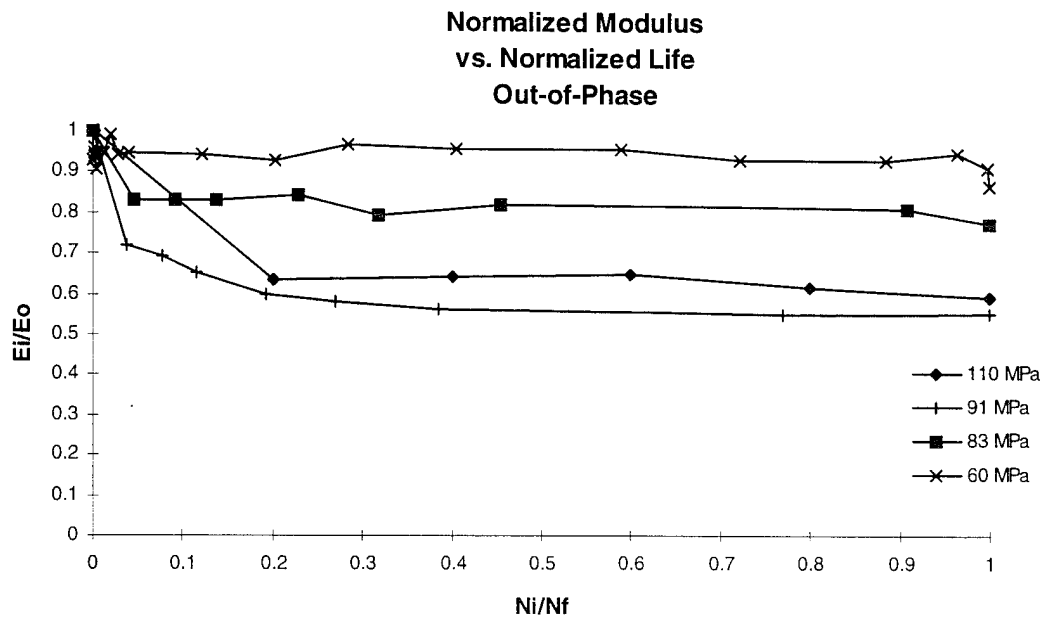


Figure 61. Normalized Modulus Degradation, Out-of-Phase

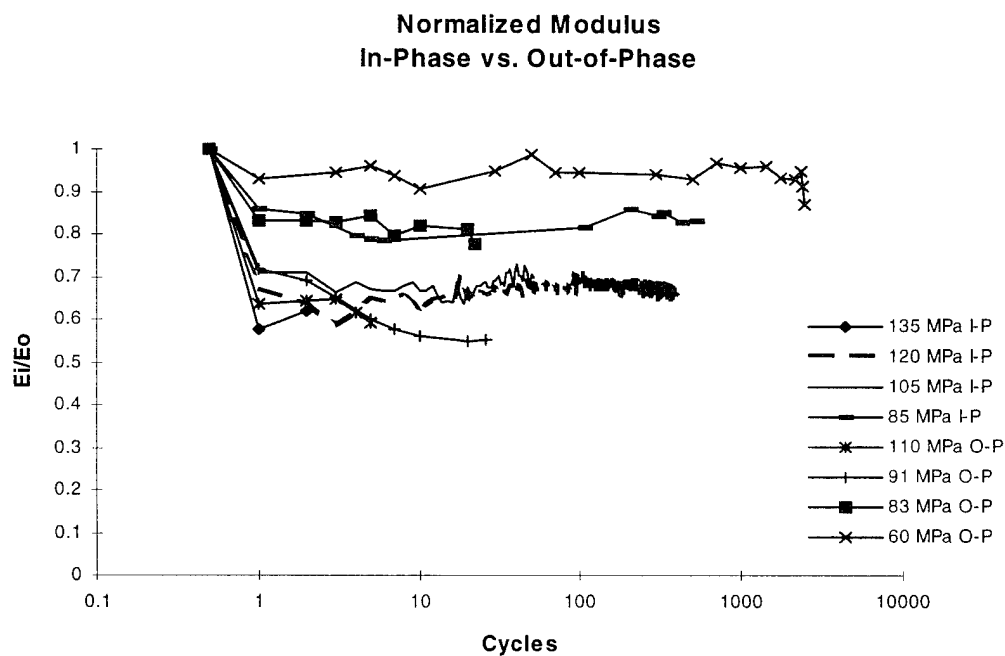


Figure 62. Normalized Modulus: In-Phase TMF vs. Out-of-Phase TMF

degradation for the same stress level. The only difference between them is that the in-phase TMF shows a slow modulus recovery.

566°C Isothermal

Figure 63 shows how the modulus changed over the fatigue life of the specimens tested under isothermal conditions at 566°C. At high stress levels there was a large reduction in initial modulus in the first cycle, then the modulus tended to remain fairly constant. The fact that the modulus did not decrease indicates that the small strain increase experienced was a creep phenomenon. The initial reduction in modulus indicates that there is a large amount of damage occurring in the first cycle. The modulus of the specimen tested at 110 MPa decreased very slowly. This indicates that there is gradual damage accumulating in the matrix, and strain ratcheting.

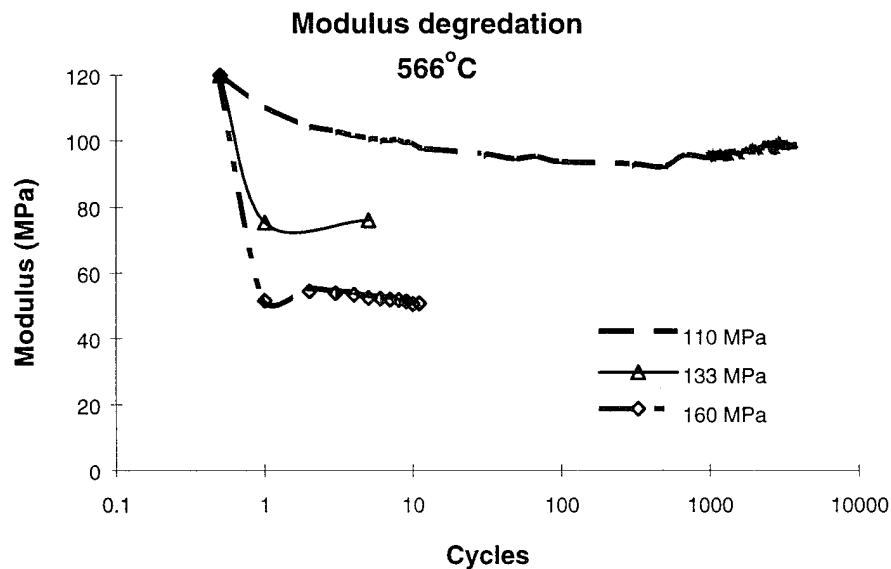


Figure 63. Modulus Degradation: 566°C

Figure 64 shows the normalized modulus degradation for the specimens tested under isothermal fatigue conditions at 566°C. The stress level of 160 MPa degraded the modulus to about 45%, most of which occurred in the first cycle, indicating that first ply failure occurred in the first cycle. The specimen run at a stress level of 133 MPa degraded the modulus to 58%. Again most of the damage occurred in the first cycle. A stress level of 110 MPa degraded to about 78%. There is no recovery in modulus at this temperature, indicating no increase in shear stress between the fibers and matrix.

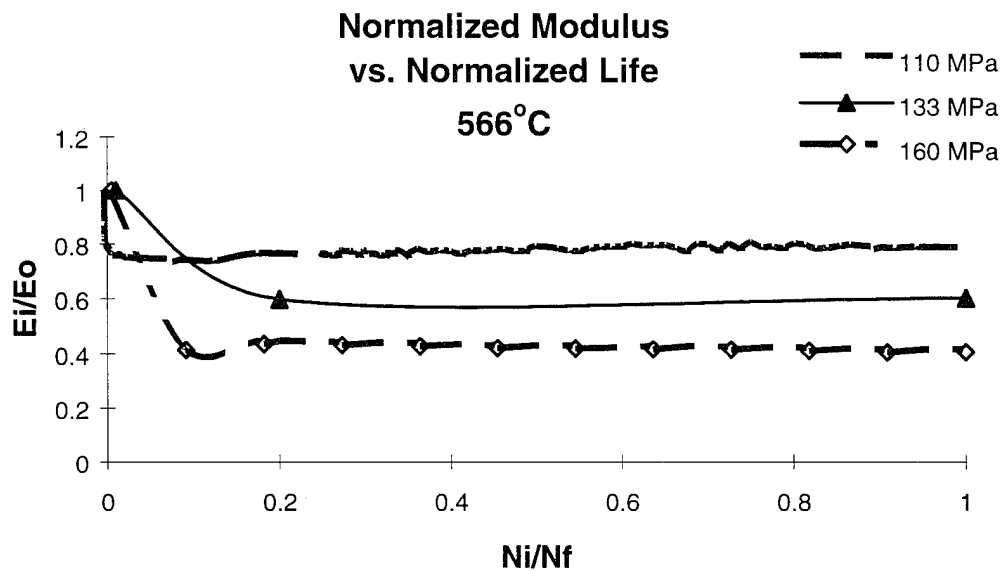


Figure 64. Normalized Modulus Degradation: 566°C

1093°C Isothermal

Figure 65 shows the modulus degradation for the isothermal fatigue specimens tested at 1093°C. The modulus experienced a sharp drop during the first cycle. The degradation is due to damage in the form of matrix cracking in the 90° plies, which occurs

during the first cycle. The higher stress level experienced no decrease in modulus after the first cycle, indicating that the damage level was saturated. The lower stress level experience the gradual decrease in modulus caused by damage accumulation. This is the same effect as discussed in the previous section dealing with strain, and more evidence will be discussed in later sections.

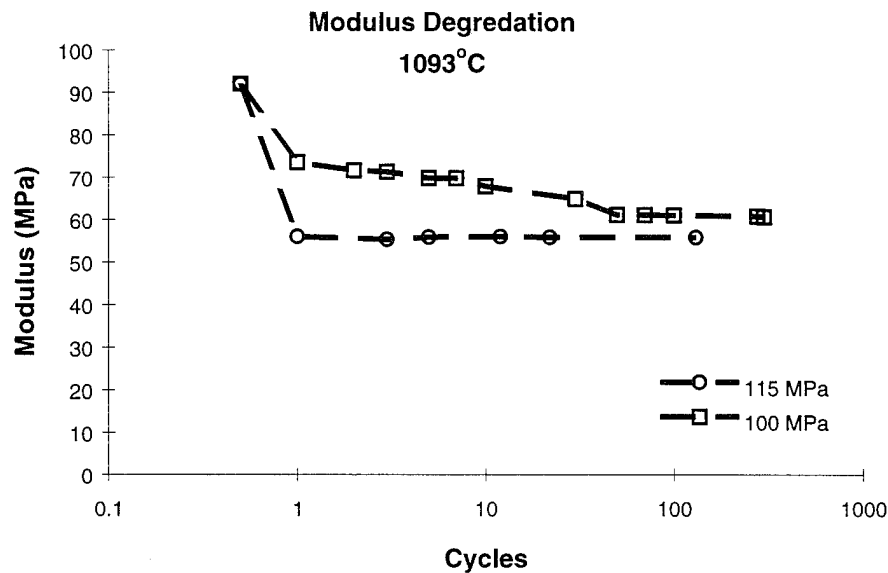


Figure 65. Modulus Degradation: 1093°C

Figure 66 shows the normalized modulus data for the isothermal fatigue specimens tested at 1093°C. The maximum stress level of 115 MPa degraded the modulus to about 60%, most of which occurred in the first cycle, less than 1% of the total life. This indicates that first ply failure occurred in the first cycle. The maximum stress level of 100 MPa degraded the modulus to 80%. Again most of the damage occurred in the first cycle. The modulus then decreased slowly to 65%. This shows that first ply failure did not occur, but matrix cracks did form, and they continued to develop during

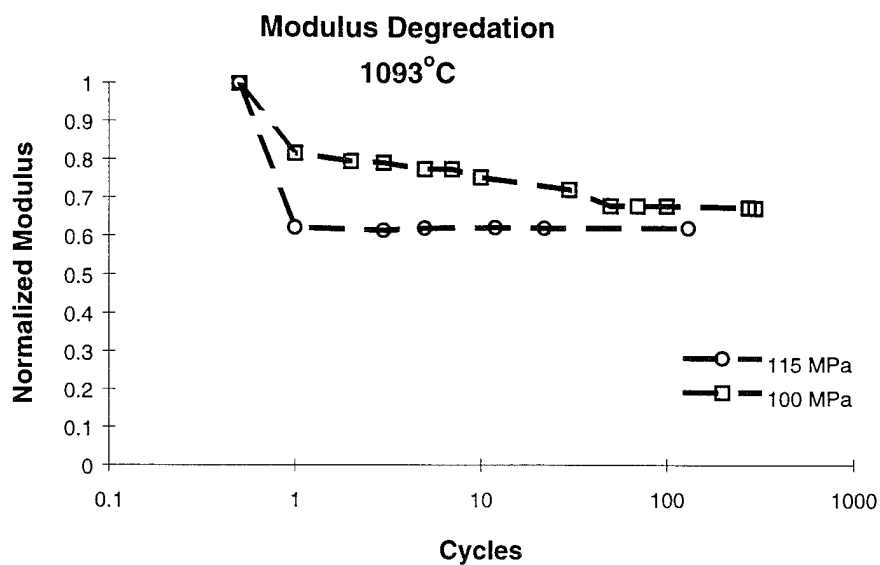


Figure 66. Normalized Modulus Degradation: 1093°C

cycling, until the matrix became saturated with cracks. After saturation, the modulus remained constant.

566°C vs. 1093°C

Figure 67 shows the normalized modulus for both isothermal fatigue cases, 566°C and 1093°C. The isothermal fatigue at 1093°C degraded much more than the isothermal fatigue at 566°C. This shows that there is an effect of the temperature on damage.

TMF vs. Isothermal Fatigue

A comparison was made among the moduli under TMF conditions and the moduli under isothermal fatigue conditions. For clarity, these were separated into two charts, high stress levels and low stress levels. Figure 68 shows the modulus degradation at high

stress levels (110 MPa - 160 MPa). Figure 69 shows the modulus degradation at low stress levels (60 MPa - 110 MPa).

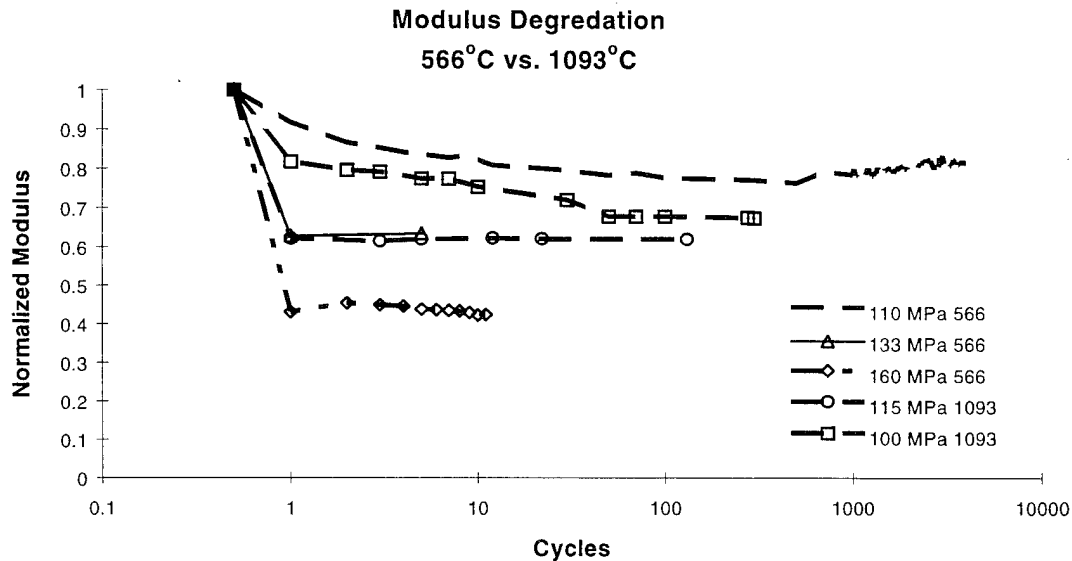


Figure 67. Normalized Modulus: 566°C vs. 1093°C

The high stress levels show that the modulus for in-phase TMF, out-of-phase TMF, and 566°C degrade about the same amount for any given stress level. The modulus at 1093°C degraded the most for any given stress level. The modulus for the in-phase TMF exhibited a slow recovery, due to the increased shear stressed from oxidation of the fiber/matrix interface and the small movement between the fibers and matrix.

At low stress levels, the modulus at 566°C degraded relatively less. The in-phase and out-of-phase TMF showed the same amount of degradation for any given stress level. The 1093°C modulus degraded much more than any other condition. This shows the effects of temperature on oxidation. The lower temperature isothermal test at 566°C showed little damage since it was exposed to the least amount of temperature, and thus

oxidized the least. The most oxidation corresponded to the highest exposure to temperature, the isothermal condition at 1093°C.

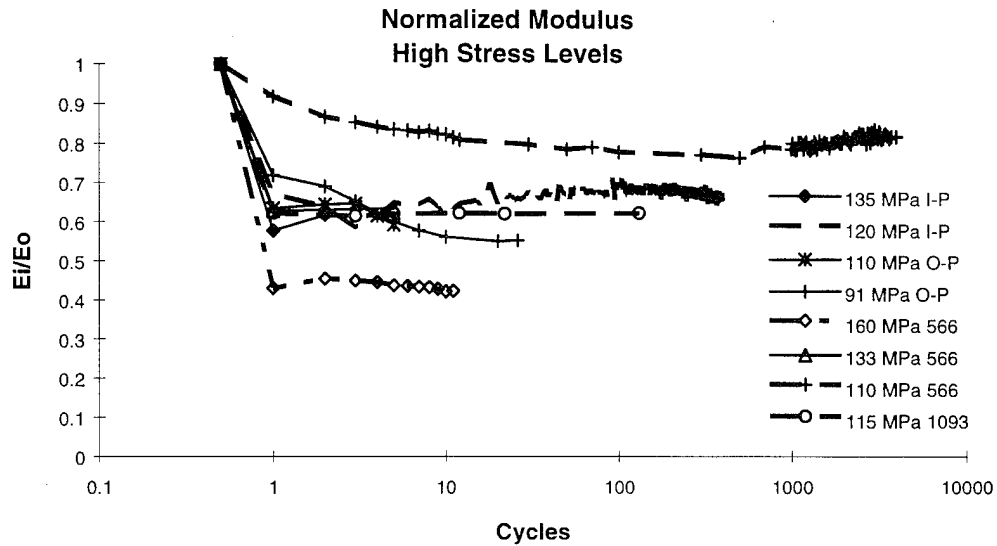


Figure 68. Normalized Modulus: High Stress Levels

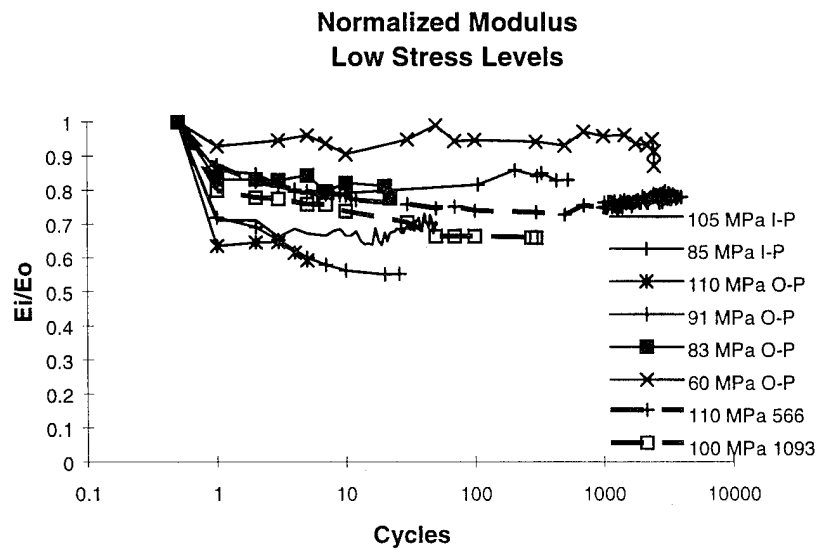


Figure 69. Normalized Modulus: Low Stress Levels

Summary

In summary, there are several stages of thermo-mechanical fatigue damage. The first is matrix cracking of the ninety degree plies, occurring in the first few cycles. Next, fiber/matrix debonding occur. At sufficiently high stresses, fibers will begin to fail, and the matrix cracks will open, but will be bridged by the fibers. Soon more fibers will fail, until the area is reduced to the point of failure stress. This is fiber controlled failure, and is reflected in a large and quick reduction in secant modulus of elasticity. This fiber controlled failure will have a fracture surface with long fiber pull-out.

If the stresses are not high enough to fail the fibers, more matrix cracks will form as the specimen is fatigued. The cracks cannot grow, they are deflected by the fiber/matrix debonds. New cracks continue to form until a saturation level is reached, these cracks cause permanent strain deformation in each cycle, known as strain ratcheting. The material is undergoing a small amount of creep as well, evidenced by an increase in strain without an increase in modulus. Meanwhile, the high temperature is creating a harsh, highly oxidative environment. This oxidation makes the interface between the fiber and matrix strong and brittle; it also degrades the fiber. The brittle interface allows the cracks to propagate from the matrix to the fibers, failing the fibers in a brittle fashion, causing total failure of the specimen. This is matrix controlled failure and is recognized by a quick reduction in modulus over the first few cycles, then a leveling of the secant modulus until failure. Occasionally a slight reduction in modulus is observed immediately preceding failure, presumably due to the fiber breakage. This is

not always captured due to the frequency of data acquisition during relatively high cycle fatigue.

All of the load and temperature conditions resulted in moduli that decreased rapidly in the first few cycles, then reached a stabilized value. The in-phase TMF and the isothermal fatigue at 1093°C shared the common trait of slight modulus recovery due to an increase in friction between fiber and matrix. The out-of-phase TMF and 566°C isothermal tests do not exhibit this small increase in modulus after matrix crack saturation. This is due to the residual stresses allowing frictional fiber sliding, which eventually reduces the shear stress between the fiber and matrix due to abrasion of the interface.

Hysteresis Loops

One way to analyze the stress-strain data acquired from fatigue tests is to examine their hysteresis loops. These loops are created by the difference in strain response during loading and unloading. This difference results in hysteresis. The hysteresis data can provide a great deal of information, from the migration of the curves over time, the magnitude of the difference, the area inside the curve, and the orientation of the curves.

Loop migration over time indicates how the strain progresses, similar to the strain histories. The area inside the curve indicates the amount of energy the material is absorbing during the cycle. The orientation of the curve indicates the current modulus, similar the modulus degradation curves.

In-Phase TMF

Figure 70 shows the hysteresis loops for in-phase TMF at 120 MPa. The first loop is open, there is a great deal of damage and the material is absorbing a great deal of energy. There is a large lateral shift over the first few cycles, then the shift gets smaller. All the remaining loops have very similar areas and orientations, showing that there is not a large change in modulus of elasticity after the first few cycles. This indicates that there is no fiber breakage occurring. They do tend to migrate with each cycle. This migration is an indicator of strain ratcheting and creep. Notice that the curves are not quite closed, indicating a small amount of plastic like behavior. The area within each curve does not change, indicating no change in frictional shear stress between the fiber and the matrix, which is one of the predominant energy absorbing mechanisms.

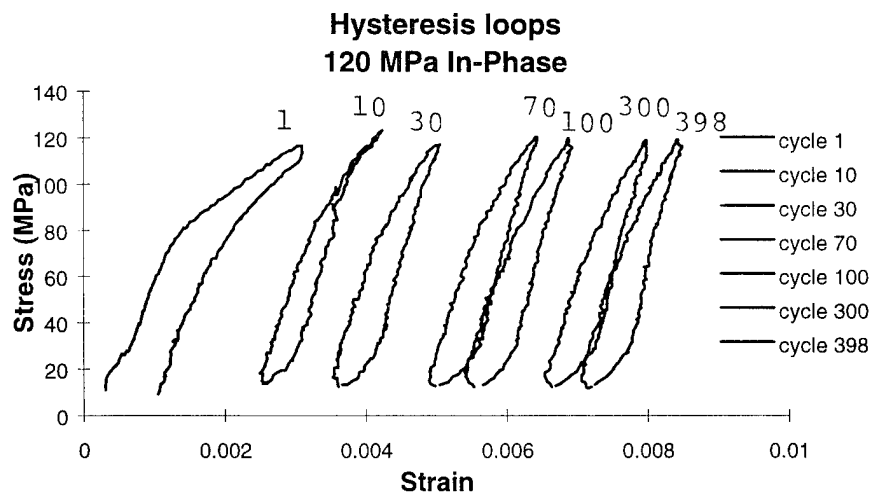


Figure 70. Hysteresis: 120 MPa, In-Phase TMF

Figure 71 represents the hysteresis loops for in-phase TMF at a maximum stress level of 105 MPa. These curves remain fairly similar with a slow lateral migration. This shows the gradual increase in strain during the cycling due to creep that was reflected in the strain data. The curves are not closed, showing the small amount of unrecovered strain each cycle. The area within the curves does not change much, showing the energy absorption rate remains constant throughout the life of the specimen.

Figure 72 shows the stress strain hysteresis for in-phase TMF cycling at 85 MPa. This shows a very small migration of curves throughout the life cycle, showing time related environmental effects and creep. There is very little matrix damage accumulation occurring. Recall in a previous section discussing strain data, the strain at this stress level did not increase much. For this low maximum stress case, the area within the curves tends to increase with cycles, indicating the energy being absorbed is increasing with the number of cycles.

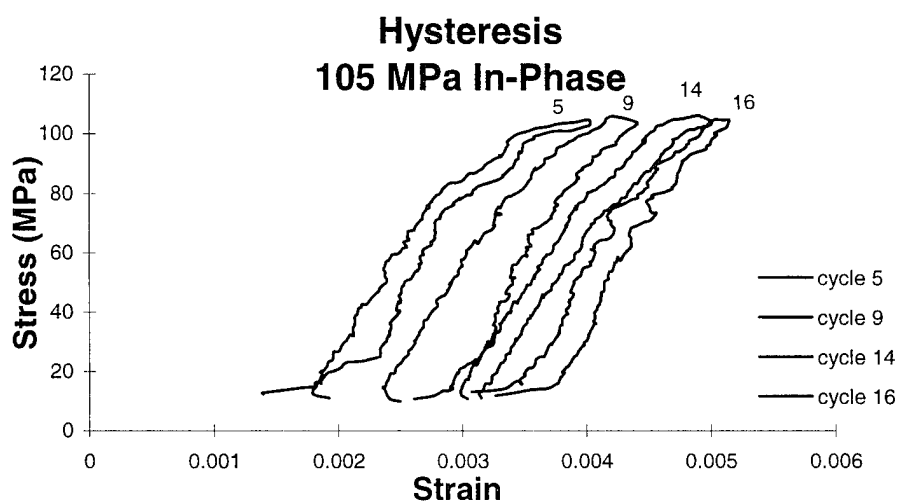


Figure 71. Hysteresis: 105 MPa, In-Phase TMF

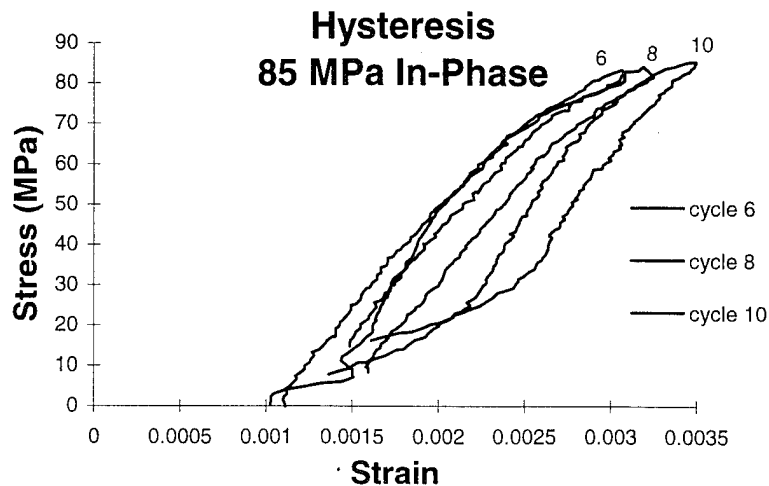


Figure 72. Hysteresis: 85 MPa, In-Phase TMF

Out-of-Phase TMF

The out-of-phase TMF cycling produced some unusual hysteresis loops. There is a large amount of hysteresis present. However, the magnitudes of the strains were very small, with very little movement with cycles.

Figure 73 shows the stress strain response of out-of-phase TMF cycling, with a maximum stress of 110 MPa. These loops are open. The actual area inside the curves is relatively small, due to the magnitude of the strain. This indicates there is a large amount of frictional sliding occurring. The loops are not perfectly closed, but the strain at the end of the cycle is slightly less than the strain at the beginning of the cycle. There is a minuscule amount of migration of the curves, showing the lack of strain ratcheting that occurred over the life of the specimen.

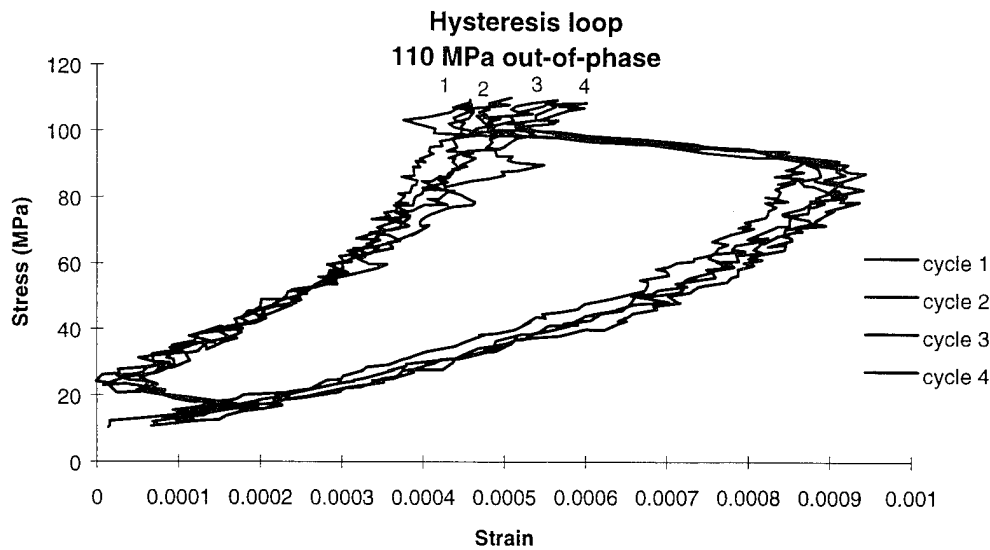


Figure 73. Hysteresis: 110 MPa, Out-of-Phase TMF

Figure 74 shows the out-of-phase TMF cycling hysteresis loops at 91 MPa. The area within the loop is relatively large. After the first cycle, the area does not change with cycles, indicating a constant energy absorption each cycle. The loops are not perfectly closed, but the strain at the end of the cycle is slightly less than the strain at the beginning of the cycle. The migration of the curves is small, reflecting the constant strain observed in the previous section dealing with strain data.

Figure 75 shows the out-of-phase TMF cycling hysteresis loops at 83 MPa. The area within the loop is very large. The area does not change with cycles, indicating a large, but constant energy absorption within each cycle. The loops are not perfectly closed, but the strain at the end of the cycle is slightly less than the strain at the beginning of the cycle. The migration of the curves is very small.

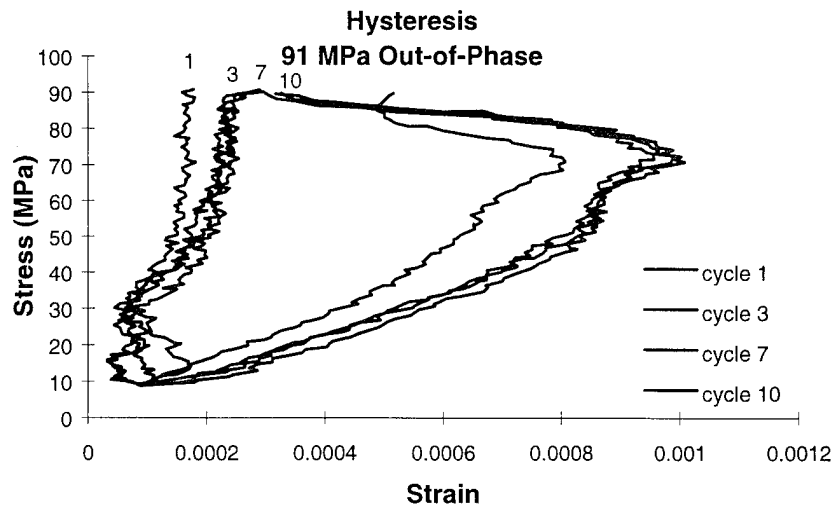


Figure 74. Hysteresis: 91 MPa, Out-of-Phase TMF

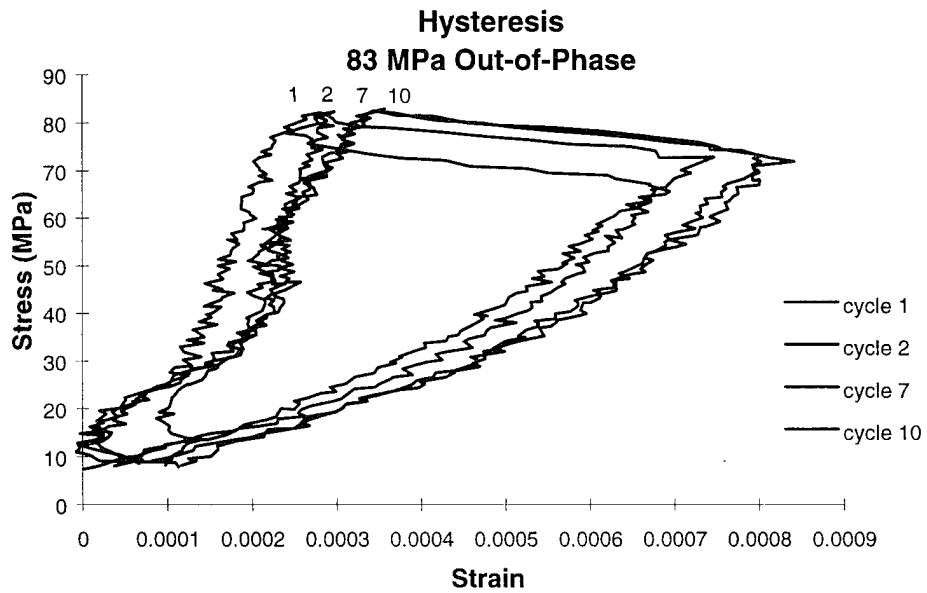


Figure 75. Hysteresis: 83 MPa, Out-of-Phase TMF

Figure 76 shows the out-of-phase TMF cycling hysteresis loops at 60 MPa. The area within the loop is much smaller than the higher stress out-of-phase TMF cycling. The area does not change with cycles, indicating a constant energy absorption within each cycle. The loops are not perfectly closed, but the strain at the end of the cycle is slightly less than the strain at the beginning of the cycle. There is almost no migration of the curves.

It is clear that a higher maximum stress level results in a larger area within each loop. This shows a direct correlation between maximum stress level and the amount of energy absorbed in the form of frictional sliding for each cycle.

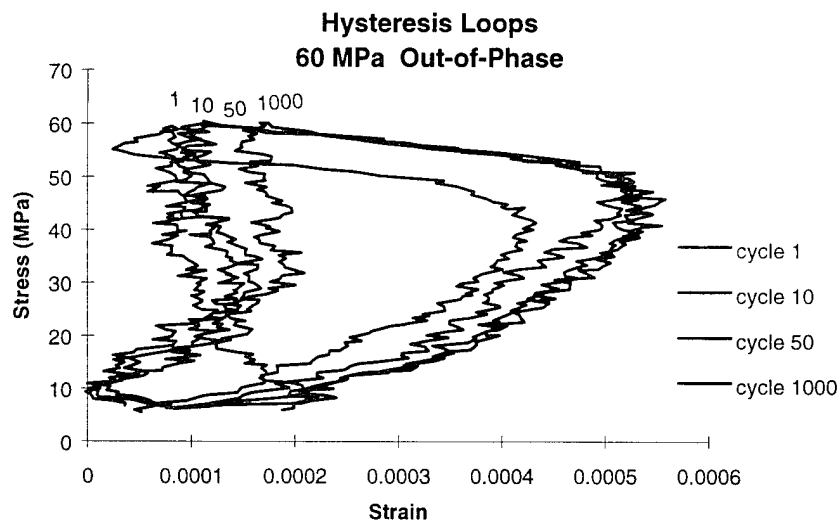


Figure 76. Hysteresis: 60 MPa, Out-of-Phase TMF

566°C Isothermal

As Figure 77 shows, at 160 MPa and 566°C, the initial stress-strain curve is open, with a large internal area. The subsequent curves are closed with much smaller areas.

These areas remain virtually constant. The curves tilt downward over time. The large area and open end of the first cycle loop indicate a large amount of unrecoverable damage occurring, and frictional fiber sliding. The remaining cycles show a much smaller amount of energy absorption, which remains constant for the remainder of the life. The curve of the first cycle changes dramatically at the point where first ply failure occurred during the monotonic tensile tests. This damage is the primary cause of the large hysteresis of the first cycle. The slope of the secant for the remainder of the curves is slowly decreasing, showing a gradual decrease in measured modulus of elasticity, as damage accumulates. The curves do not migrate after the first few cycles, indicating very little ratcheting.

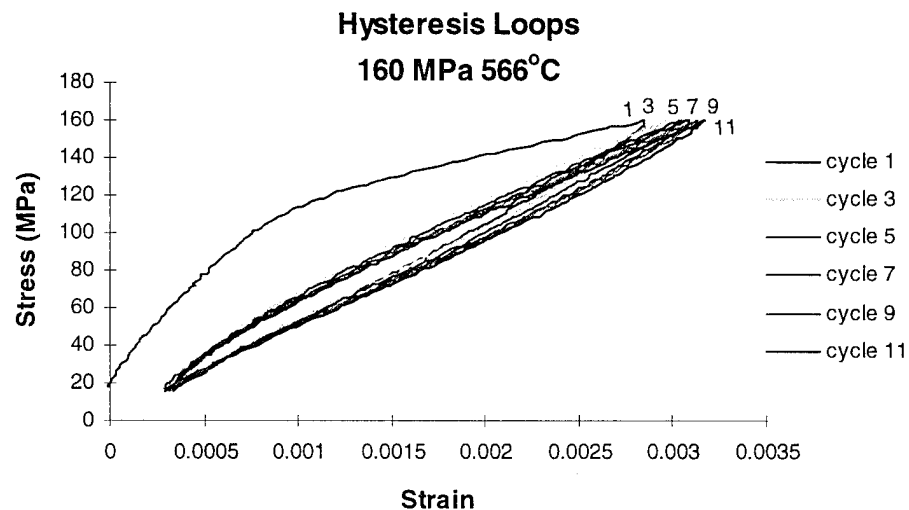


Figure 77. Hysteresis: 160 MPa, 566°C

Figure 78 shows the stress-strain hysteresis during each cycle at 133 MPa. The initial curve has a large area within it, mainly due to a great deal of damage occurring

during the first cycle. The area grows smaller with subsequent cycles. This indicates a decrease in the amount of damage that is accumulating, as well as a decrease in fiber sliding as the number of cycles increases.

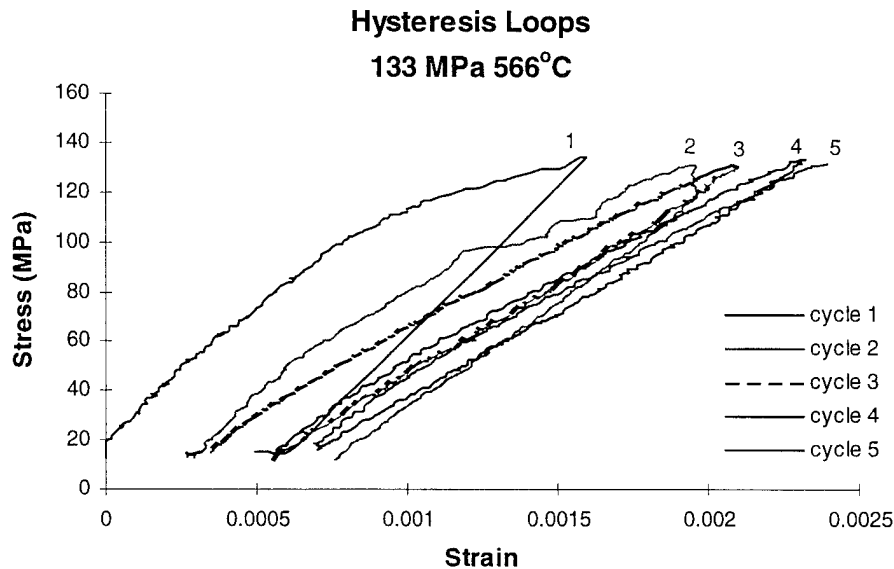


Figure 78. Hysteresis: 133 MPa, 566°C

Figure 79 shows the stress-strain hysteresis for isothermal fatigue at 110 MPa and 566°C. The figure shows the loop for the first cycle is slightly larger than the rest. This indicates most of the damage is occurring in the first cycle, but failure of the ninety degree plies has not occurred, as it did in the higher stress levels. There is a large shift in the location of the curve for the first few cycles, then it stabilizes, with very little shift throughout the remainder of the life. The first loop is larger, showing more energy is absorbed in the first cycle. The remaining life shows very little hysteresis.

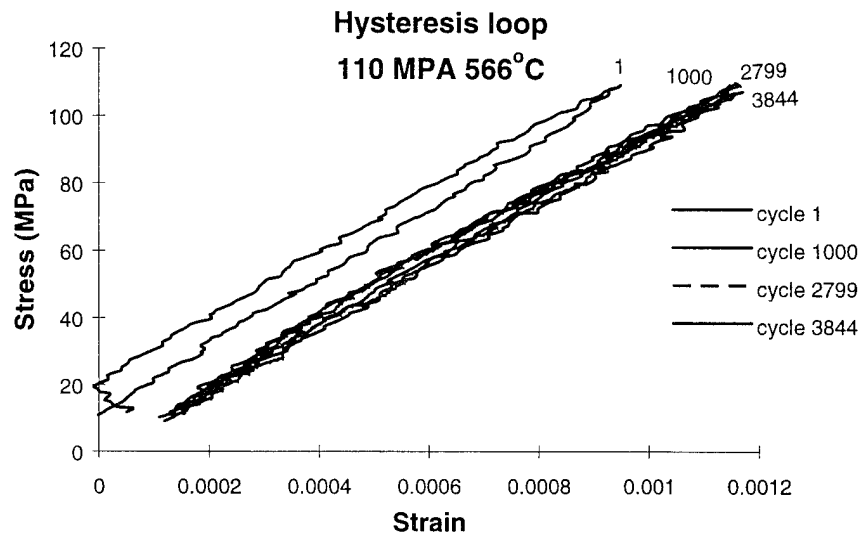


Figure 79. Hysteresis: 110 MPa, 566C

1093°C Isothermal

Figure 80 shows the hysteresis loops of isothermal cycling at 1093°C, with a maximum stress of 100 MPa. The first few curves are open with a relatively large area inside. The remainder of the curves are very narrow, with just a small amount of hysteresis. The curves do migrate over the life of the specimen, indicating much more strain ratcheting than the tests at 566°C.

Summary

In summary, under in-phase TMF conditions, the loops tend to be slightly open, mostly due to the energy absorbing effects of damage accumulation. There is a large amount of ratcheting, with a dependence on maximum stress. These out-of-phase TMF tests are relatively wide, showing the effects of energy lost due to friction of fiber sliding,

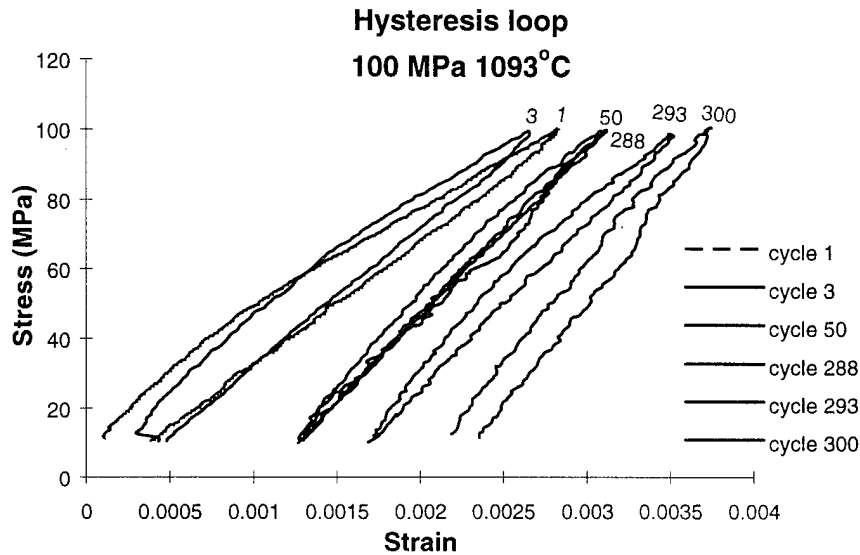


Figure 80. Hysteresis: 100 MPa, 1093°C

as well as damage accumulation. The movement was negligible, indicating very little strain ratcheting.

Under isothermal conditions, the stress-strain hysteresis curves show a small area within the loops, and very little movement. At higher temperatures, the loops were more open, showing the effect of residual stresses on fiber sliding. They also tended to migrate more at the higher temperature. The material is not absorbing much energy relative to the TMF conditions. The orientation does show some decrease in slope over time, indicating a loss in modulus due to damage accumulation. The loops are closed, indicating almost full strain recovery.

Damage Mechanisms

The failure mechanisms were investigated using post-mortem microscopic examination of specimens. The fracture surface, the fiber pull-out and the fiber condition

were viewed using the scanning electron microscope. Damage to the specimen that did not produce failure was also examined by looking at the polished edge of the specimen under an optical microscope.

Metals typically have a large plastic region where internal defects move about. Ceramics do not exhibit this behavior and experience brittle failure. Fiber reinforcement allows ceramic matrix composites to behave in a plastic fashion. Ceramic matrix composites are unusual in that the ultimate strain of the fibers is greater than the ultimate strain of the matrix. The initial damage in these ceramic matrix composites is matrix cracking. Weak interfacial bonds allow some fiber sliding relative to the matrix. This results in crack deflection, frictional fiber sliding, crack bridging and fiber pull-out. Ultimate failure is a result of fiber failure. These properties allow the very brittle ceramic to behave in almost a metallic fashion. They add toughness to the material by absorbing energy, making the stress strain response nonlinear. Prolonged exposure to elevated temperatures can, however, cause the fiber/matrix interface to oxidize, embrittling it. This also makes it stronger, preventing debonds, and not allowing fiber sliding. The embrittlement reduces the toughness of the laminate. The high temperature TMF environment can also degrade the fibers, making them weaker. The fibers fail easily and in a brittle fashion. Ultimate failure is a result of fiber failure.

A visual evaluation of the fracture surface of the specimens gives insight to the mechanisms that occur during its life. A side view of the specimens shows the damage accumulation as well as the nature of the cracking that occurred. A mesoscopic view of

the entire fracture surface provides the damage condition and the extent of fiber pull-out. A closer, microscopic view of the fibers indicates the fiber condition at failure.

In-Phase TMF

Under in-phase TMF conditions, the time to failure was inversely proportional to the stress level. The previous section dealing with fatigue life shows this clearly. A lower stress level increases the exposure time and the fiber/matrix bond becomes highly oxidized when final failure occurs. This is shown by the great deal of fiber pull out at high stress levels, and the very flat fracture surfaces at low stress levels.

Figure 81 shows the fracture surface of the in-phase TMF test run at a maximum stress level of 145 MPa. The fiber pull-out is long and the fracture surface is slightly irregular. The long fiber pull-out indicates the fiber/matrix interface was weak, and allowed fiber pull-out and crack bridging. The debond between the fibers and the matrix deflected the crack tips, resulting in the uneven surface. Final failure was fiber controlled, with a great deal of damage and energy absorption.

The fracture surface under in-phase TMF conditions at 135 MPa, shown in Figure 82, had long fiber pull out indicating the weak interfacial bond that is desired for a high toughness composite. The surface is slightly irregular, the irregularity is due to the high number of matrix cracks that form in the ninety degree plies. Most of these cracks form in the first cycle, but cannot propagate due to debond between the fiber and matrix.

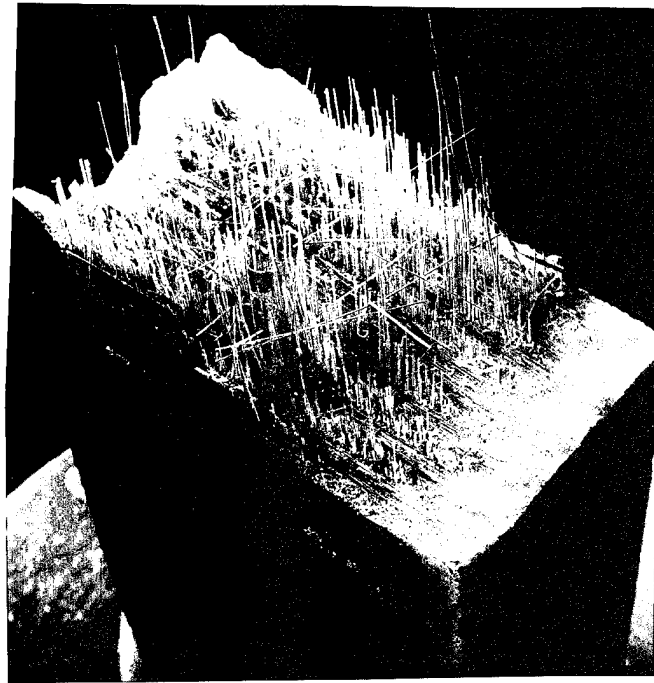


Figure 81. In-Phase TMF: 145 MPa, Fracture Surface, 12x

The in-phase TMF test at 120 MPa again exhibits fiber pull-out, showing the environment had not fully oxidized the fiber/matrix interface. The edges had no fiber pull-out, showing the fiber/matrix interface at the edges had been oxidized, making it strong but brittle. The oxidation allowed cracks to propagate from the matrix to the fibers, breaking the fibers level with the matrix failure. This can be seen in Figure 83. The surface is planar, except a small region seen in the lower left side of the photograph. This shows a combination of fiber controlled failure and matrix controlled failure controlled the fatigue life at this stress level.

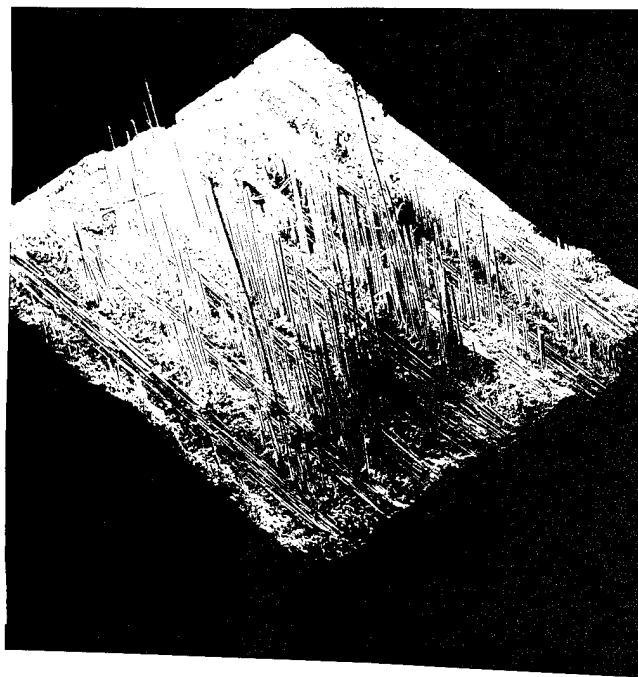


Figure 82. In-Phase TMF: 135 MPa, Fracture Surface, 13x

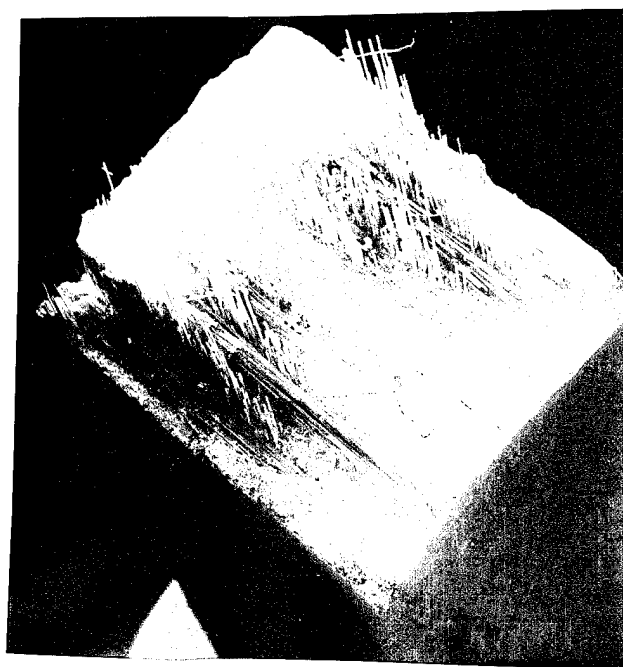


Figure 83. In-Phase TMF: 120 MPa Fracture Surface, 12x

The surface at 105 MPa shows very little fiber pull-out. The fracture surface, shown in Figure 84, is slightly irregular. The failure was matrix controlled phenomenon. Figure 85 shows the polished edge of the same specimen, looking at the ends of the ninety degree plies. This shows the typical damage accumulation of the matrix cracking in the ninety degree plies. This is in the form of small cracks in the matrix material, and is consistent with the results from the previous section dealing with modulus degradation. Most of the cracks form in the first couple of cycles, and soon afterwards the matrix becomes saturated with cracks. As these matrix cracks accumulate, the stiffness of the material declines, which is manifested in a reduction of the modulus of elasticity.

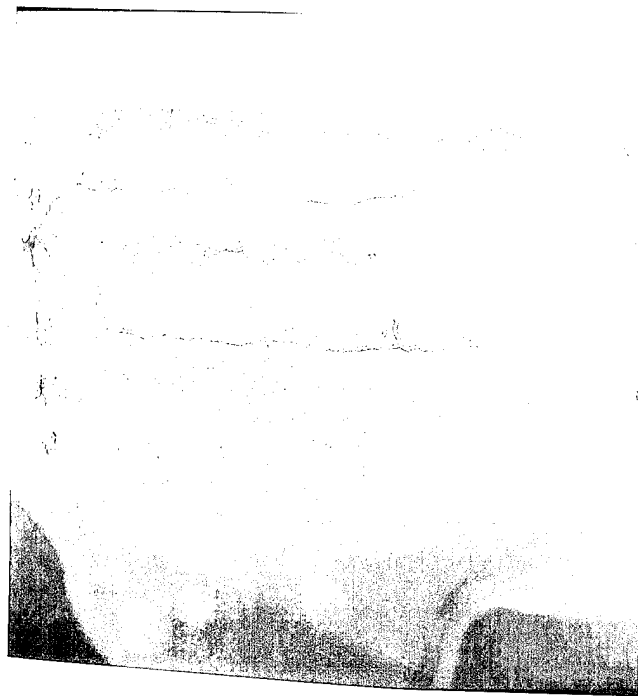


Figure 84. In-Phase TMF: 105 MPa, 13x



Figure 85. In-Phase TMF: 105 MPa, Damage Accumulation, 100x

At a maximum stress of 100 MPa, Figure 86 shows the fracture surface is level with no fiber pull-out. The fibers show concoidal fracture in Figure 87, typical of brittle materials. The matrix cracking was uninhibited by the fibers and went straight through them, as seen in Figure 88. This is evidence of the undesirable strong interfacial bond that occurs with oxidation. The cracks also crossed the ply interfaces easily. This failure was a matrix controlled phenomenon.

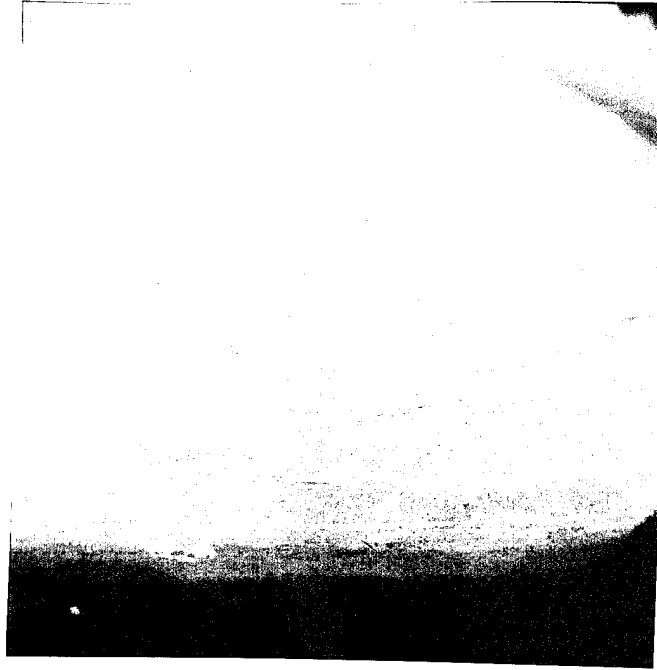


Figure 86. In-Phase TMF: Fracture Surface, 100 MPa, 13x

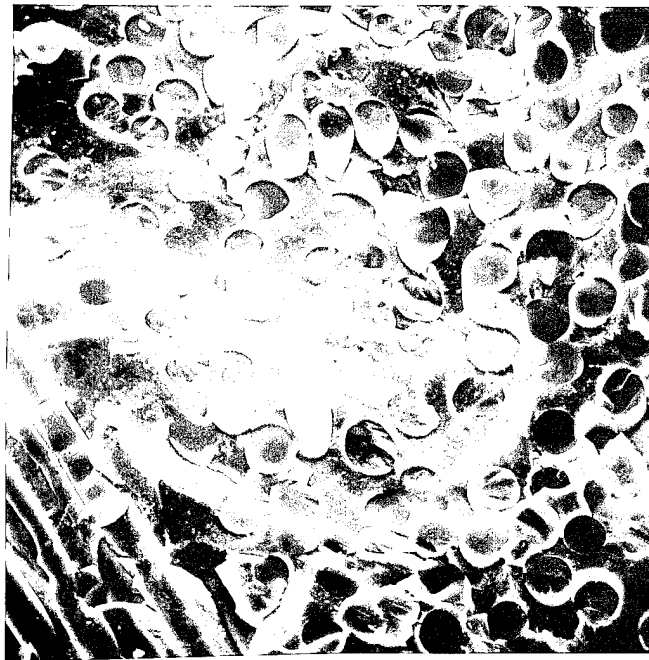


Figure 87. In-Phase TMF: 100 MPa, Concoidal Fiber Fracture, 600x

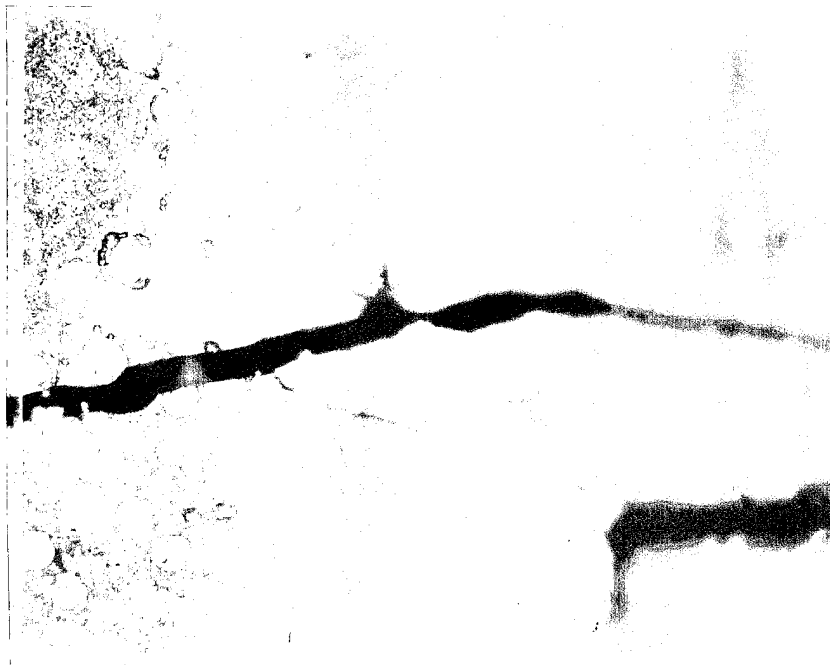


Figure 88. In-Phase TMF: 100 MPa, Matrix Crack, 100x

Out-of-Phase TMF

Out-of-phase TMF tests show signs of environmental effects, as well as damage accumulation due to the mechanical fatigue. There are several factors involved with TMF cycling that reduce fiber strength, oxidation of the fiber/matrix interface, abrasion of the fiber caused by fiber sliding and oxidation of the fiber. Oxidation of the interface is time and temperature dependent; the accumulation of cracks can accentuate this problem. Abrasion occurs gradually, with each cycle caused by the sliding along the interfaces. It is most detrimental in out-of-phase TMF which accentuates the sliding.

With more time at elevated temperature, the failure behavior changes from a fiber controlled failure, to a matrix controlled failure. The fiber controlled failure is damage tolerant and plastic like, where the matrix controlled failure is brittle and abrupt.

The failure mechanisms seen in the out-of-phase TMF specimens indicate the material properties seemed to degrade much quicker than the in-phase TMF specimens. The maximum stress level occurs at the minimum temperature point. This is the point of highest residual stresses, causing more damage to the matrix. This also allows the environmental effects to propagate rapidly through the composite due to paths provided by open matrix cracks.

Figure 89 shows the fracture surface of the specimen tested under out-of-phase TMF conditions at a maximum stress level of 145 MPa. There is extensive fiber pull-out, as well as an irregular fracture surface. This indicates a large amount of fiber sliding with



Figure 89. Out-of-Phase TMF: 145 MPa, Fracture Surface, 12x

respect to the surrounding matrix. This sliding absorbs large amounts of energy, which is reflected in the previous section dealing with stress-strain hysteresis. The fibers, shown in Figure 90, have a very little degradation. The short amount of exposure time did not allow for the temperature effects to damage the fibers.

The fracture surface of the out-of-phase TMF test at 110 MPa is shown in Figure 91. The fracture surface is smooth, with a small amount of short fiber pull-out. The fibers were weakened by a combination of fiber oxidation and frictional sliding. This reduces the amount of fiber bridging, and the fiber pull-out is much shorter. The weaker fibers have higher numbers of breaks, allowing for a more matrix controlled failure, resulting in a planar fracture surface.



Figure 90. Out-of-Phase TMF: 145 MPa, Fiber Condition, 600x

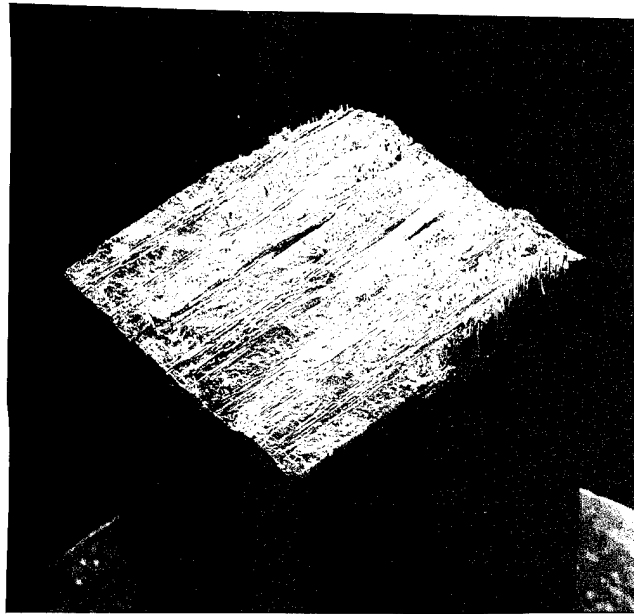


Figure 91. 110 MPa, Out-of-Phase TMF, fracture surface, 11x

Figure 92 shows the fracture surface of the specimen tested under out-of-phase TMF conditions at a maximum stress level of 83 MPa. The fracture surface is even, but there is still a small amount of fiber pull-out. The condition of the fibers in Figure 93 indicates that they have degraded. The fiber degradation is due to the frictional sliding that wears the interface, allowing the fibers to oxidize quickly. This oxidation weakens the fibers, causing the failure to be matrix controlled, and thus the fracture surface is planar.



Figure 92. Out-of-Phase TMF: 83 MPa, Fracture Surface, 13x

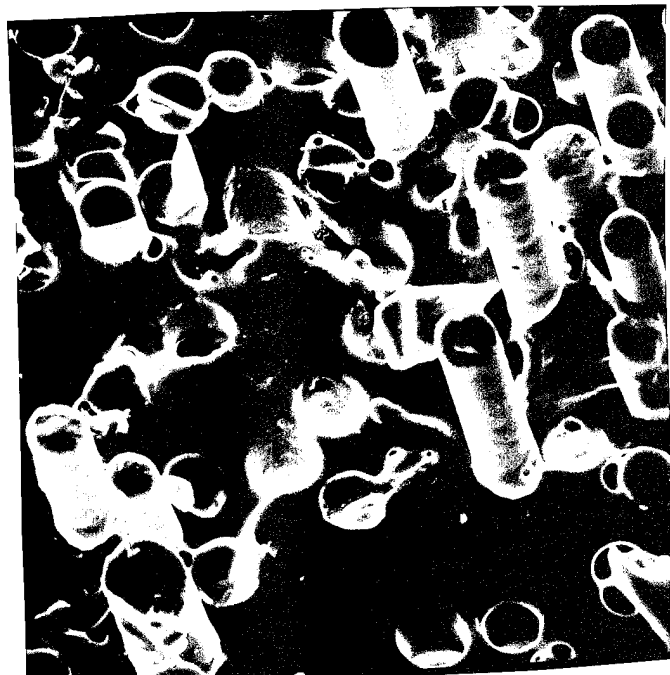


Figure 93. Out-of-Phase TMF: 83 MPa, Fiber Condition, 600x

Figure 94 shows the typical deflection of a matrix crack. This is at a stress level of only 83 MPa, and may seem to contradict the previous statement that there is a strong mechanically created interfacial bond, but consider that the time to failure was also very short, and the interface had not oxidized yet. The fiber and matrix could still move relative to each other when the temperature was at a maximum. This crack could have also formed in the first couple of cycles.

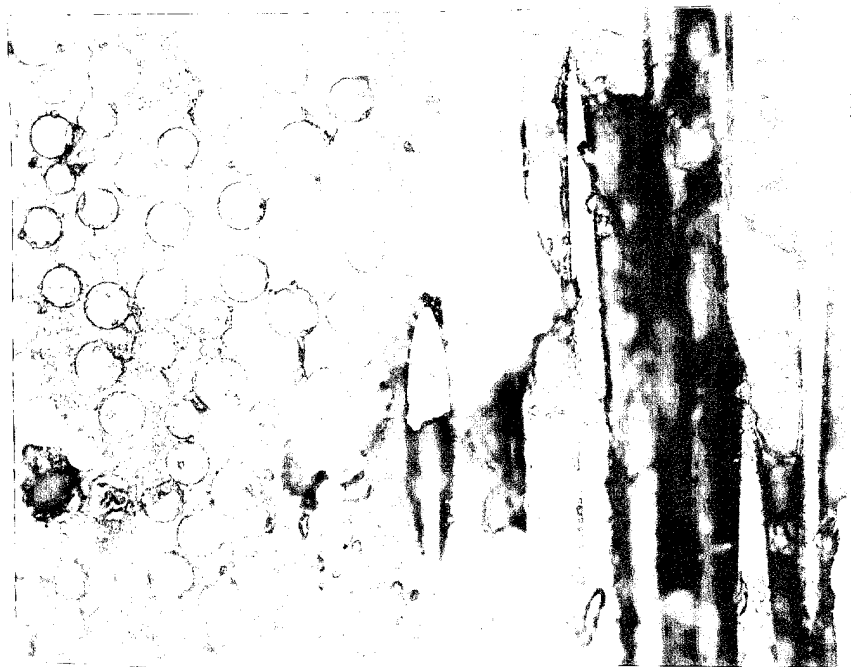


Figure 94. Out-of-Phase TMF: 83 MPa, Debond, Crack Deflection, 100x

Isothermal Fatigue

Under isothermal conditions the residual thermal stresses do not cycle, hence reducing their impact. As a result the predominant mechanism was the time dependent high temperature oxidation. The fiber/matrix interface oxidized much quicker at 1093°C than at 566°C. The specimens under isothermal fatigue condition followed the same trend of fiber controlled failure at high stress levels, and matrix controlled failure at low stress levels, as in the case of TMF conditions.

566°C Isothermal

The fracture surface of the test conducted at 160 MPa under isothermal conditions of 566°C is shown in Figure 95. There is long fiber pull out, but the fibers get shorter close to the free edge, until there is no fiber pull out at all at the free edge. The oxygen is diffusing through the specimen, and the edges become oxidized first, making a brittle structure near the edges.

At higher stress levels, the material failed quickly. As Figure 96 shows, there was a great deal of fiber pull-out under isothermal conditions at 566°C, 133 MPa. The failure surface is jagged, and the plies failed at different locations. The final failure was fiber controlled. This is evidence of the weaker interfacial bond, that allows the fibers to move relative to the matrix, absorbing energy, and deflecting the matrix crack. A typical crack is shown in Figure 97. Note how the crack circumvents the transverse fibers. The fibers remain undamaged by either cracks or oxidation. Figure 98 shows a couple of

undamaged fibers from the 133 MPa 566°C test. The fibers retain their strength because the time to failure is short enough to prevent oxidation of the fiber.



Figure 95. Isothermal Fatigue 566°C: 160 MPa, Fracture Surface, 11x



Figure 96. Isothermal Fatigue 566°C: 133 MPa, Fiber Pull-Out, 550x



Figure 97. Isothermal Fatigue 566°C: 133 MPa, Matrix Crack Deflection, 100x



Figure 98. Isothermal Fatigue 566°C: 133 MPa, Fiber Condition, 1020x

1093°C Isothermal

Specimens tested under isothermal fatigue conditions at 1093°C showed the environmental effects permeated much quicker than at 566°C, or TMF testing. At a slightly higher stress level, short fiber pull-out is beginning to occur, although not much, as seen in Figure 99. The fracture surface, Figure 100, is still fairly clean, although rougher than the surface at 100 MPa. Matrix cracks that accumulate in the ninety degree plies do not so easily propagate into the 0 degree plies. Although they are difficult to see, penetrant shows the evidence of numerous matrix cracks that accumulated during the cycling of this specimen, in Figure 101.

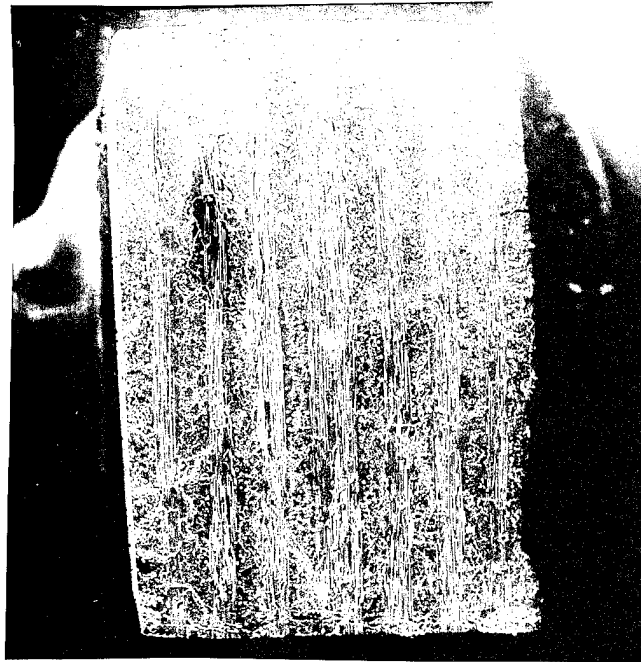


Figure 99. 1093°C Isothermal Fatigue: 115 MPa, Short Fiber Pull-Out, 12x

At low stress levels, the specimens were exposed to the high temperature environment much longer, causing oxidation of the fiber matrix interface. This toughened the bond, which then caused the composite to behave essentially as a monolithic ceramic, where cracks propagate uninhibited, and there is no plasticity, and thus no toughness. The isothermal fatigue specimen tested at 100 MPa and 1093°C shows this effect. This is also reflected by a very small area within the hysteresis loops, shown in a previous section. Figure 102 shows how cracks went easily through the material transverse to the load, through the matrix, across the 90 degree fibers, across the ply interface and straight through the 0 degree fibers. The fracture surface is clean, with no fiber pullout, as shown in Figure 103. Figure 104 shows the damaged fibers as result of oxidation.

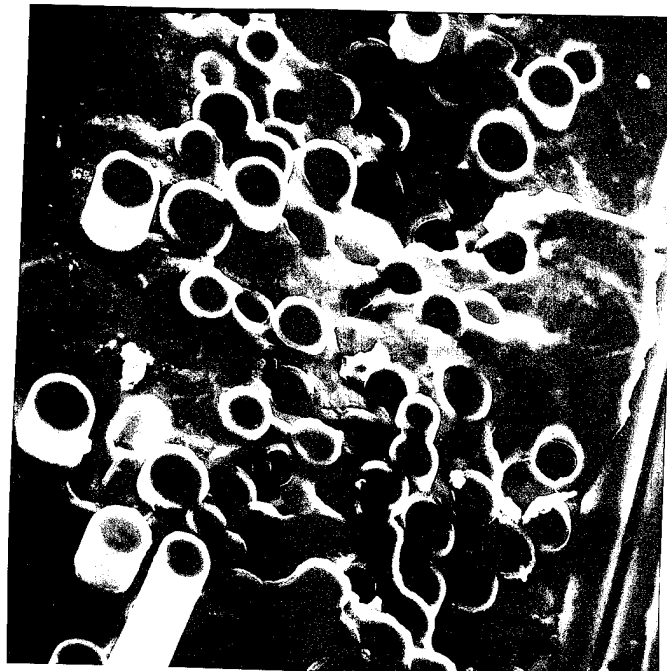


Figure 100. 1093°C Isothermal Fatigue: 115 MPa, Fracture Surface, 550x



Figure 101. 1093°C Isothermal Fatigue: 115 MPa, Matrix Crack Accumulation, 10x



Figure 102. 1093°C Isothermal Fatigue: 100 MPa, Matrix and Fiber Crack, 100x



Figure 103. 1093°C Isothermal Fatigue: 100 MPa, Clean Fracture Surface, 12x



Figure 104. 1093°C Isothermal Fatigue: 100 MPa, Fiber Condition, 550x

Summary

In summary, the typical failure at the higher stress level is fiber controlled, with the material exhibiting the tough characteristics that are desired with the fiber reinforcement of the ceramic. These tough characteristics are caused by energy absorbing mechanisms, such as frictional fiber sliding, and crack bridging by the fibers. The absorbed energy results in the hysteresis of the stress-strain curves. Damage occurred in the form of matrix cracks which could not propagate through the composite due to the debonds between the fiber and the matrix. This damage accumulation manifests itself in the form of strain accumulation. The damage occurs quickly, very early in the life of the specimen, and results in a modulus of elasticity that degrades very rapidly and then levels off. High temperature effects cause the fiber/matrix interface to oxidize, resulting in a matrix controlled failure. This matrix controlled failure is characterized by a planar surface, with little or no fiber pull-out. The planar surface is due to easy crack propagation through both fiber and matrix. This is a result of the oxidation of the fiber/matrix interface. When the interface is oxidized, it becomes strong, but brittle, which cannot stop cracks from propagating. This alters the material characteristics such that the failure stress becomes lower with a high number of cycles. This can be seen in the fatigue life curves, which reflect the downward trend of failure stress with higher cycles. The fatigue life curves also show the environmental effects on the composite. A harsher environment allows a faster oxidation, thus reducing the failure strength in a fewer number of cycles.

In-phase TMF conditions allow for oxidation of the interface over time. The combination of thermal stresses and mechanical stresses do not allow for easy fiber sliding, thus there is less energy absorbed per cycle, and the fibers do not degrade in strength much because the lack of frictional sliding limits the abrasion of the fibers. The cyclic mechanical loading causes matrix cracking, which allows for more rapid oxidation of the fibers. The in-phase TMF conditions are the least damaging, only the isothermal condition at 566°C is less damaging, simply because the environment is less severe at 566°C than a cycling temperature between 566°C and 1093°C.

Out-of-phase TMF conditions are much more damaging to the material. The residual stresses increase fiber sliding. This is evident from the large hysteresis effects observed in out-of-phase loading. Also, this sliding abrades the fiber surface, allowing the fiber to oxidize. This causes the strength of the composite to degrade rapidly, which is reflected in the modulus degradation discussed in a previous section.

Isothermal conditions do not have the change in residual stresses during cycling that are present in the TMF tests. This reduces the damage mechanisms to time dependent environmental effects. The higher temperature of 1093°C is a harsher environment than 566°C, and thus the composite degrades more rapidly. The degradation is caused chiefly by the oxidation of the fiber/matrix interface. Higher temperatures cause a more rapid oxidation. This oxidation causes the normally weak interface to become stronger and more brittle. Cracks that are normally stopped by the debond between the fiber and the matrix are unabated and propagate easily across the material,

resulting in a matrix controlled failure that is similar to the brittle failure of a monolithic ceramic.

V. Conclusions

The purpose of this study was to investigate the thermo-mechanical fatigue behavior and damage mechanisms of a model ceramic matrix composite with a cross-ply lay-up. The material was a potassium borosilicate glass (BSG) doped (5%) magnesium aluminosilicate (MAS) cordierite matrix reinforced with Nicalon fibers in a $[0/90]_{4s}$ lay-up. The composite had 39 percent fiber by volume. The BSG dopant serves as a source of boron which alters the fiber matrix interface, increasing its resistance to oxidation.

Monotonic tensile tests to failure were performed at two temperatures, 566°C and 1093°C. Thermo-mechanical fatigue testing between 566°C and 1093°C was performed under in-phase and out-of-phase conditions, at a various maximum stress levels.

Isothermal tests at 566°C and 1093°C were also performed at various maximum stress levels. All fatigue tests had a load ratio of 0.1 and a period of 180 seconds.

The experimental data was analyzed in the form of S-N curves, S-T curves, strain data, modulus degradation, and stress-strain hysteresis. A scanning electron microscope was then used to examine the fracture surface. From these, the fatigue behavior and damage mechanisms were inferred for all four fatigue conditions.

The S-N and S-T curves indicated that the thermo-mechanical fatigue life was not dependent on the number of cycles, but more on the total exposure time. The in-phase TMF fatigue life was almost equal to the isothermal fatigue life at 1093°C temperatures. The out-of-phase TMF life was consistently one twentieth of the fatigue life under isothermal conditions at 566°C. The fatigue life data also indicated that there were more

than one mechanism occurring, depending on the stress level. At higher stresses, the failure was fiber controlled phenomenon, and at lower stresses, the failure was matrix controlled phenomenon. The stress level that marked the transition between the two damage mechanisms varied according to the fatigue conditions. The transition for in-phase TMF was at 120 MPa, as was the transition for the isothermal fatigue at 1093°C. The transition for out-of-phase TMF was at 90 MPa. The transition for isothermal fatigue at 566°C was at 145 MPa. The threshold for failure under TMF conditions was found to be 60 MPa, which was also the proportional limit at 1093°C under static tensile loading.

VI. Recommendations

Further research should include tests at a variety of temperatures, to find the temperature threshold of the material. The effect of thickness should be investigated. A thinner specimen would be less likely to include existing flaws, but a thicker specimen would take longer for the oxidation to permeate through the entire laminate. There is also the difference between plane stress and plane strain, which would occur with a thicker specimen. Thermo-mechanical fatigue should be investigated in an argon environment, and compared to this data, to determine the effects of oxygen on the material. An analytical study of this material should be made.

Bibliography

1. Butkus, L.M. and Holmes, J.W. Thermomechanical Fatigue of Nicalon-Reinforced Calcium Aluminosilicate Glass-Ceramic. Abstract No.. CB92-134, Ceramic Composites Research Laboratory, University of Michigan
2. Daniel, I.M., Anastassopoulos, G. and Lee, J.W. The Behavior of Ceramic Matrix Fiber Composites Under Longitudinal Loading. Composites Science and Technology 46: 105-113 1993.
3. Grant, S., Fatigue Behavior of a Cross-Ply Ceramic Matrix Composite Subjected to Tension-Tension Cycling with Hold Time, MS Thesis AFIT/GAE/ENY/94D-1, Graduate School of Engineering, Air Force Institute of Technology (AETC), Wright-Patterson AFB, Ohio, December 1994.
4. Hurwitz, F. I. "Ceramic Matrix Composites; Ceramic Fiber Reinforced." International Encyclopedia of Composites v1, New York: VHC Publisher, 1990.
5. Ishikawa, T. Recent Developments of the SiC Fiber Nicalon and Its Composites, Including Properties of the SiC Fiber Hi-Nicalon for Ultra-High Temperature. Composites Science and Technology 51: 135-144 1994.
6. Karandikar, P. and Chou T. Characterization And Modeling Of Microcracking And Elastic Moduli Changes In Nicalon/CAS Composites. Composites Science and Technology 46: 253-263 1992.
7. Larsen, D.C. Thermally Durable Glass-Ceramic Matrix Composites: Interim Report, 13 December 1992. Contract F33615-90-C-5909. Corning, New York: Corning Inc., December 1992 (P-92-222-13-TP).
8. Mall, S. and Kim, R.Y., Failure Mechanisms In Laminates Of Silicon Carbide/Calcium-Aluminosilicate Ceramic Composite. Composites 23: 215-222 1992.
9. Mall, S. and Schubbe J.J. Thermomechanical Fatigue Behavior of a Cross-Ply SCS-6/Ti-15-3 Metal Matrix Composite. Composites Science and Technology 50: 49-57 1994.
10. Nair, S.V. and Jakus, K. High Temperature Mechanical Behavior of Ceramic Composites. Butterworth-Heinemann, Newton, MA 1995.
11. Powell, K.L., Smith, P.A. and Yeomans, J.A. Aspects of Residual Thermal Stresses in Continuous-Fibre-Reinforced Ceramic Matrix composites. Composites Science and Technology 47: 359-367 1993.

12. Prewo, K.M., Brennan J.J., and Layden G.K. Silicon Carbide Fiber Reinforced Glass-Ceramics For High Performance Applications. American Ceramic Society Bulletin 65: 305-313 1986.
13. Simon, G. and Bunsell, A.R. Mechanical Behavior And Structural Characterization Of The Nicalon Silicon Carbide Fibres. Journal of Materials Science 19: 3649-3657 1984.
14. Simon, G. and Bunsell, A.R. Creep Behavior And Structural Characterization At High Temperatures Of Nicalon SiC Fibers. Journal of Materials Science 19: 3658-3670 1984.
15. Steiner, C., Fatigue Behavior of a Cross-Ply Ceramic Matrix Composite at Elevated Temperature Under Tension-Tension Loading, MS Thesis AFIT/GAE/ENY/94D, Graduate School of Engineering, Air Force Institute of Technology (AETC), Wright-Patterson AFB, Ohio, December 1994.
16. Toreki W., Batich, C.D., Sacks, Slaem, M., Choi, G.J., and Morrone, A.A. Polymer derived Silicon Carbide Fibers with Low Oxygen Content and Improved Thermomechanical Stability. Composites Science and Technology 51: 145-159 1992.
17. Worthem, D. W. Thermomechanical Fatigue Behavior of Three Ceramic Matrix Composites. Contract NAS3-25266. Brookpark, OH: Sverdup Technology, Inc. 1993.
18. Worthem D.W. and Ellis J.R. Thermomechanical Fatigue of Nicalon/CAS Under In-Phase and Out-of-Phase Cyclic loadings. CP-10104, 5th Annual HITEMP Review, NASA Lewis Research Center, Cleveland OH 1992.

APPENDIX A

This appendix contains the calculations for the lamina (ply) properties of Nicalon/MAS-5.

These calculations were based on a simple rule of mixtures.

The laminate properties were then calculated from the lamina properties, based on a $[0/90]_{4s}$

lay-up. The significant properties are Elastic Modulus, Coefficient of Thermal Expansion (CTE), and the A matrix.

Calculate lamina properties

$$E_f := 200 \cdot 10^9 \quad E_m := 138 \cdot 10^9 \quad t := .1275 \cdot .0254$$

$$t = 0.00324$$

$$v_f := .25 \quad v_m := .25$$

$$v_f := .39 \quad v_m := .61$$

$$G_f = \frac{E_f}{2 \cdot (1 + v_f)} = 8 \cdot 10^{10}$$

$$\alpha_f := 4 \cdot 10^{-6} \quad \alpha_m := 2.4 \cdot 10^{-6}$$

$$G_f := 8 \cdot 10^{10} \quad G_m := 5.52 \cdot 10^{10}$$

$$G_m = \frac{E_m}{2 \cdot (1 + v_m)} = 5.52 \cdot 10^{10}$$

$$E_1 = E_f \cdot v_f + E_m \cdot v_m = 1.6218 \cdot 10^{11}$$

$$v_f \cdot v_f + v_m \cdot v_m = 0.25$$

$$E_2 = \frac{E_f \cdot E_m}{E_f \cdot v_m + E_m \cdot v_f} = 1.56979 \cdot 10^{11}$$

$$G_{12} = \frac{G_f \cdot G_m}{G_f \cdot v_m + G_m \cdot v_f}$$

$$v_{21} = \frac{1.57 \cdot 10^8}{1.622 \cdot 10^8} \cdot 0.25 = 0.24199$$

$$G_{12} = 6.27915 \cdot 10^{10}$$

$$\alpha_1 = \frac{\alpha_f \cdot E_f \cdot v_f + \alpha_m \cdot E_m \cdot v_m}{E_f \cdot v_f + E_m \cdot v_m} \quad \alpha_1 = 3.16952 \cdot 10^{-6}$$

Calculate Laminate properties

Values for constants

$$E_1 := 1.622 \cdot 10^{11} \quad E_2 := 1.57 \cdot 10^{11} \quad G_{12} := 6.279 \cdot 10^{10} \quad v_{21} := 0.242$$

$$v_{12} := .25 \quad t = 0.00324 \quad \alpha_2 := (1 + v_f) \cdot \alpha_f \cdot v_f + (1 + v_m) \cdot \alpha_m \cdot v_m - \alpha_1 \cdot v_{12}$$

$$\alpha_2 = 2.98762 \cdot 10^{-6}$$

Q matrix (stiffness) plane stress

$$\begin{bmatrix} \frac{E_1}{1 - \nu_{12} \cdot \nu_{21}} & \frac{\nu_{12} \cdot E_2}{1 - \nu_{12} \cdot \nu_{21}} & 0 \\ \frac{\nu_{12} \cdot E_2}{1 - \nu_{12} \cdot \nu_{21}} & \frac{E_2}{1 - \nu_{12} \cdot \nu_{21}} & 0 \\ 0 & 0 & G_{12} \end{bmatrix} = \begin{bmatrix} 1.72645 \cdot 10^{11} & 4.17775 \cdot 10^{10} & 0 \\ 4.17775 \cdot 10^{10} & 1.6711 \cdot 10^{11} & 0 \\ 0 & 0 & 6.279 \cdot 10^{10} \end{bmatrix}$$

$$Q := \begin{bmatrix} 1.726 \cdot 10^{11} & 4.178 \cdot 10^{10} & 0 \\ 4.178 \cdot 10^{10} & 1.671 \cdot 10^{11} & 0 \\ 0 & 0 & 6.279 \cdot 10^{10} \end{bmatrix}$$

generate Qbar 90 $\theta := \frac{\pi}{2}$

$$\alpha_{px} := \alpha_1 \cdot \cos(\theta)^2 + \alpha_2 \cdot \sin(\theta)^2$$

$$\alpha_{px} = 2.98762 \cdot 10^{-6}$$

$$\alpha_{py} := \alpha_2 \cdot \cos(\theta)^2 + \alpha_1 \cdot \sin(\theta)^2$$

$$\alpha_{py} = 3.16952 \cdot 10^{-6}$$

$$\alpha_{p6} := 2 \cdot \sin(\theta) \cdot \cos(\theta) \cdot (\alpha_1 - \alpha_2)$$

$$\alpha_{p6} = 0$$

T 90

T neg trans matrix

$$\begin{bmatrix} \cos(\theta)^2 & \sin(\theta)^2 & \sin(\theta) \cdot \cos(\theta) \\ \sin(\theta)^2 & \cos(\theta)^2 & -\sin(\theta) \cdot \cos(\theta) \\ -2 \cdot \sin(\theta) \cdot \cos(\theta) & 2 \cdot \sin(\theta) \cdot \cos(\theta) & \cos(\theta)^2 - \sin(\theta)^2 \end{bmatrix} = \begin{bmatrix} 0 & 1 & 0 \\ 1 & 0 & 0 \\ 0 & 0 & -1 \end{bmatrix}$$

$$T_{negt} := \begin{bmatrix} 0 & 1 & 0 \\ 1 & 0 & 0 \\ 0 & 0 & -1 \end{bmatrix}$$

$$T^- := \begin{bmatrix} \cos(\theta)^2 & \sin(\theta)^2 & -2 \cdot \sin(\theta) \cdot \cos(\theta) \\ \sin(\theta)^2 & \cos(\theta)^2 & 2 \cdot \sin(\theta) \cdot \cos(\theta) \\ \sin(\theta) \cdot \cos(\theta) & -\sin(\theta) \cdot \cos(\theta) & \cos(\theta)^2 - \sin(\theta)^2 \end{bmatrix} = \begin{bmatrix} 0 & 1 & 0 \\ 1 & 0 & 0 \\ 0 & 0 & -1 \end{bmatrix}$$

$$T_{neg} := \begin{bmatrix} 0 & 1 & 0 \\ 1 & 0 & 0 \\ 0 & 0 & -1 \end{bmatrix}$$

$$Qbar = T_{neg} \cdot Q \cdot T_{negt} = \begin{bmatrix} 1.671 \cdot 10^{11} & 4.178 \cdot 10^{10} & 0 \\ 4.178 \cdot 10^{10} & 1.726 \cdot 10^{11} & 0 \\ 0 & 0 & 6.279 \cdot 10^{10} \end{bmatrix}$$

$$Qp := \begin{bmatrix} 1.671 \cdot 10^{11} & 4.178 \cdot 10^{10} & 0 \\ 4.178 \cdot 10^{10} & 1.726 \cdot 10^{11} & 0 \\ 0 & 0 & 6.279 \cdot 10^{10} \end{bmatrix}$$

generate A matrix

$$A := (8 \cdot Q + 8 \cdot Qp) \cdot t \quad h := t \cdot 16$$

$$A = \begin{bmatrix} 8.80095 \cdot 10^9 & 2.16487 \cdot 10^9 & 0 \\ 2.16487 \cdot 10^9 & 8.80095 \cdot 10^9 & 0 \\ 0 & 0 & 3.25353 \cdot 10^9 \end{bmatrix}$$

$$E_{xx} := \frac{1}{h} \cdot \frac{[A_{0,0} \cdot A_{1,1} \cdot A_{2,2} - A_{0,0} \cdot (A_{1,2})^2 - (A_{0,1})^2 \cdot A_{2,2} + 2 \cdot A_{0,1} \cdot A_{0,2} \cdot A_{1,2} - (A_{0,2})^2 \cdot A_{1,1}]}{[A_{1,1} \cdot A_{2,2} - (A_{1,2})^2]}$$

$$E_{xx} = 1.59573 \cdot 10^{11}$$

$$v_{xy} := \frac{(A_{0,1} \cdot A_{2,2} - A_{0,2} \cdot A_{1,2})}{[A_{1,1} \cdot A_{2,2} - (A_{1,2})^2]} \quad v_{xy} = 0.24598 \quad \alpha := \begin{bmatrix} \alpha_1 \\ \alpha_2 \\ 0 \end{bmatrix} \quad \alpha_p := \begin{bmatrix} \alpha_{px} \\ \alpha_{py} \\ \alpha_{p6} \end{bmatrix}$$

$$N := 8 \cdot t \cdot (Q \cdot \alpha + Qp \cdot \alpha_p) \quad N = \begin{bmatrix} 3.3772 \cdot 10^4 \\ 3.3772 \cdot 10^4 \\ 3.6236 \cdot 10^{-14} \end{bmatrix}$$

$$E_{yy} := \frac{1}{h} \cdot \frac{[A_{0,0} \cdot A_{1,1} \cdot A_{2,2} - A_{0,0} \cdot (A_{1,2})^2 - (A_{0,1})^2 \cdot A_{2,2} + 2 \cdot A_{0,1} \cdot A_{0,2} \cdot A_{1,2} - (A_{0,2})^2 \cdot A_{1,1}]}{[A_{0,0} \cdot A_{2,2} - (A_{0,2})^2]}$$

$$E_{yy} = 1.59573 \cdot 10^{11}$$

$$v_{xy} = \frac{(A_{0,1} \cdot A_{2,2} - A_{0,2} \cdot A_{1,2})}{[A_{0,0} \cdot A_{2,2} - (A_{0,2})^2]} = 0.24598 \quad v_{xy} = 0.24598$$

$$G_{xy} := \frac{1}{h} \cdot \frac{[A_{0,0} \cdot A_{1,1} \cdot A_{2,2} - A_{0,0} \cdot (A_{1,2})^2 - (A_{0,1})^2 \cdot A_{2,2} + 2 \cdot A_{0,1} \cdot A_{0,2} \cdot A_{1,2} - (A_{0,2})^2 \cdot A_{1,1}]}{[A_{0,0} \cdot A_{1,1} - (A_{0,1})^2]}$$

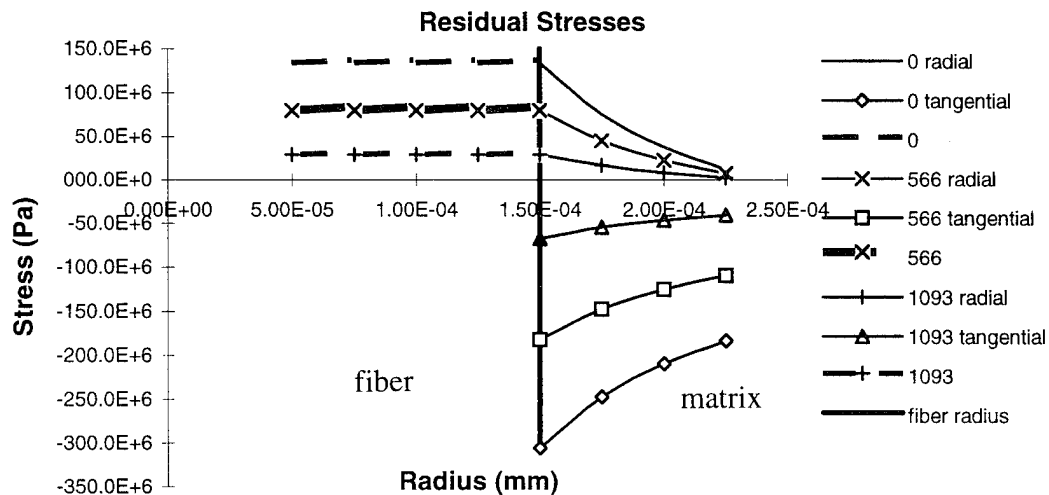
$$G_{xy} = 6.279 \cdot 10^{10}$$

$$\alpha_x := \frac{A_{1,1} \cdot N_0 - A_{0,1} \cdot N_1}{A_{0,0} \cdot A_{1,1} - (A_{0,1})^2} \quad \alpha_x = 3.07975 \cdot 10^{-6} \quad \alpha_y := \frac{-(A_{0,1} \cdot N_0 - A_{0,0} \cdot N_1)}{A_{0,0} \cdot A_{1,1} - (A_{0,1})^2} \quad \alpha_y = 3.07975 \cdot 10^{-6}$$

APPENDIX B

This appendix contains figures graphically representing the results of calculations for the residual stresses between the fibers and matrix in this composite. The reference temperature is 1400°C. The calculations were based on a basic elasticity problem of a cylinder within a cylinder with different CTE's.

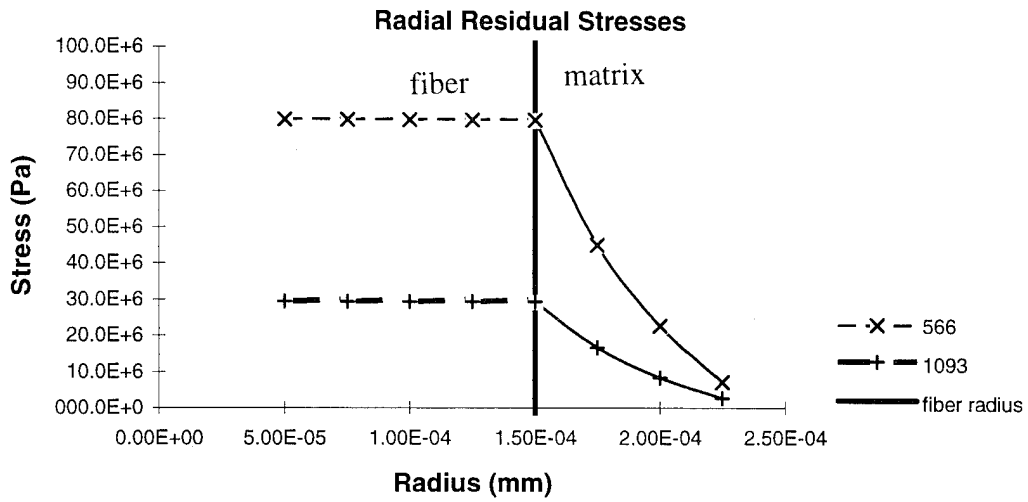
The first two figures show the tangential and hoop stresses between the fiber and matrix. The last four figures show the longitudinal stresses, and they are under in-phase TMF and out-of-phase TMF conditions. The mechanical stress is linearly superimposed on the residual stress, and the resultant total stress is shown.



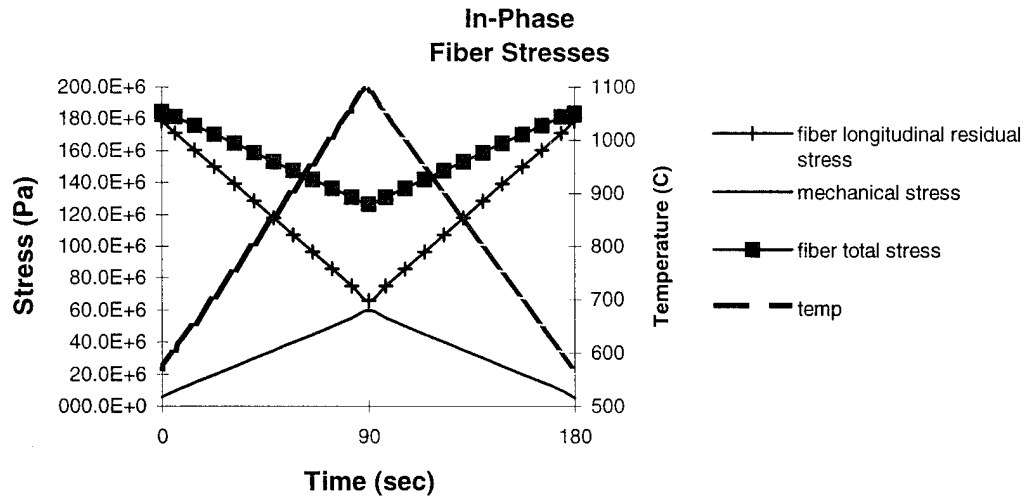
Radial and Tangential Residual Stresses in the Fiber and Matrix.

The vertical black line is the fiber/matrix interface.

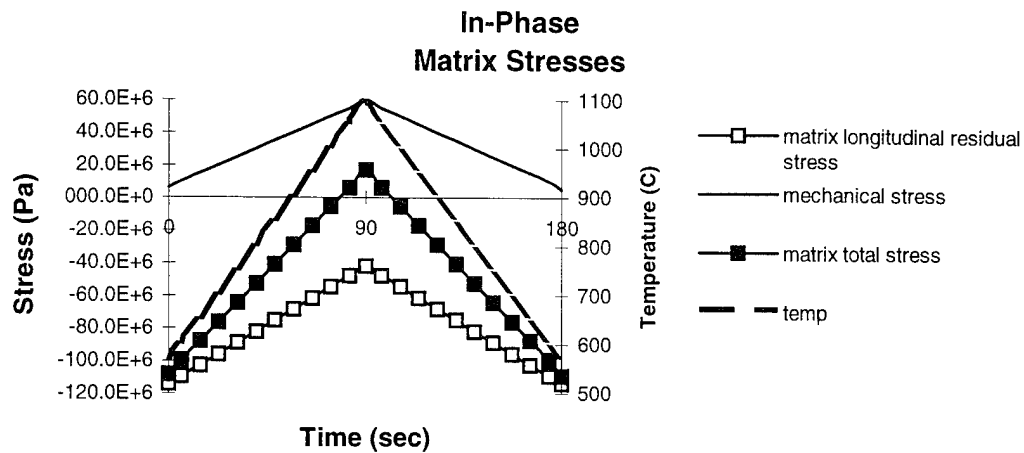
fiber tangential stress = fiber radial stress



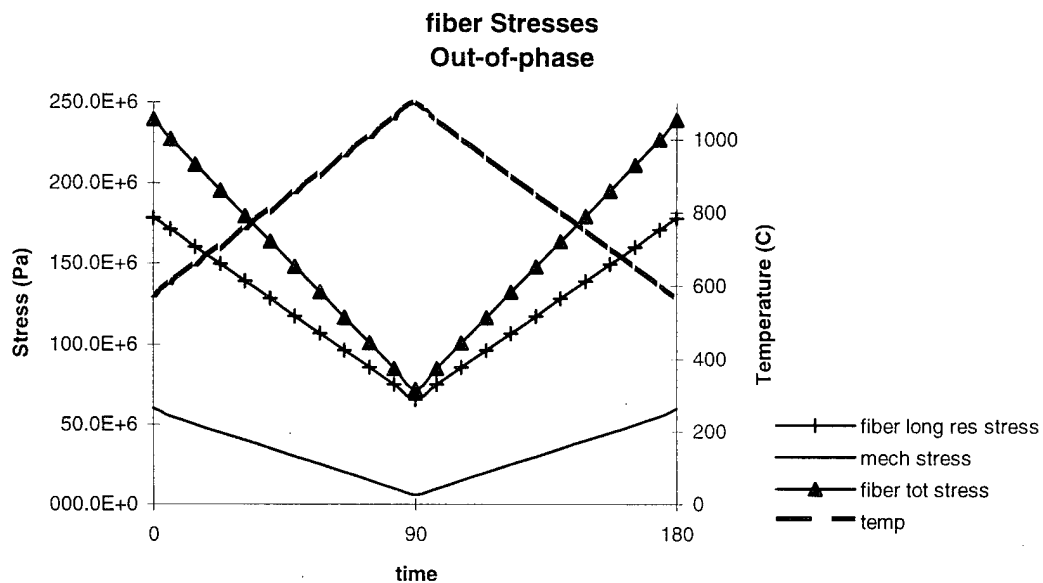
Radial Residual Stresses in the Fiber and Matrix at 566°C and 1093°C.



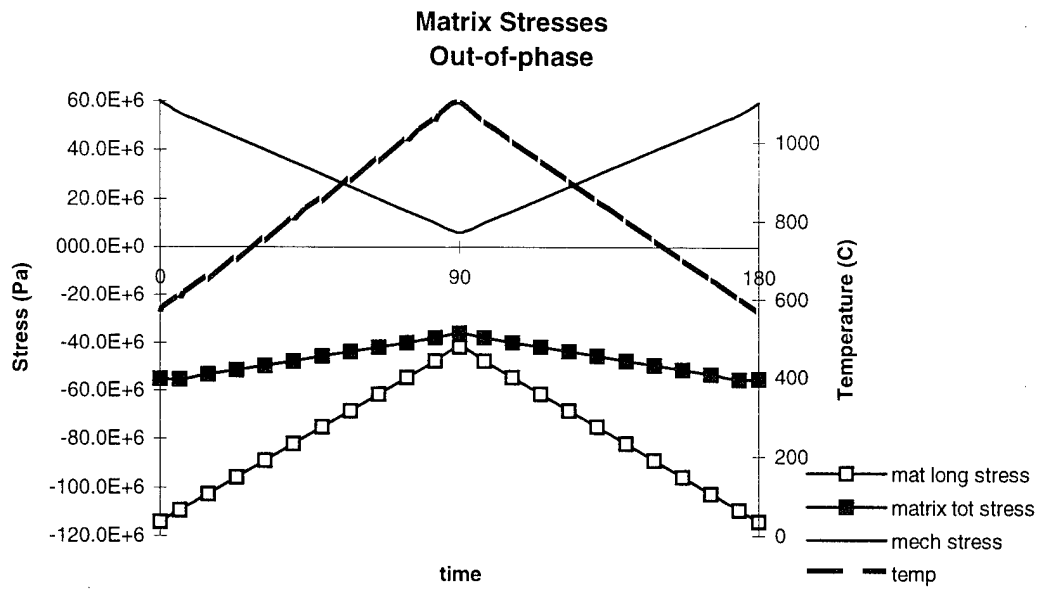
Fiber Stresses during one In-Phase TMF Cycle, due to a 60 MPa mechanical load and temperature cycle between 566°C and 1093°C



Matrix Stresses during one In-Phase TMF Cycle, due to a 60 MPa mechanical load and temperature cycle between 566°C and 1093°C



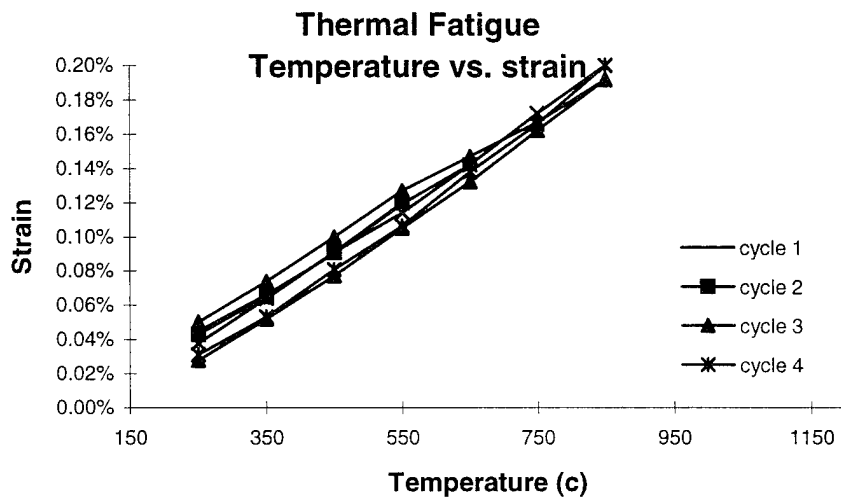
Fiber Stresses during one Out-of-Phase TMF Cycle, due to a 60 MPa mechanical load and temperature cycle between 566°C and 1093°C



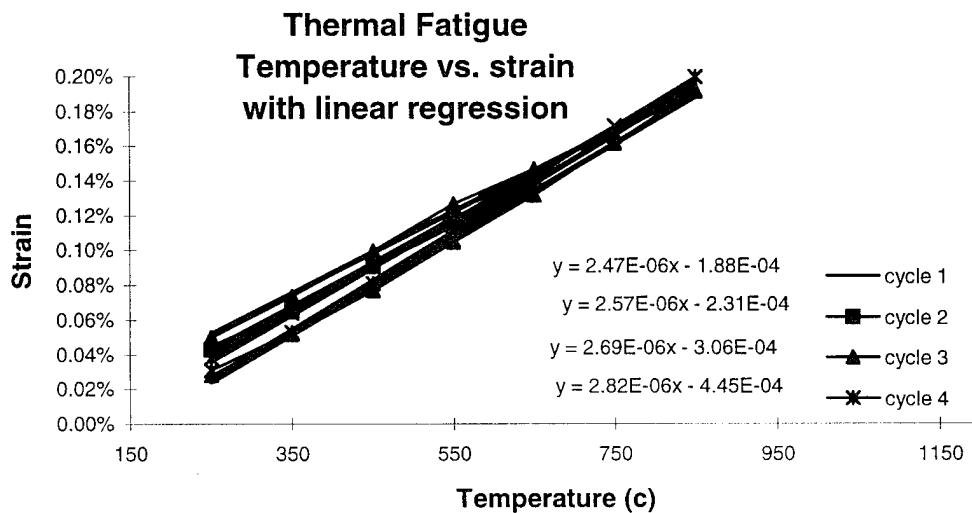
Matrix Stresses during one Out-of-Phase TMF Cycle, due to a 60 MPa mechanical load and temperature cycle between 566°C and 1093°C

APPENDIX C

This appendix contains the results of a thermal fatigue test of a Nicalon/MAS-5 specimen. The first figure shows the data for four cycles. The second figure shows the best fit curves based on linear regression of each cycle, with each curves slope labeled. The slope is the coefficient of thermal expansion (CTE).



Thermal Fatigue: Strain vs. Temperature



Thermal Fatigue: Linear Regression, CTE Each Cycle

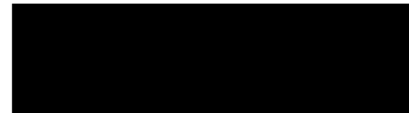
Vita

Captain Dana G. Allen [REDACTED]. He graduated from North Reading High School, North Reading, Massachusetts in 1987. A few weeks later he arrived at the United States Air Force Academy in Colorado Springs, Colorado. He graduated in 1991 with a Bachelor of Science in Aeronautical Engineering.

Captain Allen's military assignment was as a Structural Engineer for the Lockheed C-141 Starlifter at Robins Air Force Base, Warner-Robins, Georgia.

Captain Allen entered the School of Engineering, Air Force Institute of Technology, in May 1994.

Permanent Address:



REPORT DOCUMENTATION PAGE			Form Approved OMB No. 0704-0188	
Public reporting burden for this collection of information is estimated to average 1 hour per response, including the time for reviewing instructions, searching existing data sources, gathering and maintaining the data needed, and completing and reviewing the collection of information. Send comments regarding this burden estimate or any other aspect of this collection of information, including suggestions for reducing this burden, to Washington Headquarters Services, Directorate for Information Operations and Reports, 1215 Jefferson Davis Highway, Suite 1204, Arlington, VA 22202-4302, and to the Office of Management and Budget, Paperwork Reduction Project (0704-0188), Washington, DC 20503.				
1. AGENCY USE ONLY (Leave blank)		2. REPORT DATE December 1995		3. REPORT TYPE AND DATES COVERED Master's Thesis
4. TITLE AND SUBTITLE TERMO-MECHANICAL FATIGUE OF CROSS-PLY CERAMIC MATRIX COMPOSITE UNDER TENSION-TENSION LOADING			5. FUNDING NUMBERS	
6. AUTHOR(S) Dana G. Allen				
7. PERFORMING ORGANIZATION NAME(S) AND ADDRESS(ES) Air Force Institute of Technology WPAFB, OH 45433-6583			8. PERFORMING ORGANIZATION REPORT NUMBER AFIT/GAE/ENY/95D-01	
9. SPONSORING / MONITORING AGENCY NAME(S) AND ADDRESS(ES) AFOSR/NA			10. SPONSORING / MONITORING AGENCY REPORT NUMBER	
11. SUPPLEMENTARY NOTES				
12a. DISTRIBUTION / AVAILABILITY STATEMENT Approved for public release; distribution unlimited			12b. DISTRIBUTION CODE	
13. ABSTRACT (Maximum 200 words) This study investigated failure modes and associated damage in a [0/90] _{4s} Nicalon/MAS-5 ceramic matrix composite when subject to in-phase and out-of-phase thermo-mechanical fatigue (TMF). Also isothermal fatigue (IF) tests were conducted at the same frequency as that of the TMF. Stress and strain hysteresis, total strain and stiffness were monitored to characterize material behavior. Post-mortem microscopic and fractographic analysis were performed to characterize damage. Failure was dominated by fiber failure when the maximum stress was above first ply failure, and by matrix damage accumulation when the maximum stress was below first ply failure. TMF conditions cause a shorter fatigue life than IF. Out-of-phase TMF has the shortest fatigue life, with in-phase faring better except at very high stress levels. The IF life at 1093°C was worse than IF at 566°C.				
14. SUBJECT TERMS Thermo-mechanical Fatigue, Ceramic Matrix Composites			15. NUMBER OF PAGES 129	
			16. PRICE CODE	
17. SECURITY CLASSIFICATION OF REPORT Unclassified	18. SECURITY CLASSIFICATION OF THIS PAGE Unclassified	19. SECURITY CLASSIFICATION OF ABSTRACT Unclassified	20. LIMITATION OF ABSTRACT UL	

GENERAL INSTRUCTIONS FOR COMPLETING SF 298

The Report Documentation Page (RDP) is used in announcing and cataloging reports. It is important that this information be consistent with the rest of the report, particularly the cover and title page. Instructions for filling in each block of the form follow. It is important to **stay within the lines** to meet **optical scanning requirements**.

Block 1. Agency Use Only (Leave blank).

Block 2. Report Date. Full publication date including day, month, and year, if available (e.g. 1 Jan 88). Must cite at least the year.

Block 3. Type of Report and Dates Covered. State whether report is interim, final, etc. If applicable, enter inclusive report dates (e.g. 10 Jun 87 - 30 Jun 88).

Block 4. Title and Subtitle. A title is taken from the part of the report that provides the most meaningful and complete information. When a report is prepared in more than one volume, repeat the primary title, add volume number, and include subtitle for the specific volume. On classified documents enter the title classification in parentheses.

Block 5. Funding Numbers. To include contract and grant numbers; may include program element number(s), project number(s), task number(s), and work unit number(s). Use the following labels:

C - Contract	PR - Project
G - Grant	TA - Task
PE - Program Element	WU - Work Unit Accession No.

Block 6. Author(s). Name(s) of person(s) responsible for writing the report, performing the research, or credited with the content of the report. If editor or compiler, this should follow the name(s).

Block 7. Performing Organization Name(s) and Address(es). Self-explanatory.

Block 8. Performing Organization Report Number. Enter the unique alphanumeric report number(s) assigned by the organization performing the report.

Block 9. Sponsoring/Monitoring Agency Name(s) and Address(es). Self-explanatory.

Block 10. Sponsoring/Monitoring Agency Report Number. (If known)

Block 11. Supplementary Notes. Enter information not included elsewhere such as: Prepared in cooperation with...; Trans. of...; To be published in.... When a report is revised, include a statement whether the new report supersedes or supplements the older report.

Block 12a. Distribution/Availability Statement. Denotes public availability or limitations. Cite any availability to the public. Enter additional limitations or special markings in all capitals (e.g. NOFORN, REL, ITAR).

DOD - See DoDD 5230.24, "Distribution Statements on Technical Documents."

DOE - See authorities.

NASA - See Handbook NHB 2200.2.

NTIS - Leave blank.

Block 12b. Distribution Code.

DOD - Leave blank.

DOE - Enter DOE distribution categories from the Standard Distribution for Unclassified Scientific and Technical Reports.

NASA - Leave blank.

NTIS - Leave blank.

Block 13. Abstract. Include a brief (*Maximum 200 words*) factual summary of the most significant information contained in the report.

Block 14. Subject Terms. Keywords or phrases identifying major subjects in the report.

Block 15. Number of Pages. Enter the total number of pages.

Block 16. Price Code. Enter appropriate price code (*NTIS only*).

Blocks 17. - 19. Security Classifications. Self-explanatory. Enter U.S. Security Classification in accordance with U.S. Security Regulations (i.e., UNCLASSIFIED). If form contains classified information, stamp classification on the top and bottom of the page.

Block 20. Limitation of Abstract. This block must be completed to assign a limitation to the abstract. Enter either UL (unlimited) or SAR (same as report). An entry in this block is necessary if the abstract is to be limited. If blank, the abstract is assumed to be unlimited.